

**PHASE EQUILIBRIUM STUDIES OF NFM AND TOLUENE WITH  
HEAVY HYDROCARBONS AND THE CONCEPTUAL PROCESS  
DESIGN OF AN AROMATICS RECOVERY UNIT**

by

NIVAAR BRIJMOHAN

(BSc Eng)

University of KwaZulu-Natal

Submitted in fulfilment of the academic requirements for  
the degree of Master of Science in Engineering at the School  
of Chemical Engineering, University of KwaZulu-Natal

Durban

2017

## ABSTRACT

Distillation and extraction are commonly employed phase separation techniques, and improved efficiency and cost reduction in these large-scale processes are motivating factors behind thermodynamic equilibrium investigations. This first objective of the research undertaken was phase equilibrium studies of two ternary systems comprising of a heavy hydrocarbon and toluene, with the suitability of NFM as an extraction solvent investigated, due to its good selectivity and heat stability (Xia et al., 2008). The other objective was the development and simulation of a conceptual process design using Aspen Plus V8.4 to demonstrate the separation and recovery of aromatics using NFM, and to make a comparison to an existing process in terms of energy and cost efficiency.

Ternary liquid-liquid equilibrium (LLE) phase compositions were generated for the systems *n*-nonane (1) + toluene (2) + NFM (3), as well as *n*-decane (1) + toluene (2) + NFM (3). The measurements were conducted at 303.15 K, 323.15 K, and 343.15 K for each system. The modified apparatus of Raal and Brouckaert (1992) was used, with the latest modifications to the cell incorporating an adjustable temperature sleeve and magnetic stirrer (Narasigadu et al., 2014). The uncertainty in temperature of each cell was 0.02 and 0.01 respectively. Composition uncertainty was minimized by ensuring that phase composition samples were within 1% of the repeatability error for the average absolute deviation of at least 3 samples taken. Samples were analysed using gas chromatography.

The ternary systems measured in this work were modelled in terms of the NRTL model (Renon and Prausnitz, 1968) and the UNIQUAC model (Abrams and Prausnitz, 1975). Calculated RMSD values were between 0.002 and 0.02 for both models, indicating that the models represented the data satisfactorily, with the NRTL model displaying superior representation due to lower RMSD values compared to UNIQUAC. The effectiveness of using NFM an alternative solvent to extract toluene from a mixture containing *n*-nonane and *n*-decane was evaluated by determining the distribution coefficient, selectivity, and separation factor.

A process design simulation was developed using Aspen Plus V8.4 for the separation of benzene, toluene, ethylbenzene and xylene (BTEX) isomers from a hydrocarbon mixture using NFM as the

solvent. Process conditions and column specifications were optimized by investigating numerous unit configurations and running sensitivity analyses on these parameters. The aim was to target a recovery of at least 99% aromatics, which was achieved. A sequence of columns was used to effect the aromatics recovery, consisting of a counter-current liquid-liquid extraction column, followed by four distillation columns in series. The simulation results indicated that the process would consume at least 11 kcal/kg extract less energy than the sulfolane process. This manifests as lower heating and steam requirements, resulting in reduced costs of at least R19 million per annum.

## PREFACE

The research outcomes presented in this dissertation were achieved by work performed at the University of KwaZulu-Natal from August 2015 to September 2017. The work was supervised by Doctor C. Narasigadu and Professor D. Ramjugernath. This dissertation is submitted as the full requirement for the degree Master of Science Engineering (Chemical). I declare that:

1. The research reported in this thesis, except where otherwise indicated, is my original research.
2. This thesis has not been submitted for any degree or examination at any other university.
3. This thesis does not contain other persons' data, pictures, graphs or other information, unless specifically acknowledged as being sourced from other persons.
4. This thesis does not contain other persons' writing, unless specifically acknowledged as being sourced from other researchers. Where other written sources have been quoted, then:
  - i. Their words have been re-written but the general information attributed to them has been referenced
  - ii. Where their exact words have been used, then their writing has been placed in italics and inside quotation marks, and referenced.
5. This thesis does not contain text, graphics or tables copied and pasted from the Internet, unless specifically acknowledged, and the source being detailed in the thesis and in the References sections.

---

N. Brijmohan

As supervisor of this candidate, I approve this dissertation for submission:

---

Doctor C. Narasigadu

---

Professor D. Ramjugernath

## ACKNOWLEDGEMENTS

The following people are acknowledged for their contribution to this work:

- My supervisors, Doctor C. Narasigadu and Professor D. Ramjugernath for affording me this opportunity, and their expert knowledge, guidance and support.
- SASOL Ltd. for their financial assistance.
- The technical staff at the School of Chemical Engineering, University of KwaZulu-Natal for their work done on the equipment used in this project.
- My family and friends for their motivation and encouragement.

# TABLE OF CONTENTS

ABSTRACT.....	i
PREFACE.....	iii
ACKNOWLEDGEMENTS.....	iv
LIST OF FIGURES.....	viii
LIST OF TABLES.....	xi
NOMENCLATURE.....	xiii
CHAPTER ONE: INTRODUCTION.....	1
CHAPTER TWO: LITERATURE REVIEW.....	7
2.1 LLE Techniques.....	7
2.1.1 Titration Method.....	7
2.1.2 Turbidity Method.....	8
2.1.3 Laser-light Scattering Technique.....	8
2.1.4 Continuous Measurement.....	9
2.1.5 Direct Analytical Method.....	10
CHAPTER THREE: THEORETICAL BACKGROUND.....	12
3.1 Criterion for Phase Equilibrium.....	13
3.2 Liquid Phase Activity Coefficient Models.....	14
3.2.1 The NRTL (Non-Random Two Liquid) Model.....	14
3.2.2 The UNIQUAC (UNIversal QUasi-Chemical) Equation.....	15
3.3 Regression Algorithms.....	17
3.4 Liquid – Liquid Extraction.....	19
3.4.1 Type 1: Formation of One Pair of Partially Miscible Liquids.....	21
3.4.2 Type 2: Formation of Two Pairs of Partially Miscible Liquids.....	22

3.4.3 Type 3: Formation of Three Pairs of Partially Miscible Liquids.....	22
3.4.4 Identification of Plait Point.....	23
CHAPTER FOUR: EQUIPMENT DESCRIPTION .....	25
4.1 The Liquid-Liquid Equilibrium Apparatus.....	25
4.2 Temperature Measurement and Control .....	28
4.3 Sampling and Composition Analysis.....	29
4.4 Auxiliary Equipment.....	29
CHAPTER FIVE: EXPERIMENTAL PROCEDURE.....	30
5.1 Gas Chromatograph Calibration .....	30
5.2 Calibration of Temperature Sensors .....	32
5.3 The Liquid-Liquid Equilibrium Apparatus.....	33
5.3.1 Cleaning the LLE Cell .....	33
5.3.2 Operating Procedure .....	33
CHAPTER SIX: EXPERIMENTAL RESULTS.....	35
6.1 Chemical Purity .....	36
6.2 Phase Equilibrium of Test Systems .....	36
6.2.2 Liquid-Liquid Equilibrium Result .....	37
6.4 Phase Equilibrium of New Systems.....	38
6.4.1 Ternary Liquid-Liquid Equilibrium (LLE).....	39
CHAPTER SEVEN: DATA ANALYSIS AND DISCUSSION .....	48
7.1 Ternary Systems Correlation .....	48
7.1.1 n-Nonane (1) + Toluene (2) + NFM (3) .....	49
7.1.2 n-Decane (1) + Toluene (2) + NFM (3).....	53
7.2 Systems Comparison.....	57
7.3 Solvent Parameters.....	58

CHAPTER EIGHT: PROCESS DESIGN SIMULATION .....	62
8.1 Process Requirements .....	62
8.2 Thermodynamic Modelling .....	64
8.3 Process Modeling and Simulation .....	64
8.4 System Specifications .....	67
8.4.1 Liquid-Liquid Extraction Column .....	67
8.4.2 Extractive Distillation Column .....	68
8.4.3 Solvent Feed.....	69
8.4.4 Solvent Recovery Column .....	70
8.4.5 Benzene Recovery Column.....	72
8.4.6 Toluene Recovery Column .....	74
8.5 Energy Comparison .....	77
CHAPTER NINE: CONCLUSION .....	80
CHAPTER TEN: RECOMMENDATIONS .....	82
REFERENCES .....	83
APPENDIX A.....	89
APPENDIX B .....	92
APPENDIX C .....	102

## LIST OF FIGURES

Figure 1-1: Process flow diagram of a naphtha cracker (Meindersma and de Haan, 2008).....	4
Figure 1-2: Process flow diagram of the sulfolane process (Johnson, 1986) .....	5
Figure 2-1: Turbid mixture on addition of a third component (Naidoo, 2003). .....	8
Figure 2-2: A schematic diagram of the apparatus used for mutual solubility measurements with laser-light scattering (Benjamin et al., 1993).....	9
Figure 2-3: Apparatus for determining continuous liquid-liquid equilibria (Naidoo, 2003).....	10
Figure 2-4: Illustration of the direct analytical method of measuring LLE (Naidoo, 2003). .....	11
Figure 3-1: Flow chart illustrating the process followed in regression of predicted binary interaction parameters. ....	18
Figure 3-2: Illustration of the various elements in a liquid – liquid extraction system. ....	19
Figure 3-3: Plotting of points on a ternary LLE diagram (Treybal, 1963). ....	20
Figure 3-4: Type 1 ternary system in equilibrium (Treybal, 1963). ....	21
Figure 3-5: Type 2 ternary system in equilibrium (Treybal, 1963). ....	22
Figure 3-6: Type 3 ternary system in equilibrium (Treybal, 1963). ....	22
Figure 3-7: The graphical Coolidge method of determining the plait point (Treybal, 1963).....	23
Figure 3-8: Alternative method of determining the plait point (Treybal, 1963).....	24
Figure 4-1: LLE still used by Raal and Brouckaert (1992). ....	26
Figure 4-2: LLE still of Ndlovu (2005). ....	27
Figure 4-3: Schematic of the double-walled glass cell (Narasigadu et al., 2014). ....	28
Figure 6-1: The $T-x^I-x^{II}$ plot for the methanol (1) + <i>n</i> -heptane (2) system at 101.3 kPa.....	38
Figure 6-2: Ternary diagram for the <i>n</i> -nonane (1) + toluene (2) + NFM (3) system at 303.15 K and 1 atm.....	40
Figure 6-3: Ternary diagram for the <i>n</i> -nonane (1) + toluene (2) + NFM (3) system at 323.15 K and 1 atm.....	41
Figure 6-4: Ternary diagram for the <i>n</i> -nonane (1) + toluene (2) + NFM (3) system at 343.15 K and 1 atm.....	42
Figure 6-5: Ternary diagram for the <i>n</i> -decane (1) + toluene (2) + NFM (3) system at 303.15 K and 1 atm.....	43

Figure 6-6: Ternary diagram for the <i>n</i> -decane (1) + toluene (2) + NFM (3) system at 323.15 K and 1 atm.....	44
Figure 6-7: Ternary diagram for the <i>n</i> -decane (1) + toluene (2) + NFM (3) system at 343.15 K and 1 atm.....	45
Figure 7-1: Fit of the NRTL model with $\alpha = 0.35$ for the predicted tie-lines and binodal curve for the ternary plot of the <i>n</i> -nonane (1) + toluene (2) + NFM (3) system at 303.15 K and 1 atm. ....	50
Figure 7-2: Fit of the NRTL model with $\alpha = 0.35$ for the predicted tie-lines and binodal curve for the ternary plot of the <i>n</i> -nonane (1) + toluene (2) + NFM (3) system at 323.15 K and 1 atm. ....	51
Figure 7-3: Fit of the NRTL model with $\alpha = 0.2$ for the predicted tie-lines and binodal curve for the ternary plot of the <i>n</i> -nonane (1) + toluene (2) + NFM (3) system at 343.15 K and 1 atm. ....	52
Figure 7-5: Fit of the NRTL model with $\alpha = 0.4$ for the predicted tie-lines and binodal curve for the ternary plot of the <i>n</i> -decane (1) + toluene (2) + NFM (3) system at 323.15 K and 1 atm.....	55
Figure 7-6: Fit of the NRTL model with $\alpha = 0.2$ for the predicted tie-lines and binodal curve for the ternary plot of the <i>n</i> -decane (1) + toluene (2) + NFM (3) system at 343.15 K and 1 atm.....	56
Figure 7-7: Measured and predicted distribution coefficients with NRTL model for the <i>n</i> -nonane (1) + toluene (2) + NFM (3) system. ....	59
Figure 7-8: Measured and predicted distribution coefficients with NRTL model for the <i>n</i> -decane (1) + toluene (2) + NFM (3) system. ....	59
Figure 7-9: Measured and predicted separation factor by NRTL model for the <i>n</i> -nonane (1) + toluene (2) + NFM (3) system. ....	60
Figure 7-10: Measured and predicted separation factor by NRTL model for the <i>n</i> -decane (1) + toluene (2) + NFM (3) system. ....	60
Figure 7-11: Measured and predicted selectivity by NRTL model for the <i>n</i> -nonane (1) + toluene (2) + NFM (3) system. ....	61
Figure 7-12: Measured and predicted selectivity by NRTL model for the <i>n</i> -nonane (1) + toluene (2) + NFM (3) system. ....	61
Figure 8-1: Process flow diagram illustrating aromatics recovery process using NFM as the solvent. ....	65
Figure 8-2: Sensitivity comparison of solvent feed to extractor against toluene distillate. ....	70
Figure 8-3: Sensitivity comparison of solvent recycle rate against feed stage. ....	71
Figure 8-4: Sensitivity comparison of solvent recycle rate against number of stages.....	72

Figure 8-5: Sensitivity comparison of benzene distillate against feed stage. ....	73
Figure 8-6: Sensitivity comparison of benzene distillate against number of stages. ....	74
Figure 8-7: Sensitivity comparison of benzene distillate against benzene column boil up ratio..	74
Figure 8-8: Sensitivity comparison of toluene distillate against feed stage.....	76
Figure 8-9: Sensitivity comparison of toluene distillate against number of stages. ....	76
Figure 8-10: Sensitivity comparison of toluene distillate against column boil up ratio. ....	77
Figure B-1: Temperature calibration plot of cell 1 temperature sensor.....	92
Figure B-2: Temperature deviation plot of cell 1 temperature sensor. ....	93
Figure B-3: Temperature calibration plot of cell 2 temperature sensor.....	93
Figure B-4: Temperature deviation plot of cell 2 temperature sensor. ....	94
Figure B-5: GC calibration graph of methanol (1) + <i>n</i> -heptane (2) (methanol dilute region).....	96
Figure B-6: GC calibration graph of methanol (1) + <i>n</i> -heptane (2) ( <i>n</i> -heptane dilute region).....	96
Figure B-7: Composition deviation plot for the methanol (1) + <i>n</i> -heptane (2) system .....	97
Figure B-8: GC calibration graph for the nonane (1) + NFM (2) pair ( <i>n</i> -nonane dilute region)..	97
Figure B-9: GC calibration graph for the <i>n</i> -nonane (1) + NFM (2) pair (NFM dilute region).....	98
Figure B-10: Composition deviation plot for the <i>n</i> -nonane (1) + NFM (2) system .....	98
Figure B-11: GC calibration graph for <i>n</i> -decane (1) + NFM (2) pair ( <i>n</i> -decane dilute region) ...	99
Figure B-12: GC calibration graph for the <i>n</i> -decane (1) + NFM (2) pair (NFM dilute region) ...	99
Figure B-13: Composition deviation plot for the <i>n</i> -decane (1) + NFM (2) system.....	100
Figure B-14: GC calibration graph for the toluene (1) + NFM (2) pair (toluene dilute region). 100	
Figure B-15: GC calibration graph for the toluene (1) + NFM (2) pair (NFM dilute region)....	101
Figure B-16: Composition deviation plot for the toluene (1) + NFM (2) system .....	101
Figure C-1: Aspen Plus flowsheet for aromatics recovery unit using NFM as the solvent.....	102

# LIST OF TABLES

Table 1-1: Summary of existing separation techniques (Weissermel and Arpe, 2003).....	2
Table 1-2: Commercial solvent extraction processes (Weissermel and Arpe, 2003).....	3
Table 6-1: Chemical purities and refractive indices for all reagents used in this study. ....	36
Table 6-2: Experimental LLE data for the methanol (1) + <i>n</i> -heptane (2) system at 101.3 kPa....	37
Table 6-3: Liquid-liquid equilibrium data for the <i>n</i> -nonane (1) + toluene (2) + NFM (3) system at 303.15 K and 101.3 atm. ....	39
Table 6-4: Liquid-liquid equilibrium data for the <i>n</i> -nonane (1) + toluene (2) + NFM (3) system at 323.15 K and 101.3 atm. ....	40
Table 6-5: Liquid-liquid equilibrium data for the <i>n</i> -nonane (1) + toluene (2) + NFM (3) system at 343.15 K and 101.3 atm. ....	41
Table 6-6: Liquid-liquid equilibrium data for the <i>n</i> -decane (1) + toluene (2) + NFM (3) system at 303.15 K and 101.3 atm. ....	43
Table 6-7: Liquid-liquid equilibrium data for the <i>n</i> -decane (1) + toluene (2) + NFM (3) system at 323.15 K and 101.3 atm. ....	44
Table 6-8: Liquid-liquid equilibrium data for the <i>n</i> -decane (1) + toluene (2) + NFM (3) system at 343.15 K and 101.3 atm. ....	45
Table 6-9: Experimental data of the distribution coefficient ( $\kappa$ ), separation factor ( $\beta$ ) and selectivity (S) of the <i>n</i> -nonane (1) + toluene (2) + NFM (3) system .....	46
Table 6-10: Experimental data of the distribution coefficient ( $\kappa$ ), separation factor ( $\beta$ ) and selectivity (S) of the <i>n</i> -decane (1) + toluene (2) + NFM (3) system .....	47
Table 7-1: Model parameters for the tie-lines of the <i>n</i> -nonane (1) + toluene (2) + NFM (3) system at 303.15 K and 1 atm. ....	49
Table 7-2: Model parameters for the tie-lines of the <i>n</i> -nonane (1) + toluene (2) + NFM (3) system at 323.15 K and 1 atm. ....	50
Table 7-3: Model parameters for the tie-lines of the <i>n</i> -nonane (1) + toluene (2) + NFM (3) system at 343.15 K and 1 atm. ....	51
Table 7-4: Modelled liquid-liquid equilibrium data for the <i>n</i> -nonane (1) + toluene (2) + NFM (3) system at 303.15, 323.15, 343.15 K and 101.3 atm. ....	53

Table 7-5: Model parameters for the tie-lines of the <i>n</i> -decane (1) + toluene (2) + NFM (3) system at 303.15 K and 1 atm. ....	54
Table 7-6: Model parameters for the tie-lines of the <i>n</i> -decane (1) + toluene (2) + NFM (3) system at 323.15 K and 1 atm. ....	55
Table 7-7: Model parameters for the tie-lines of the <i>n</i> -decane (1) + toluene (2) + NFM (3) system at 343.15 K and 1 atm. ....	56
Table 7-8: Modelled liquid-liquid equilibrium data for the <i>n</i> -decane (1) + toluene (2) + NFM (3) system at 303.15, 323.15, 343.15 K and 101.3 atm. ....	57
Table 7-9: Plait point of ternary systems measured at different temperatures. ....	58
Table 8-1: Typical composition of feed naphtha (Meindersma and de Haan, 2008). ....	63
Table 8-2: Operating conditions of main streams in separation process. ....	65
Table 8-3: Aromatics recovery achieved in separation process. ....	67
Table 8-4: Specifications for the liquid-liquid extraction column. ....	68
Table 8-5: Specifications for the extractive distillation column simulated using Radfrac. ....	69
Table 8-6: Specifications for the solvent recovery column simulated using Radfrac. ....	71
Table 8-7: Specifications for the benzene recovery column simulated using Radfrac. ....	73
Table 8-8: Specifications for the toluene recovery column simulated using Radfrac. ....	75
Table 8-9: Duty of major energy consumers and specific energy consumption. ....	78
Table B-1: Calibration results for temperature sensors in this investigation. ....	92
Table B-2: Operating conditions for the Shimadzu 2014 gas chromatograph. ....	94
Table B-3: Summary of calibrations with average absolute deviations ....	95
Table C-1: Stream operating conditions and molar flows from Aspen Plus V8.4 ....	103
Table C-2: Summary of process heat exchangers required - from Aspen Plus V8.4 ....	104

# NOMENCLATURE

## English Letters

$A_i^*$	Peak area obtained from the gas chromatograph
$D^*$	Parameter used for the LLE charts of Renon and Prausnitz (1968)
$F_i$	Response factor
$F$	Fugacity [kPa]
$\hat{f}_i$	Fugacity in solution [kPa]
$G$	Molar or specific Gibbs energy [J/mol]
$\bar{G}$	Partial molar Gibbs energy [J/mol]
$G_{ij}$	Parameter in the NRTL model of Renon and Prausnitz (1968)
$g_{ij} - g_{ii}$	Parameter representing energy interactions between species in the NRTL model of Renon and Prausnitz (1968)
$H$	Enthalpy [J/mol]
$k_{ij}$	Binary interaction parameter
$l_i$	Parameter in the UNIQUAC model of Abrams and Prausnitz (1975)
$K$	Distribution coefficient
$M$	Represents a general thermodynamic property
$N$	Number of moles
$P$	System Pressure [kPa]
$q_i$	Pure component area parameter in the UNIQUAC model of Abrams and Prausnitz (1975)
$q'_i$	Pure component area parameter in the modified UNIQUAC model (Anderson and Prausnitz, 1978)
$R$	Universal gas constant [J/mol.K]
$r_i$	Pure component volume parameter in the UNIQUAC model of Abrams and Prausnitz (1975)
$S$	Selectivity
$S^*$	Parameter used for the LLE charts of Renon and Prausnitz (1968)

$T$	System temperature [ $^{\circ}\text{C}$ or $\text{K}$ ]
$u_{ij} - u_{ii}$	Parameter representing energy interactions between species in the UNIQUAC model of Abrams and Prausnitz (1975)
$V$	Molar or specific volume [ $\text{cm}^3/\text{mol}$ ]
$X$	Liquid phase mole fraction or composition
$Y$	Vapour phase mole fraction or composition
$Z$	Coordination number in the UNIQUAC model of Abrams and Prausnitz (1975)

### Greek Letters

$\alpha_{ij}$	Non-randomness parameter in the NRTL model of Renon and Prausnitz (1968) representing solution non-randomness
$\delta$	Denotes a residual (e.g. $\delta P$ )
$\Gamma_i$	Temperature dependent constant of integration
$\gamma$	Activity coefficient
$\mu_i$	Chemical potential of component $i$
$\theta_i$	Area fraction in the modified UNIQUAC model of Abrams and Prausnitz (1975)
$\theta'_i$	Area fraction in the modified UNIQUAC model (Anderson and Prausnitz, 1978)
$\tau_{ij}$	Dimensionless interaction parameter in the NRTL model of Renon and Prausnitz (1968)

### Subscript

$1$	Denotes component 1
$2$	Denotes component 2
$3$	Denotes component 3
$Ad$	Denotes an absolute deviation
$C$	Denotes a critical property

<i>Calc</i>	Denotes a calculated value
<i>Exp</i>	Denotes an experimental value
<i>R</i>	Denotes a reduced property

**Superscripts**

<i>C</i>	Denotes a combinatorial property for the UNIQUAC model of Abrams and Prausnitz (1975)
<i>E</i>	Denotes an excess property
<i>L</i>	Denotes a liquid phase
$\alpha$	Denotes a thermodynamic phase
$\beta$	Denotes a thermodynamic phase / separation factor
$\pi$	Denotes a thermodynamic phase

# 1

## CHAPTER ONE

### INTRODUCTION

Aromatics are an important group of chemicals used as a feedstock for the chemical manufacture of plastics, synthetic rubbers, and synthetic fibers. It consists primarily of benzene, toluene, and xylene isomers and is produced by separation from petroleum naphtha, coking naphtha, and pyrolysis gasoline through different techniques (Chen et al., 2017). Table 1-1 summarizes the various separation techniques applied in this industry in different processes.

Conventional distillation is not an effective technique in this process due to the formation of azeotropes between alkanes and aromatics in the stream mixture. Solvent extraction is the most commonly used technique in ensuring high aromatic purities from feedstocks of low aromatic content. The method entails the use of solvents to selectively absorb certain components in a mixture with conventional distillation used thereafter to separate the solvent and desired component. Additional benefits realized by utilizing this technique include reduced capital investment and operating costs (Cho et al., 2002).

**Table 1-1: Summary of existing separation techniques (Weissermel and Arpe, 2003).**

Process	Separation Problem	Operational Requirements
Azeotropic Distillation	BTX separation from pyrolysis gasoline	High aromatic content (>90%)
Extractive Distillation	BTX separation from pyrolysis gasoline	Medium aromatic content (65–90%)
Liquid-Liquid Extraction	BTX separation from reformate gasoline	Lower aromatic content (20- 65%)
Crystallization by Freezing	Isolation of <i>p</i> -xylene from <i>m/p</i> -mixtures	Distillate pre-separation of <i>o</i> - xylene and ethylbenzene from C <sub>8</sub> aromatic fractions
Adsorption on Solids	Isolation of <i>p</i> -xylene from C <sub>8</sub> aromatic fractions	Continuous, reversible, and selective adsorption

Commonly used solvents include N-formylmorpholine (NFM), sulfolane, N-methyl-2-pyrrolidinone (NMP) and glycols (Weidlich et al., 1987). Compatible solvents need to have a high selectivity for aromatics, rapidly form two phases at the operating temperature, and possess non-corrosive and non-reactive properties (Saha et al., 1999). Research on using combinations of solvents is also ongoing, with reported benefits being that of lower energy consumption and solvent to feed ratio (Saha et al., 1999). Krummen and Gmehling (2004) investigated the use of water as a co-solvent with NMP and NFM, finding that the presence of water lead to an increase in the selectivity of the solvent, but a decrease in capacity. A summary of the commercial processes utilizing solvent extraction is presented in Table 1-2:

**Table 1-2: Commercial solvent extraction processes (Weissermel and Arpe, 2003).**

Process	Company	Solvent	Extraction Conditions
Udex	UOP-Dow	Mono-, di-, tri- or tetraethylene glycol/H <sub>2</sub> O and mixtures	130 - 150°C, 5 - 7 bar
Tetra	UCC	Tetraethylene glycol/H <sub>2</sub> O	Not disclosed
Sulfolane	Shell-UOP	Tetrahydrothiophene dioxide (sulfolane)	50 - 100°C
Arosolvan	Lurgi	N-Methylpyrrolidone/H <sub>2</sub> O	20 - 40°C, 1 bar
DMSO	IFP	Dimethyl sulfoxide/H <sub>2</sub> O	20 - 30°C
CIS	-	Propylene carbonate	20 - 50°C
Duo-Sol	Milwhite Co.	Propane/cresol or phenol	Not disclosed
Formex	Snamprogetti	N-Formylmorpholine/H <sub>2</sub> O	40°C, 1 bar
Aromex	Koppers	N-Formylmorpholine/H <sub>2</sub> O	80°C, 2 bar
Morphylex	Krupp-Koppers	N-Formylmorpholine/H <sub>2</sub> O	Not disclosed
Mofex	Leuna-Werke	Monomethylformamide/H <sub>2</sub> O	20 - 30°C, 0.1 - 0.4 bar
Arex	Leuna-Werke	N-Methyl- $\epsilon$ -caprolactam	60°C

Azeotropic distillation is cost-effective when a small recovery of aliphatics is required, as seen in Table 1-1, when streams of pyrolysis gasoline aromatics are greater than 90%. Strongly polar ancillary solvents such as amines and water enable separation of cycloalkanes and alkanes as lower boiling point azeotropes.

Extractive distillation is another employed separation technique, involving blending polar solvents with hydrocarbon mixtures, resulting in higher volatilities of naphthenes in relation to aromatics, and more volatile paraffins relative to naphthenes, olefins, diolefins and alkynes (Zhang et al., 2005). This method lowers the column requirements in the distillation of mixtures which would otherwise not be feasible. Typical extractive distillation processes use solvents such as NMP

(Distapex process), NFM (Morphylane and Octenar process), dimethylformamide, or sulfolane. Columns are used in series, in which the solvent is supplied with the main feed to the first column, with the aliphatics as the tops product and the aromatics and solvent as the bottoms product. The solvent is separated and recovered in subsequent columns.

The industrial application of interest in this study is the production of aromatics from pyrolysis gasoline, which occurs via the steam cracking of naphtha for the additional production of propene, ethylene and higher olefins. Figure 1-1 depicts a simplified flow diagram of a cracking process, which serves to split the naphtha feed into distributions of various products. It is industrial practice for the aromatics separation to occur subsequent to the furnace, but not from the naphtha itself. Meindersma and de Haan (2008) proposed a conceptual design for extracting aromatics directly from the feed naphtha by solvent extraction using ionic liquids, with benefits realized in terms of increased capacity and thermal efficiency, as well as reduced fouling. They estimated an annual reduction of operating costs by R 680 million (adjusted for inflation from 2008) for a 300 tph feed system by aromatic extraction from the feed system.

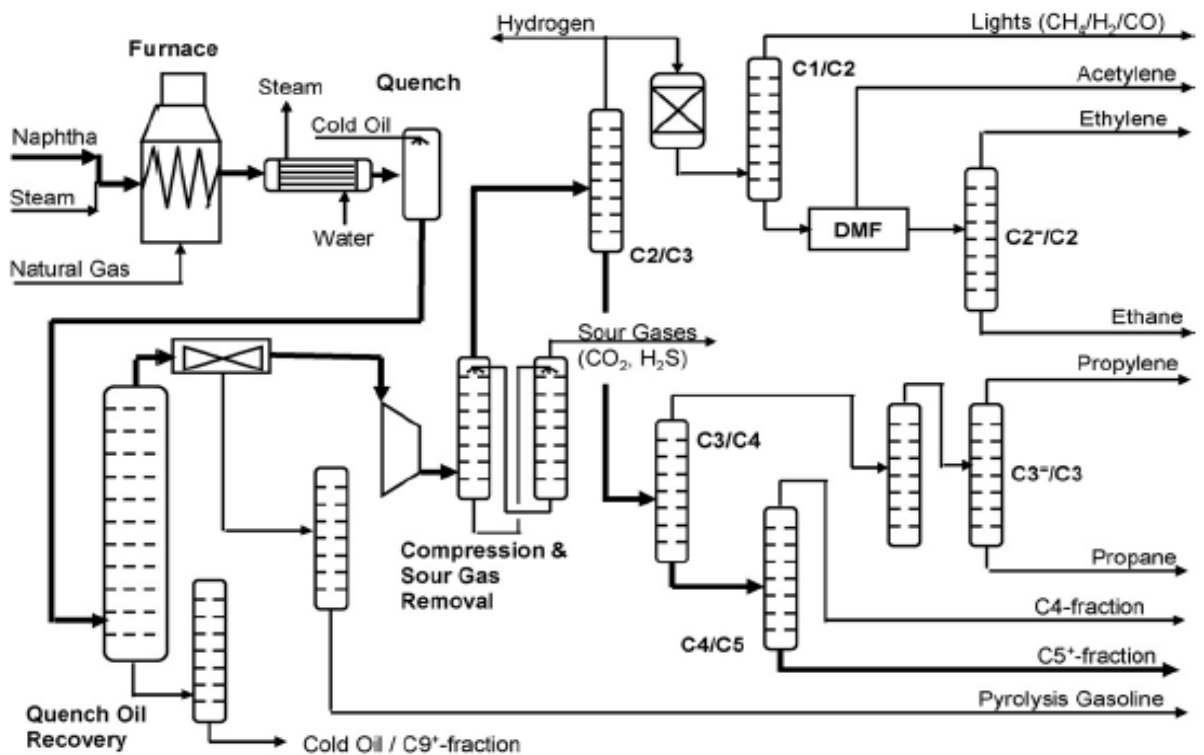


**Figure 1-1: Process flow diagram of a naphtha cracker (Meindersma and de Haan, 2008).**

Regarding solvent extraction and extractive distillation, the sulfolane process is an efficient method used in industrial applications for aromatics removal. Johnson (1986), as well as Gary and Handwerk (1984) present a detailed description of the various aromatic separation processes, also highlighting the sulfolane process. Sulfolane plants use sulfolane as the solvent, and are included for the recovery of high-purity toluene and benzene from naphtha streams. The extract is clay treated to increase the purity of the aromatic products, with benzene and toluene recovered thereafter by fractionation.

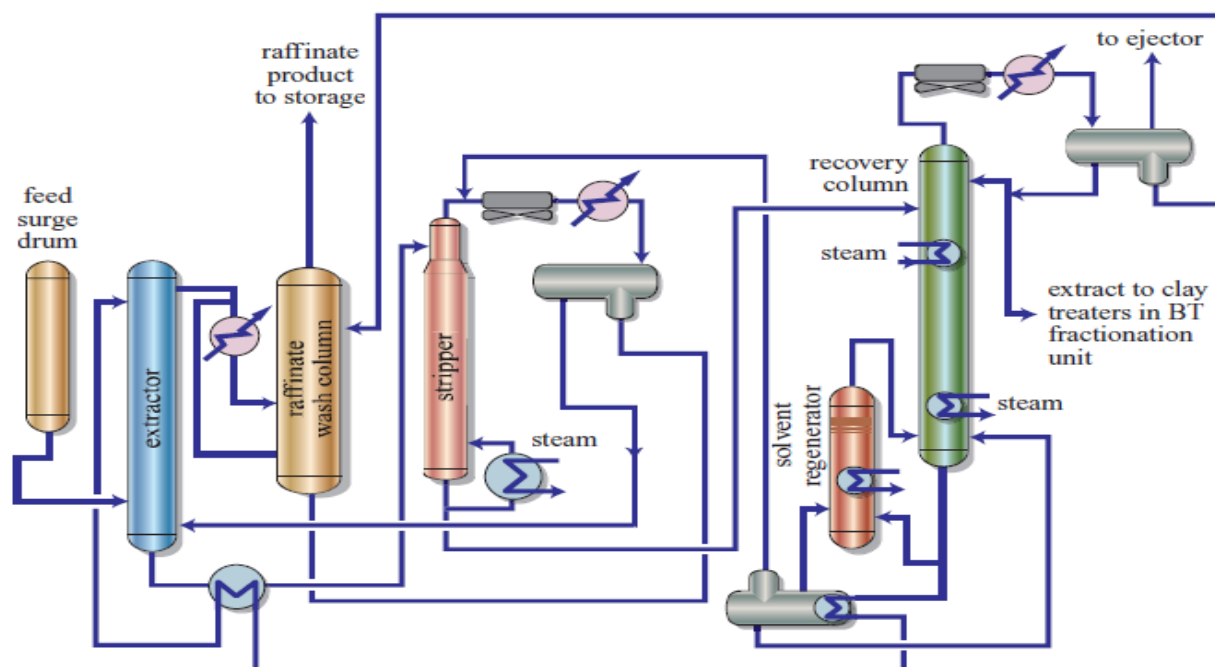


**Figure 1-2: Process flow diagram of the sulfolane process (Johnson, 1986).**

The feed is supplied to the extraction column at the bottom and interacts with the solvent entering at the top in a counter-current flow arrangement. Aromatic components are selectively absorbed by the solvent. The raffinate exits the top and contains primarily non-aromatic components, while the extract containing the aromatics, aliphatics, and the solvent exits the bottom. The extract enters an extractive distillation column to recover lighter non-aromatic components, in which the top stream is recycled back to the extractor. The bottoms is processed in a downstream column to separate aromatics from the solvent, and the resulting aromatics mixture is transported to downstream separation units to facilitate the recovery of benzene and toluene individually. The energy consumption of an aromatics recovery process is largely dependent on the desired purity

and recovery performance. Improved performance is achieved at increased solvent supply but at the cost of higher energy consumption. A typical sulfolane unit consumes 275-300 kcal of energy per kilogram of extract produced (Gary and Handwerk, 1984).

Phase equilibrium provides the underlying basis on which separation processes are designed and implemented. Information concerning phase equilibrium behaviour is necessitated by the need for optimal operation and design of chemical processing plants. LLE (liquid-liquid equilibrium) data is employed in the design of solvent extraction processes.

NFM is widely used over other solvents in the recovery of aromatics due to its good selectivity and heat stability (Xia et al., 2008). As such, the research outcomes of this investigation focus on NFM. Concerning the alkane + toluene + NFM system, equilibrium data is sufficiently available for lighter alkanes such as for hexane and heptane (Cincotti et al., 1999), while data regarding heavier alkanes appear to be limited in the open literature. This research serves to contribute measurements on heavier  $C_9 - C_{10}$  alkanes.

The following LLE measurements were conducted:

- Ternary LLE for the system *n*-nonane + toluene + NFM at 1 atm and 303.15 K.
- Ternary LLE for the system *n*-nonane + toluene + NFM at 1 atm and 323.15 K.
- Ternary LLE for the system *n*-nonane + toluene + NFM at 1 atm and 343.15 K.
- Ternary LLE for the system *n*-decane + toluene + NFM at 1 atm and 303.15 K.
- Ternary LLE for the system *n*-decane + toluene + NFM at 1 atm and 323.15 K.
- Ternary LLE for the system *n*-decane + toluene + NFM at 1 atm and 343.15 K.

The experimental LLE measurements were performed with an adapted apparatus of the original used by Raal and Brouckaert (1992). Modifications include the use of a magnetic stirrer, an adjustable thermo-well for improved temperature measurements, and a sampling port for the denser phase. The experimental data was correlated using the NRTL and UNIQUAC models, and a simulation was done thereafter using Aspen Plus V8.4, utilizing the model parameters to illustrate a process design for the extraction of aromatics using NFM and a comparison of the resulting benefits in terms of energy and cost efficiency.

# 2

## CHAPTER TWO

### LITERATURE REVIEW

The process of determining phase equilibrium behaviour of a system involves measurements of phase composition, temperature, and pressure. It is imperative for these parameters to be measured at the point where equilibrium actually exists and that removal of samples from the system does not disturb the equilibrium appreciably (Walas, 1985).

#### **2.1 LLE Techniques**

The measurement of LLE is generally considered to be easier than that of VLE. The following methods of measuring LLE will be outlined: the titration method, turbidity method, laser – light scattering method, continuous measurement method, and the direct analytical method.

##### **2.1.1 Titration Method**

The titration method involves the constant addition of a component to a known quantity of another component, or to a multi-component mixture in a stirred vessel, until turbidity appears or disappears (as illustrated in Figure 2-1). Measurement of system compositions required for phase separation allows for construction of the binodal curve, and is determined by analysis using refractive index or density. Alternatively, the tie-lines can also be obtained using the Karl-Fischer titration method, provided one of the components is water (Skoog et al., 1991).

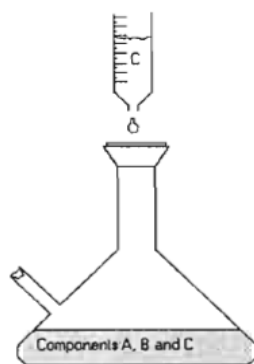


**Figure 2-1: Turbid mixture on addition of a third component (Naidoo, 2003).**

A detailed discussion on the titration method can be obtained by consulting the work of Briggs and Comings (1943), Rifai and Durandet (1962) and Letcher et al. (1989).

### **2.1.2 Turbidity Method**

This method involves charging a heterogeneous or homogeneous solution of known composition into an equilibrium cell, in which the temperature is varied. The onset or disappearance of a second phase is noted. An advantage of the turbidity method is that no phase analysis at equilibrium is necessary. Reviews of the experimental LLE cells employing the turbidity method are discussed in Raal and Muhlbauer (1998).

### **2.1.3 Laser-light Scattering Technique**

The indication of equilibrium in the titration and turbidity methods entail subjective judgement of the onset or disappearance of turbidity, leading to results of reduced accuracy. Thus, certain equipment (as illustrated in Figure 2-3) was developed to attempt to give an objective indication of equilibrium. Benjamin et al. (1993) developed an apparatus that used a photocell to detect the intensity of scattered light. The experimental cloud point is determined from a plot of intensity of scattered light versus temperature for a specific sample hence allowing for the generation of the binodal curve.

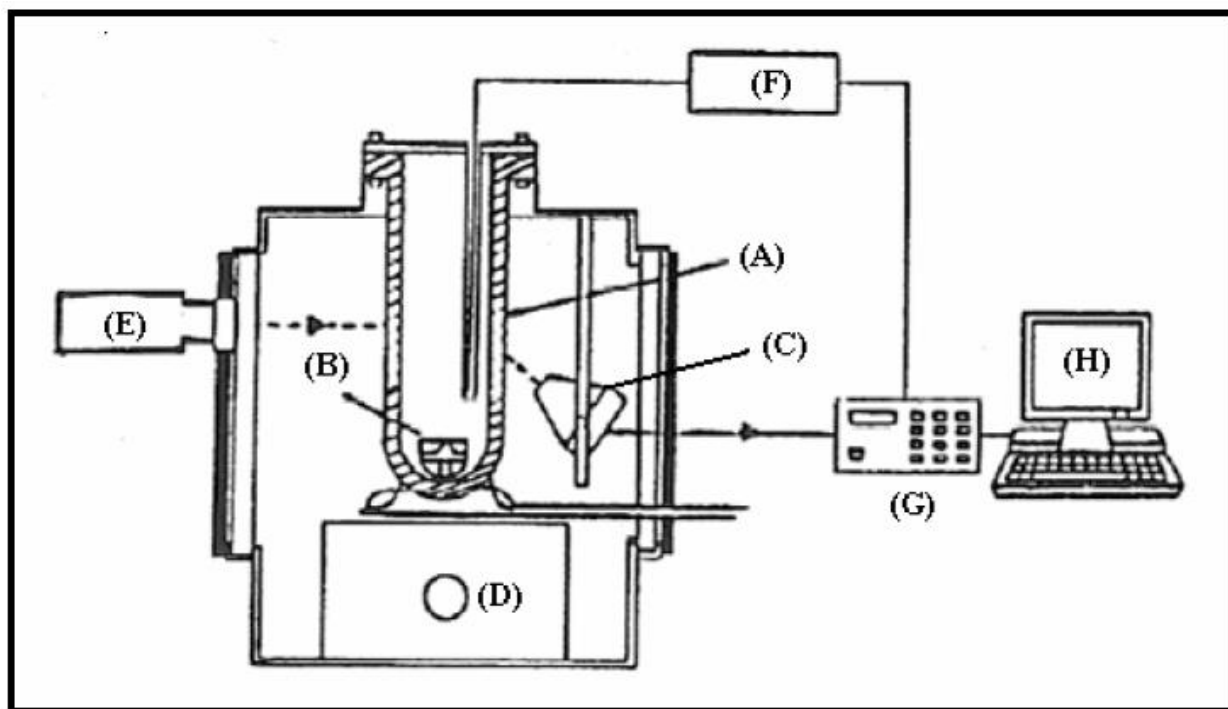


**Figure 2-2: A schematic diagram of the apparatus used for mutual solubility measurements with laser-light scattering (Benjamin et al., 1993).**

A – equilibrium vessel; B – stirrer chip; C – light sensor; D – magnetic stirrer; E – optical system; F – thermometer; G – digital multimeter; H – computer.

#### 2.1.4 Continuous Measurement

The system shown in Figure 2-3 illustrates the method of continuous measurement of Reinhardt and Rydberg (1969). Two liquid phases are mixed in the mixing chamber and separated into two outgoing pure phases in a centrifuge. Chemical reagents were added to the mixing chamber when desired. This technique involves the separation of the phases in a centrifuge, and provision is made for the recirculation of the phases and for the online determination of composition. The type of detector used depends on the system investigated. This technique does have a major drawback in that it requires sophisticated equipment and can be costly.

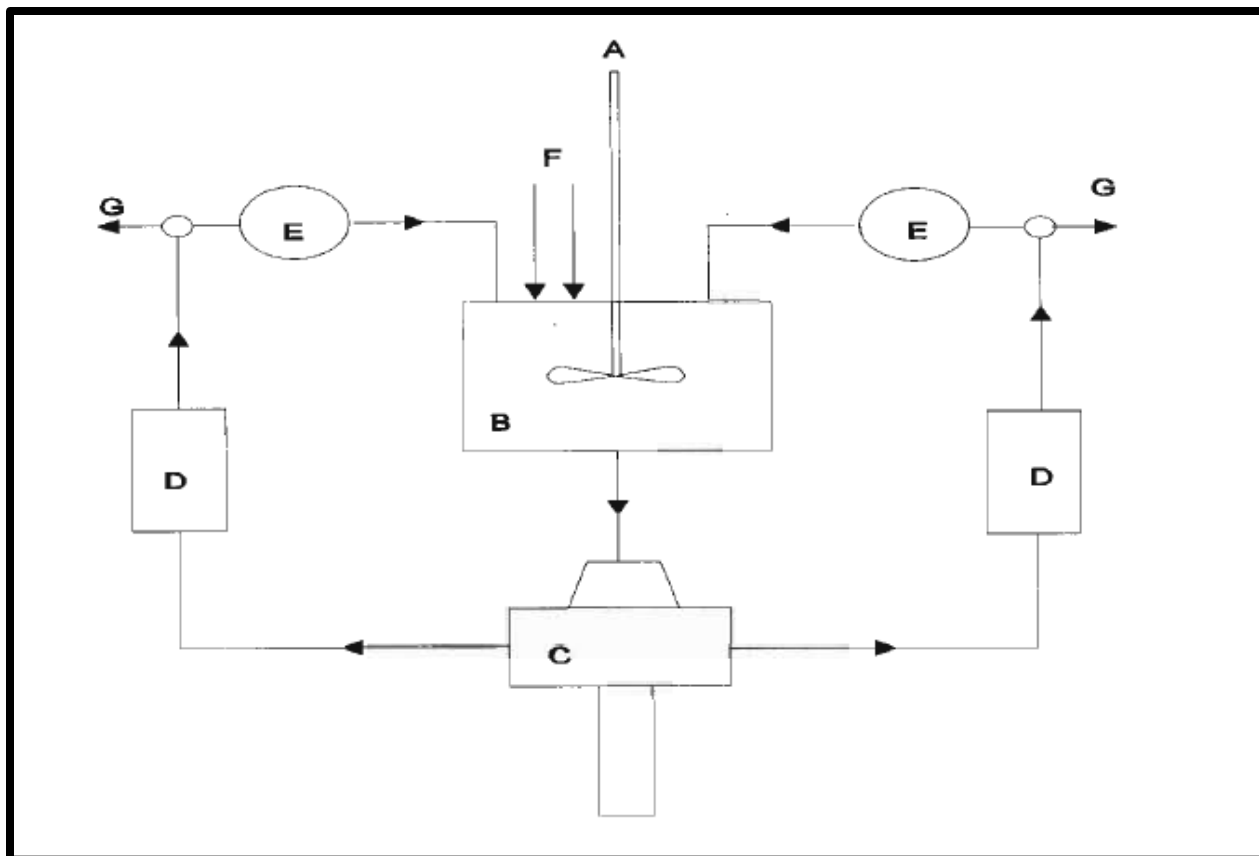


**Figure 2-3: Apparatus for determining continuous liquid-liquid equilibria (Naidoo, 2003).**

**A** – stirrer; **B** – mixing chamber; **C** – centrifuge; **D** – detector; **E** – heat control; **F** – feed; **G** – sampling point.

### 2.1.5 Direct Analytical Method

The direct analytical method is a simple method of measuring LLE. The constituents are charged to an isothermal equilibrium cell and stirred vigorously. The phases are thereafter allowed to separate and reach equilibrium. Good mixing between phases is necessary to achieve complete phase equilibria. Samples are extracted from each phase at equilibrium and analyzed. Figure 2-4 illustrates the direct analytical method.

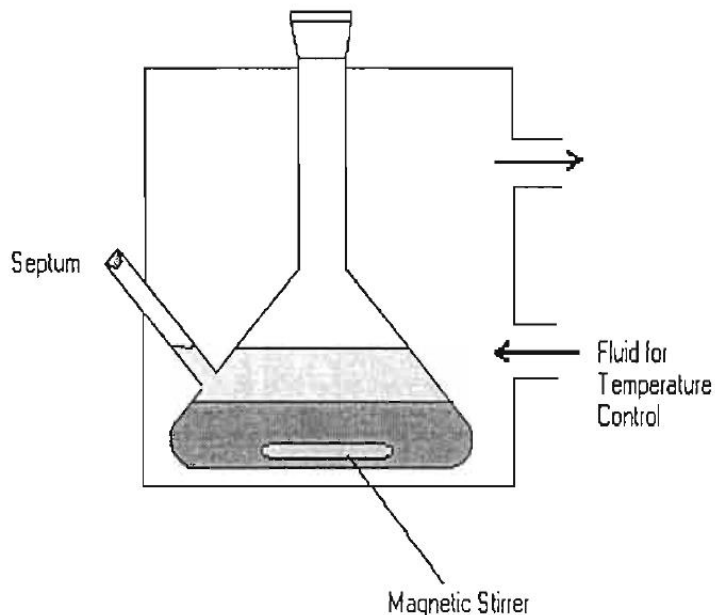


**Figure 2-4: Illustration of the direct analytical method of measuring LLE (Naidoo, 2003).**

Moriyoshi et al (1989) indicated that gas chromatography is a method that is successfully used widely to determine equilibrium compositions. The full composition range can be determined, in addition to the tie-lines, by suitable choice of overall composition. The binodal curve is then generated by taking the locus of the points indicative of the solubility limits. It is also applicable to systems containing more than three components (Novak et al., 1987).

The direct analytical method was used to obtain the LLE data required for this project using a double-walled glass cell, with tie-line compositions determined by gas chromatography. The cell is an adapted apparatus of the original used by Raal and Brouckaert (1992), with modifications undertaken by Ndlovu (2005) and Narasigadu et al. (2014) detailed in Chapter 4.

# 3

## CHAPTER THREE

### THEORETICAL BACKGROUND

The design of separation processes in industry is reliant on experimentally measured thermodynamic data to gain an appreciation for the phase equilibrium behaviour of a chemical system. Separation is usually achieved by contact between phases and the subsequent variation in composition profiles between phases (Prausnitz et al., 1999). Phase contact methodologies such as distillation and extraction are commonly employed and improved efficiency in terms of design and operating costs of these large-scale process systems are motivating factors behind extensive phase equilibrium measurements.

Practically, most processes require separation of one or more chemicals from multicomponent systems. Phase equilibrium information of such systems are difficult to obtain experimentally, however utilizing equilibrium data for binary systems can provide a sufficient indication of equilibrium behaviour of multicomponent systems (Walas, 1985). This includes utilizing binary equilibrium data to generalize phase behaviour in order to enable extrapolation at experimentally difficult conditions.

This chapter summarizes the underlying theoretical principles governing phase equilibrium behaviour beginning with the criterion for phase equilibrium. This is presented in the context of LLE with the introduction of activity coefficients. The Non-Random Two Liquid (NRTL) (Renon and Prausnitz, 1968) and UNIversal QUasi Chemical (UNIQUAC) (Abrams and Prausnitz, 1975) activity coefficient models are discussed due their capability in handling the measured systems

and the commonality of their use in industrial simulations. The Maximum-likelihood algorithm and Deming initialization method (Britt and Luecke, 1973), are reviewed due to its role in conducting the regression. Thereafter, due to the work done in creating a solvent extraction simulation in Aspen Plus, a brief overview of liquid-liquid extraction is presented, including calculation of selectivity and distribution coefficients, representation of liquid-liquid equilibrium (LLE) on an equilateral diagram, different types of LLE systems, and methods of determining the plait point.

### 3.1 Criterion for Phase Equilibrium

The criterion for phase equilibrium was established to be that the chemical potential ( $\mu$ ) of each component in each phase is the same in a system consisting of multiple phases at the same temperature and pressure. A detailed proof can be found in Smith et al. (2001). This is expressed in Equation (3-1) where  $i = 1, 2, 3 \dots N$ :

$$\mu_i^\alpha = \mu_i^\beta = \mu_i^\pi \quad (3-1)$$

The absolute values of chemical potential cannot be determined due to the fact that it is defined in terms of quantities that are not measurable. G. N. Lewis expressed chemical potential as a function of fugacity ( $f_i$ ), which is a quantity with units of pressure (Smith et al, 2001). The criterion for phase equilibrium in terms of fugacity is shown in Equation (3-2):

$$\hat{f}_i^\alpha = \hat{f}_i^\beta = \hat{f}_i^\pi \quad (3-2)$$

where  $i = 1, 2, 3 \dots N$  and  $\hat{f}_i$  is the fugacity in solution of component  $i$ . The above general criterion is applied to a system under LLE with two phases:

$$\hat{f}_i^I = \hat{f}_i^{II} \quad (3-3)$$

The activity coefficient is a factor introduced to account for non-idealities in liquid phases. In terms of fugacities, the activity coefficient for a phase is expressed in Equation (3-4):

$$\gamma_i = \frac{\hat{f}_i}{x_i f_i} \quad (3-4)$$

After expressing the criterion for equilibrium in terms of activity coefficients and cancelling the common pure component fugacity between phases, the criterion is expressed in Equation (3-5):

$$x_i^I \gamma_i^I = x_i^{II} \gamma_i^{II} \quad (3-5)$$

## 3.2 Liquid Phase Activity Coefficient Models

### 3.2.1 The NRTL (Non-Random Two Liquid) Model

The NRTL equation is a local composition model proposed by Renon and Prausnitz (1968) based on an assumption of non-randomness, and is expressed in Equation (3-6):

$$\frac{G^E}{RT} = \sum_{i=1}^n x_i \frac{\sum_{j=1}^n \tau_{ji} G_{ji} x_j}{\sum_{k=1}^n G_{ki} x_k} \quad (3-6)$$

where

$$G_{ij} = \exp(-\alpha_{ij} \tau_{ij}) \quad (3-7)$$

$$\tau_{ij} = \frac{g_{ij} - g_{ji}}{RT} \quad (3-8)$$

The form of the activity coefficient model is as follows:

$$\ln(\gamma_i) = \frac{\sum_{j=1}^n \tau_{ji} G_{ji} x_j}{\sum_{k=1}^n G_{ki} x_k} + \sum_{j=1}^n \frac{\sum_{k=1}^n G_{ij} x_j}{\sum_{k=1}^n G_{kj} x_k} \left( \tau_{ij} - \frac{\sum_{r=1}^n \tau_{rj} G_{rj} x_r}{\sum_{k=1}^n G_{kj} x_k} \right) \quad (3-9)$$

The equations contain the following parameters:  $(g_{ij} - g_{ji})$ ,  $(g_{ji} - g_{ii})$  and  $\alpha_{ij}$ . Parameters  $(g_{ij} - g_{ji})$  and  $(g_{ji} - g_{ii})$  account for the molecular interactions between components  $i$  and  $j$ . The parameter  $\alpha_{ij}$  describes the randomness of the mixture, with complete randomness defined at a value of 0. Renon and Prausnitz (1968) ascertained that  $\alpha_{ij} = \alpha_{ji}$  and recommended the usage of specific values of  $\alpha_{ij}$ . Walas (1985) specifies  $\alpha_{ij}$  to be 0.4 for aqueous organic systems and 0.3 for non-aqueous mixtures. Raal and Muhlbauer (1998) have noted that the most appropriate value of  $\alpha_{ij}$  can be determined by reduction of experimental data.

The NRTL model possesses the capability to describe completely miscible as well as partially miscible systems, and can be utilized in modelling multicomponent systems with only binary parameters (Narasigadu, 2006). Additionally, phase equilibrium behaviour of highly non-ideal

solutions is described well by the NRTL model (Raal et al., 1998). Ko et al. (2002), Zhu et al. (2007) and DongChu et al. (2007) demonstrated the effectiveness of the NRTL model to represent systems containing alkanes, toluene, and NFM.

### 3.2.2 The UNIQUAC (UNIversal QUasi-Chemical) Equation

Abrams and Prausnitz (1975) developed the UNIQUAC model illustrated in Equation (3-10):

$$\frac{G^E}{RT} = \left( \frac{G^E}{RT} \right)_{\text{combinatorial}} + \left( \frac{G^E}{RT} \right)_{\text{residual}} \quad (3-10)$$

The equation is based on the theory of localized composition and two-liquid model, and is divided into two parts. The combinatorial term accounts for differences in molecular structure between components, while the residual term takes into consideration the variation in intermolecular forces between molecules. A modification of the equation was undertaken by Anderson and Prausnitz to improve the model's applicability to mixtures consisting of water and/or lower alcohols. The two parts of the UNIQUAC equation, as stated by Prausnitz et al. (1999), for a multi-component system is given in Equation (3-11):

$$\left( \frac{G^E}{RT} \right)_{\text{combinatorial}} = \sum_{i=1}^n x_i \ln \frac{\Phi_i^*}{x_i} + \frac{z}{2} \sum_{i=1}^n q_i x_i \ln \frac{\theta_i}{\Phi_i^*} \quad (3-11)$$

$$\left( \frac{G^E}{RT} \right)_{\text{residual}} = - \sum_{i=1}^n q_i x_i \ln \left( \sum_{j=1}^n \theta'_j \tau_{ji} \right) \quad (3-12)$$

The co-ordination number ( $z$ ) is usually specified to have a value of 10, whereas the segment fraction ( $\Phi_i^*$ ) and the area fractions ( $\theta, \theta'$ ) are determined from Equations (3-13) to (3-15):

$$\Phi_i^* = \frac{r_i x_i}{\sum_{j=1}^n r_j x_j} \quad (3-13)$$

$$\theta_i = \frac{q_j x_j}{\sum_{j=1}^n q_j x_j} \quad (3-14)$$

$$\theta'_i = \frac{q'_i x_i}{\sum_{j=1}^n q_j x_j} \quad (3-15)$$

The  $r$ ,  $q$ ,  $q'$  parameters relate to the molecular structure, accounting for size of the molecules and external surface area of the molecules respectively. The inclusion of parameter  $q'$  is the modification undertaken by Anderson and Prausnitz (1978) to obtain improved model results for lower alcohols and/or water. For utilization of the original UNIQUAC equation, the condition  $q = q'$  is applied. The parameter  $\tau_{ij}$  is defined in terms of the characteristic energies ( $u_{ij} - u_{jj}$ ), which are adjustable parameters dependent on system components and given as follows:

$$\tau_{ij} = \exp\left(-\left[\frac{u_{ij} - u_{jj}}{RT}\right]\right) \quad (3-16)$$

The activity coefficient is determined for component  $i$  as follows:

$$\ln \gamma_i = \ln \gamma_i^C + \ln \gamma_i^R \quad (3-17)$$

$$\ln \gamma_i^C = \ln \frac{\Phi_i}{x_i} + \frac{z}{2} q_i \ln \frac{\theta_i}{\Phi_i} + l_i - \frac{\Phi_i}{x_i} \sum_{j=1}^n x_j l_j \quad (3-18)$$

$$\ln \gamma_i^R = -q'_i \ln \left( \sum_{j=1}^n \theta'_j \tau_{ji} \right) + q'_i - q'_i \sum_{j=1}^n \frac{\theta'_j \tau_{ij}}{\sum_{k=1}^n \theta'_k \tau_{kj}} \quad (3-20)$$

where

$$l_i = \frac{z}{2} (r_i - q_i) - (r_i - 1) \quad (3-21)$$

The UNIQUAC model can be effectively utilized to describe systems of non-electrolyte mixtures containing polar or non-polar components. The need for structural parameters and the algebraic complexity of the model itself are disadvantageous in the practical application of the equation. However, usage of advanced computing programs and software such as Aspen Plus (as used in

this work) counteract this shortcoming. Like the NRTL model, the UNIQUAC equation is applicable to multi-component mixtures in terms of binary parameters only, and displays possibly superior representation of mixtures of different varying molecular sizes (Walas, 1985). DongChu et al. (2007) and Cincotti et al. (1999) demonstrated the effectiveness of the UNIQUAC model to represent systems containing alkanes, toluene, and NFM.

### 3.3 Regression Algorithms

The binary interaction parameters for the NRTL and UNIQUAC models were regressed with Aspen Plus V8.4. The regression was implemented with the use of the Britt-Luecke algorithm (Britt and Luecke, 1973), with the binary interaction parameters being calculated by minimization of deviations between experimental data and model calculated values. This process determines the mole fractions of individual components for an initialized set of parameters using the Deming initialization method (Britt and Luecke, 1973), and thereafter a new set of parameters is determined iteratively until evaluation of the objective function is smaller than a prescribed tolerance. The maximum likelihood objective function (Q) was used as follows:

$$Q = \sum_{n=1}^{NDG} w_n \sum_{i=1}^{NP} \left[ \left( \frac{T_{e,j} - T_{m,i}}{\sigma_{T,i}} \right)^2 + \left( \frac{P_{e,j} - P_{m,i}}{\sigma_{P,i}} \right)^2 + \sum_{j=1}^{NC-1} \left( \frac{x_{e,i,j} - x_{m,i,j}}{\sigma_{x,i,j}} \right)^2 + \sum_{j=1}^{NC-1} \left( \frac{y_{e,i,j} - y_{m,i,j}}{\sigma_{y,i,j}} \right)^2 \right] \quad (3-22)$$

where:

- Q = The objective function to be minimized by data regression
- NDG = The number of data groups in the regression case
- $w_n$  = The weight of data group n
- NP = The number of points in data group n
- NC = The number of components present in the data group
- T, P, x, y = Temperature, pressure, liquid and vapor mole fractions
- e = Estimated data
- m = Measured data
- i = Data for data point  $i$
- j = Fraction data for component  $j$
- s = Standard deviation of the indicated data. If  $s=0$ , the point is not included in the objective function, and the estimated value is set equal to the measured value

The temperature and pressure are excluded from the objective function due to temperature and pressure being constant with no vapour phases, thus reducing the objective function to be in terms of liquid composition only.

To obtain an indication of the accuracy of the activity coefficient models described earlier, the root mean square deviation (*rmsd*) was calculated as follows:

$$rmsd = \sqrt{\frac{\sum_a \sum_b \sum_c \{x_{abc}(exp) - x_{abc}(calc)\}^2}{6k}} \tag{3-23}$$

Where *x* refers to the liquid phase mole fraction, and *k* the number of experimental points, with subscripts *a*, *b*, and *c* representing the component, phase, and tie-lines correspondingly. Figure 3-1 is a flow chart illustrating the process followed in performing the regression.

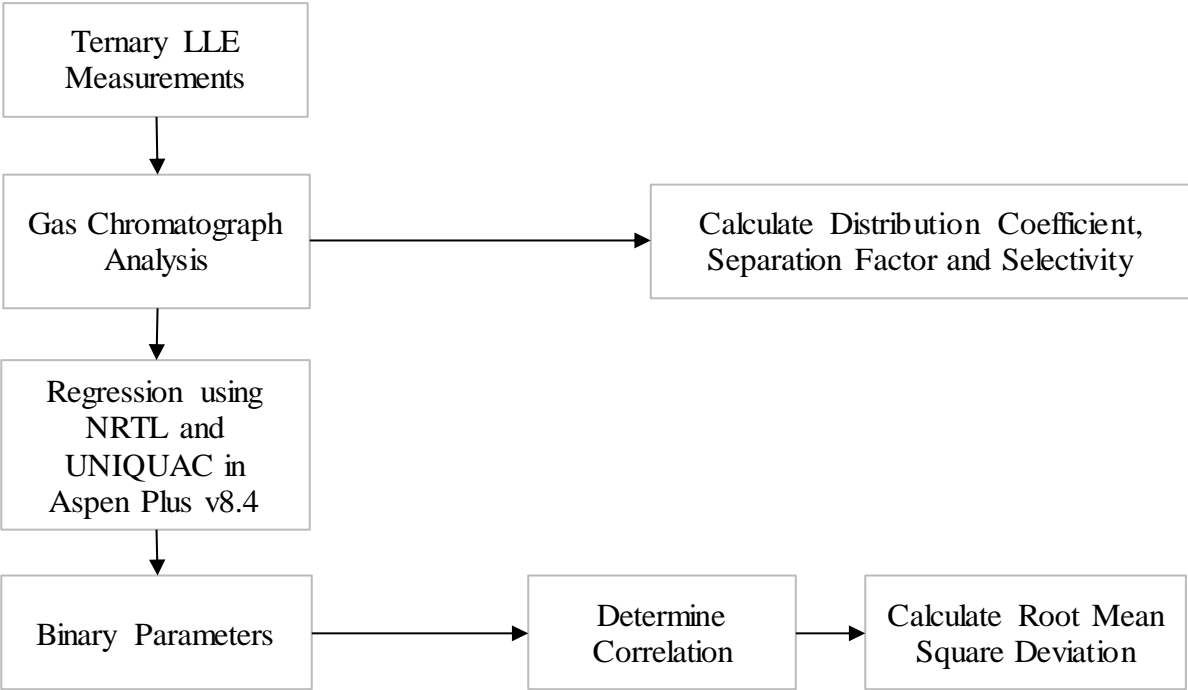


**Figure 3-1: Flow chart illustrating the process followed in regression of predicted binary interaction parameters.**

### 3.4 Liquid – Liquid Extraction

Liquid – liquid extraction involves addition of a solvent to a liquid mixture to enable a distribution of components between two immiscible liquid phases. The feed to the extraction process is the liquid mixture comprising the components to be separated. For a ternary system, the feed consists of a solute and a carrier liquid. During phase contact, mass transfer between the solute and solvent occurs. Products from the extraction process are the raffinate, which is the residual feed containing primarily the feed carrier fraction, and the extract containing the solvent and the solute (DeLancey, 2013). Figure 3-2 illustrates the basic elements of this process. The extract is the required stream if the desired product is the solute, whereas the raffinate is the preferred stream if the solute is a contaminant needing removal.

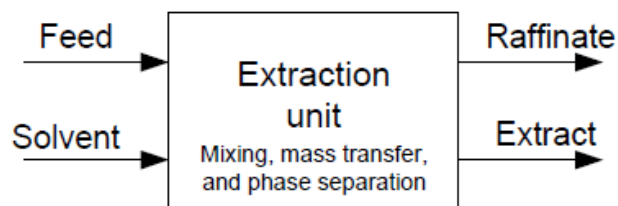


**Figure 3-2: Illustration of the various elements in a liquid – liquid extraction system.**

Solvent selection is a significant design consideration in terms of process efficiency. Relative selectivity ( $\beta$ ) is a parameter used to gauge the effectiveness of a solvent, as shown in Equation (3-24).

$$\beta = \frac{(x_2)^{\text{II}} / (x_2)^{\text{I}}}{(x_1)^{\text{II}} / (x_1)^{\text{I}}} \quad (3-24)$$

The distribution coefficient ( $K$ ) and separation factor ( $S$ ) are measures of solvent capability, and is indicated in Equations (3-25) and (3-26):

$$K = \frac{x_2^{\text{II}}}{x_2^{\text{I}}} \quad (3-25)$$

$$S = \frac{[(x_2)/(x_1 + x_2)]^{\text{II}}}{[(x_2)/(x_1 + x_2)]^{\text{I}}} \quad (3-26)$$



Type 1: formation of one pair of partially miscible liquids

Type 2: formation of two pairs of partially miscible liquids

Type 3: formation of three pairs of partially miscible liquids

### 3.4.1 Type 1: Formation of One Pair of Partially Miscible Liquids

This system is illustrated by the isotherm in Figure 3-4:

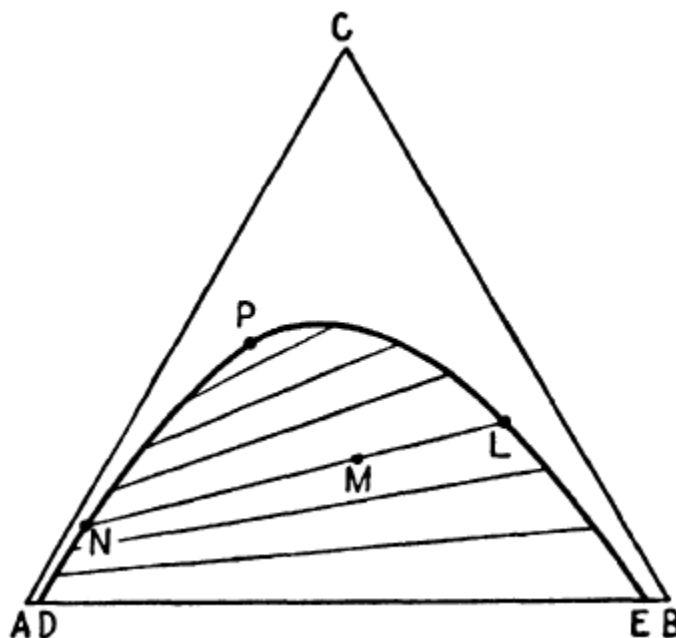
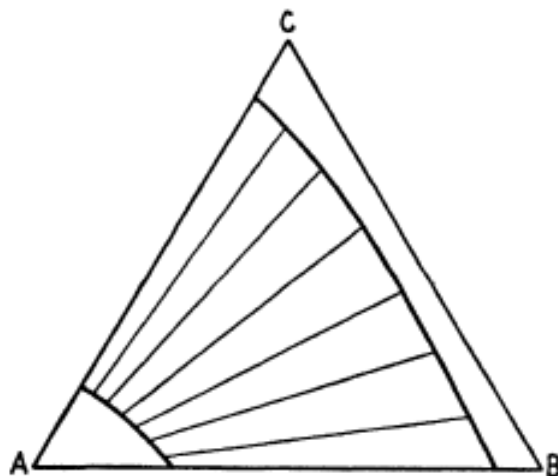


Figure 3-4: Type 1 ternary system in equilibrium (Treybal, 1963).

In this system, binary mixtures of component pairs A-C and B-C are miscible in all proportions at constant temperature. A and B are partially miscible and points D and E are binary compositions of the saturated mixture. The curve DNPLE is called the binodal curve and indicates the boundary compositions of saturated solutions. All points within the curve form two insoluble liquid phases, while all points outside the curve form a single homogenous liquid phase. A mixture with compositions indicated by point M will split to form two immiscible liquid layers with compositions indicated by points L and N respectively. Point M thus lies on the straight line LN, referred to as a tie line. Point P refers to the plait point, a juncture at which the two regions of the binodal curve merge. The tie lines decrease in length with increasing concentrations of component

C towards the plait point. At the plait point, two liquids of identical composition and density are formed. An example of such a system is benzene + water + ethanol (Treybal, 1963).

### 3.4.2 Type 2: Formation of Two Pairs of Partially Miscible Liquids



**Figure 3-5: Type 2 ternary system in equilibrium (Treybal, 1963).**

Type 2 systems are illustrated in Figure 3-5. Two pairs of binary components A-C and A-B are partially immiscible while C and B form a homogenous liquid in any proportion. The region of points lying within the band across the triangle represent liquids that form two immiscible liquid phases with compositions indicated by the edges of the tie lines. This type of ternary system has no plait point. An example of such a system is n-aniline + n-heptane + methylcyclohexane (Treybal, 1963).

### 3.4.3 Type 3: Formation of Three Pairs of Partially Miscible Liquids

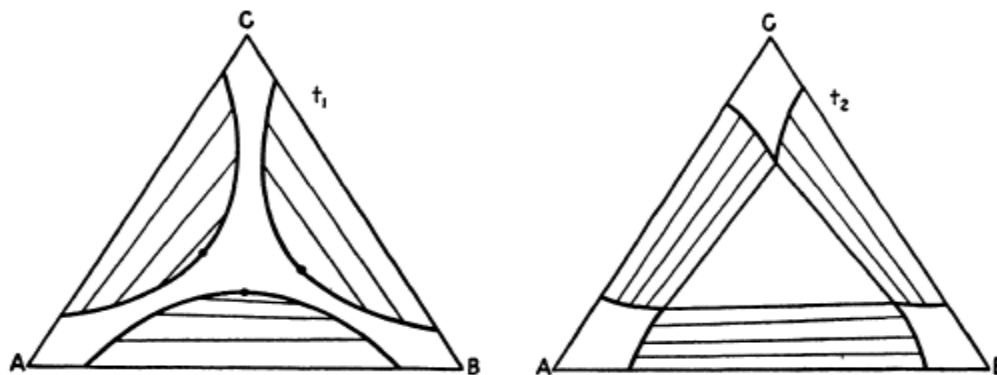


**Figure 3-6: Type 3 ternary system in equilibrium (Treybal, 1963).**



Using tie line DE, lines EF and DG are constructed parallel to AC and CB respectively. The construction lines intersect at point H. This process is implemented for all experimentally determined tie lines, until the curve JHP results. The meeting of this curve with the binodal curve is the plait point. This method is excellent for determining the plait point when several tie lines are known, but cannot be extrapolated over large distances due to the curvature of the correlation curve (Treybal, 1963). It often requires extension of the plot far below the triangular diagram. Sherwood (1937) proposed a modification (illustrated in Figure 3-8) of the method to address this difficulty.

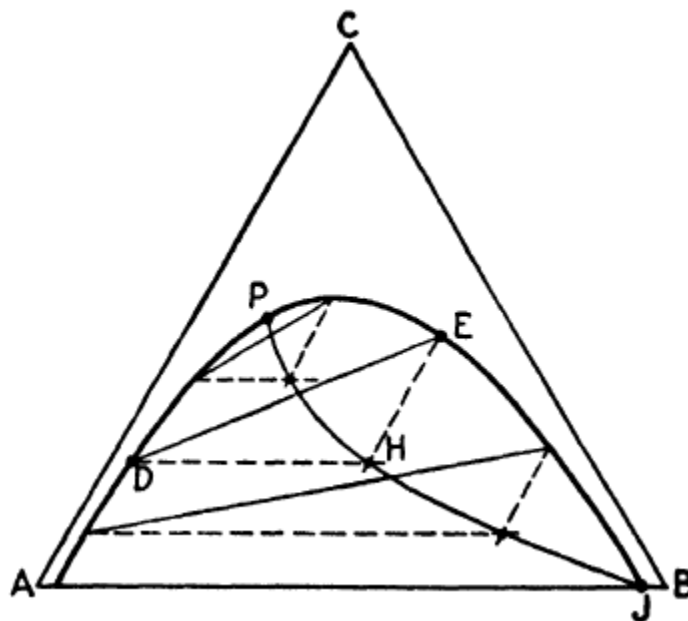


**Figure 3-8: Alternative method of determining the plait point (Treybal, 1963).**

The construction lines are developed parallel to AB rather than AC, such that the correlation curve lies within the triangle. A disadvantage of this method is the greater curvature of the curve, decreasing the accuracy with which the plait point can be determined when tie lines close to the plait point are not available.

# 4

## CHAPTER FOUR

### EQUIPMENT DESCRIPTION

#### 4.1 The Liquid-Liquid Equilibrium Apparatus

The LLE cell used to obtain measurements for the systems under consideration is a derivative of the cell used by Raal and Brouckaert (1992), resulting from several modifications. The cell of Raal and Brouckaert (1992) utilized a glass cell with fluid recirculation to maintain a fixed temperature, fitted on top of a Teflon header with o-rings as shown in Figure 4-1. A stainless steel tube (thin walled) housed the temperature probe. The mechanical stirrer was driven by a DC power supply and temperature was controlled by circulating water heated in a water bath. A disadvantage was that the sample syringe had to be injected through the top phase to sample the bottom phase thereby disturbing the liquid interface.

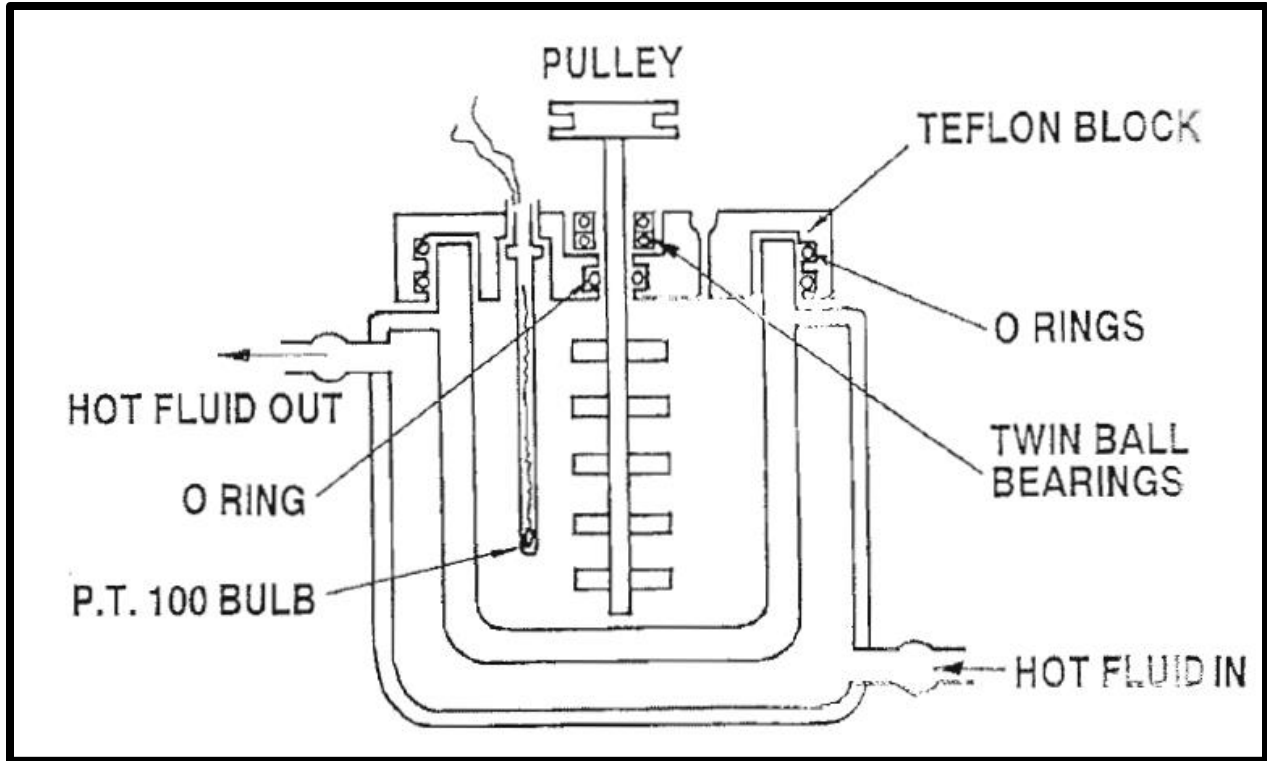


**Figure 4-1: LLE still used by Raal and Brouckaert (1992).**

The cell of Ndlovu (2005) as illustrated in Figure 4-2, is a modification of the above described cell. It utilized an additional sampling port for the denser phase so as to avoid unsettling the liquid interface between the two phases and disturbing the equilibrium. Ndlovu (2005) demonstrated that the modifications improved the accuracy of the equilibrium measurements.

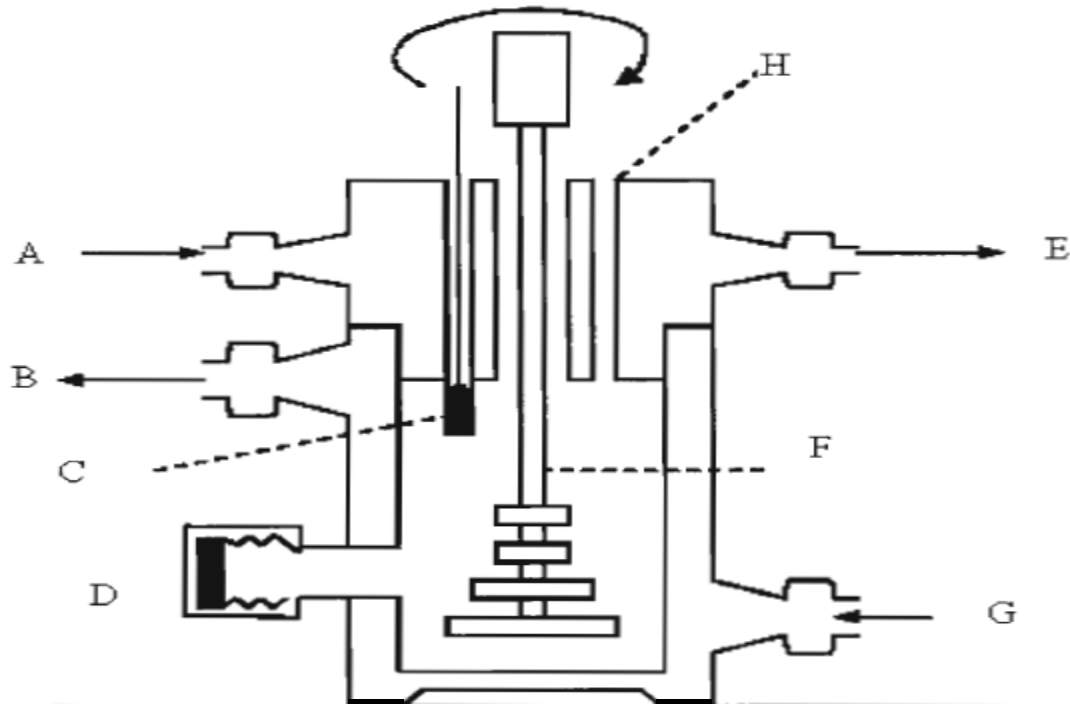


**Figure 4-2: LLE cell of Ndlovu (2005).**

A – hot fluid in; B – hot fluid out; C – Pt -1 00 thermo-well; D and H – sample points; E – hot liquid out; F – stirrer; G-hot liquid in

The subsequent modifications to the LLE cell included an adjustable thermo-well for improved temperature measurements and the use of a magnetic stirrer (Narasigadu et al., 2014). The apparatus used in Figure 4-3 was duplicated for each ternary system measured. It was successfully used in the studies of Narasigadu et al. (2009), Lasich et al. (2011), and Narasigadu et al. (2014).

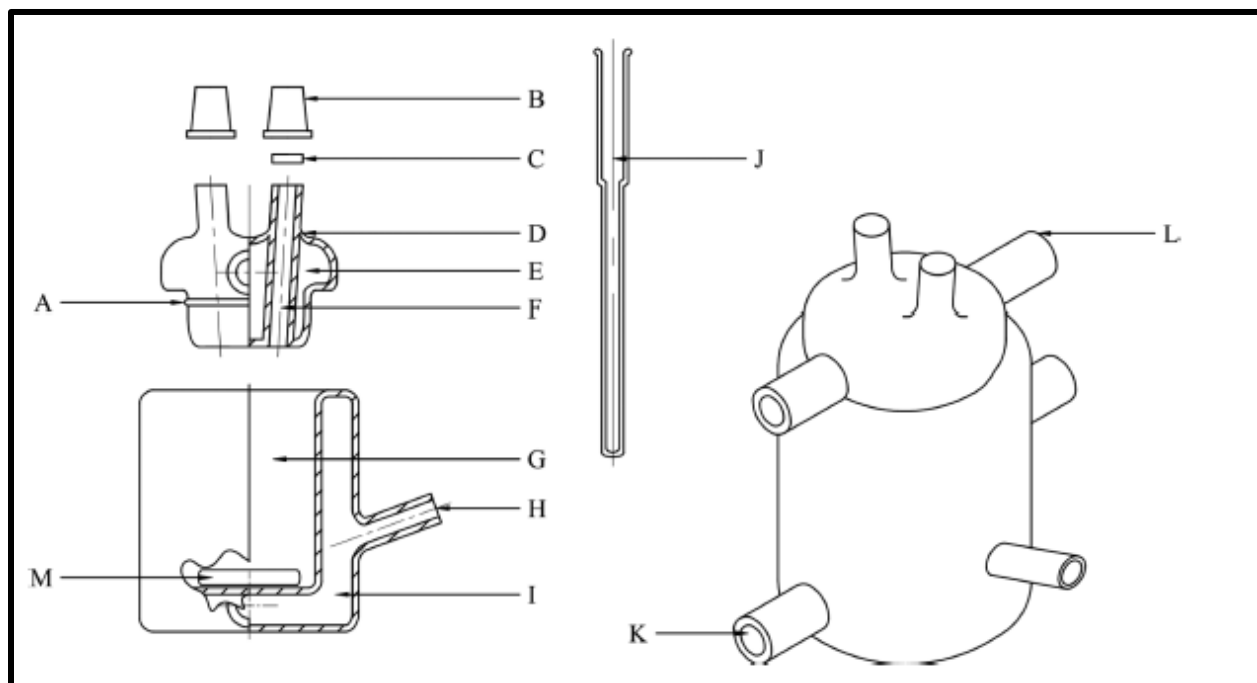


**Figure 4-3: Schematic of the double-walled glass cell (Narasigadu et al., 2014).**

A – O-ring; B – upper sampling port cap; C – septum; D – outer wall of cell cap; E – cell cap; F – upper sampling port; G – inner cell cavity; H – bottom sampling port; I – cell wall cavity for heating fluid; J – adjustable thermo-well for temperature probe; K – cell heating fluid inlet; L – cell cap heating fluid inlet; M – magnetic stirrer.

## 4.2 Temperature Measurement and Control

Two Pt-100 temperature sensors were used for temperature measurements for the equilibrium temperature of the two LLE cells. These were calibrated using the internal standard method with a pre-calibrated standard temperature probe CTB - 9100 from WIKA. The sensors were placed in the thermo-well of the cell, where a drop of silicone oil was immersed in the thermo-well to increase the contact area between the sensor and the glass wall. The temperature of the bath was determined by calibration of the temperature controller setpoint temperature against the readings of the Pt-100 sensors. The uncertainties in temperature readings of each cell were 0.02 K and 0.01 K respectively.

### **4.3 Sampling and Composition Analysis**

Once equilibrium was achieved, an air-tight syringe was used to draw liquid samples from each phase. The LLE data was analysed by gas chromatography with a Shimadzu 2014 GC that utilized helium as the carrier gas and a thermal conductivity detector. A 4 m × 1/8 inch Poropak Q packed column was used for component separation in the GC, and GC Solutions was the software program utilized. The sampling procedures, calibration, and operation are detailed further in Chapter 5. Composition uncertainty was minimized by ensuring that phase composition samples were within 1% of the repeatability error. At least three samples were taken, and at most five samples were required.

### **4.4 Auxiliary Equipment**

The isothermal environment in the LLE cell was maintained with the use of a Julabo VC circulating water bath, which heated and circulated the fluid through the cell wall cavity. Agitation of the mixture in the inner cavity cell was done using a magnetic stirrer, which was placed inside the cell at the bottom.

# 5

## CHAPTER FIVE

### EXPERIMENTAL PROCEDURE

Accurate measurement of LLE data is contingent on the correct calibration and operation of the equipment used to measure parameters such as temperature and composition. Sample preparation and analysis plays a critical role in accurately determining equilibrium compositions. This chapter focuses on the preparation, calibration and the operation of the LLE apparatus and other equipment integral to this investigation.

#### 5.1 Gas Chromatograph Calibration

The compositions of each phase was determined with the use of a Shimadzu 2014 GC that utilized helium as the carrier gas and a thermal conductivity detector. The 4 m × 1/8 inch Poropak Q packed column was used for component separation in the GC. The peak area signal was obtained by integration using the GC Solutions software package as the interface receiving the GC output signal. The integration is a built-in feature of the software package and was retrieved from the program after each run. Sample compositions were determined using the GC detector calibration.

The GC calibration required a suitable solvent to ensure that all the heterogeneous mixtures were miscible to obtain a homogenous sample composition for each calibration point. To this end, 1-propanol was used for the binary test system of methanol + heptane, while toluene was used for the calibration of the immiscible pair of NFM + alkane. The other pairs of toluene + NFM and

toluene + alkane were observed to be miscible. Molecular sieves of 10 Å were utilized to remove trace quantities of moisture in methanol and propanol.

The area ratio method was used to calibrate the GC detector, as detailed by Raal and Mühlbauer (1998). This method makes use of analyzing liquid samples that were prepared gravimetrically. Samples with mole fraction ratios evenly across the entire composition range were used. The basis of this method is the fact the number of moles passing the detector is proportional to the peak area:

$$n_i = A_i F_i \quad (5-1)$$

$n_i$  denotes the number of moles of component  $i$ ,  $A_i$  is the peak area, and  $F_i$  is a proportionality constant referred to as the response factor. The number of moles depends on the injected volume, which is difficult to duplicate for each sample injection. Thus, Raal and Mühlbauer (1998) recommend applying the above equation in terms of area and composition ratios (binary system):

$$\frac{n_1}{n_2} = \frac{F_1}{F_2} \frac{A_1}{A_2} = \frac{x_1}{x_2} \quad (5-2)$$

Where  $x$  signifies the mole fraction and subscripts 1 and 2 refer to specific components. Equation 5-2 is represented in the form of a calibration curve with the mole fraction ratio as a function of the area ratio, with the response factor ratio determined via regression. The area ratios were plotted against the mole fraction for a composition range of 0 to 1. Calibrations for the ternary systems were conducted using binary pairs as detailed by Raal and Mühlbauer (1998).

The required mass of each component in a calibration pair sample was determined theoretically to obtain the mole fraction ratios as follows:

1. Initialized masses used to determine number of moles by using the following equation:

$$n(\text{moles}) = \frac{m(\text{mass})}{MM(\text{MolarMass})} \quad (5-3)$$

2. Mole fractions for the two components were determined using the above calculated moles
3. Using the measured density, the volumes of each component were determined
4. The theoretical mole fraction ratios of components were then determined
5. The initialized masses were then varied iteratively with the use of the Microsoft Excel Solver functionality with constraints being the desired mole fraction ratios

The above algorithm allowed for the calculation of the required masses of the components to achieve the desired mole fraction ratios across the calibration range. An additional constraint was that the volumetric sum of the components be less than 8 ml to allow for the addition of the third component to create a miscible mixture. The samples were prepared in 20 ml vials with the solution filling the vial to capacity to minimize the vapour space. This was to ensure that the mixture in the sample vial did not evaporate and thus lead to an incorrect composition. Sample injections into the GC were done using a 10  $\mu$ l SGE liquid syringe. Care was taken to check for blockages, tightness of the piston plunger and needle seal of the liquid syringe. The syringe was rinsed 5 times with acetone as a cleaning agent before a sample was drawn, and additionally rinsed 3 times with the sample itself. The acetone and sample vials were air dried in a fume-hood. This was to ensure that any entrained impurities in the needle were removed. The syringe was flushed 4 times with sample to remove the entrainment of air bubbles in the syringe. After the sample was injected into the GC, the syringe was rinsed a further 5 times with acetone. The septum for the GC injector was replaced after every 100 injections to avoid errors that would result from leaks. Two pairs of components in each system were needed to determine all the component compositions. This was achieved by a simple and direct relation of the response factor ratios as outlined by Raal and Mühlbauer (1998). The accuracy of the GC analysis for the mole fraction composition was within  $1 \times 10^{-4}$ . The operating conditions for the GC as well as the GC detector calibration curves are presented in Appendix C.

## 5.2 Calibration of Temperature Sensors

The two Pt-100 temperature sensors used with the apparatus were calibrated using the internal standard method with a pre-calibrated standard temperature probe CTB - 9100 from WIKA. The Pt-100 and standard probe were immersed in a heat regulated silicon oil liquid bath. The

temperature of the bath was first varied from 293.25 K to 373.25 K, and thereafter from 373.25 K to 293.25 K, in increments of 5 K. This process is to allow for the detection of hysteresis. The temperature readings were then recorded for the three probes at each setpoint temperature, following the stabilization of the bath temperature at thermal equilibrium. The calibration curves as well as uncertainty plots are illustrated in Appendix B, Figures B-1 to B-4.

## 5.3 The Liquid-Liquid Equilibrium Apparatus

### 5.3.1 Cleaning the LLE Cell

The fluid recirculation piping was disconnected from the cell, after which the cell and all its components were rinsed thoroughly with acetone to remove traces of impurities. The disassembled components of the cell were then left in the fume-hood for a duration of thirty to forty-five minutes to allow for the evaporation of any remaining acetone. The apparatus was then reassembled.

### 5.3.2 Operating Procedure

All measurements were performed at atmospheric pressure.

#### 5.3.2.1 Binary LLE Measurements

The apparatus was cleaned as described in the previous section and the following procedure was applied:

1. The still was charged with the chemicals in suitable quantities such that the interface between the two phases was above the sampling point of the denser phase, to avoid the needle disturbing the equilibrium
2. The desired temperature setpoint was inputted to the temperature controller
3. The magnetic stirrer was activated and the solution was stirred for approximately an hour
4. The stirrer was switched off and the system was allowed to reach thermodynamic equilibrium for at least two hours, depending on the system investigated. Equilibrium was deemed established when there was no observation of emulsions, the temperature was constant within

experimental uncertainty, and the phase compositions analysed were within experimental uncertainty

5. Samples for each phase were drawn and injected into the GC for composition analysis until the peak area ratios were within a tolerance of 1% of the standard error
6. The temperature was increased incrementally and steps 2 to 5 repeated at each temperature along the interval
7. Upon completion of the measurements, the temperature controller and magnetic stirrer were switched off and the still was allowed to cool before being cleaned

### ***5.3.2.2 Ternary LLE Measurements***

The experimental procedure utilized is outlined by Alders (1959), and was applied as follows:

1. The cell was cleaned and charged with two components as was the case with the binary LLE measurements
2. After equilibrium was established with the binary mixture, a volume of the third component was added to system and distributed between the phases. This volume was approximately between 2 ml and 4 ml at each stage, depending on the spacing between tie lines in the phase envelope
3. The new mixture at each stage was stirred for an hour at a sufficiently low speed to avoid emulsification and subsequently reduce the settling time required to reach thermodynamic equilibrium
4. The mixture was allowed a minimum time of two hours to equilibrate
5. Phase compositions were analyzed following the same procedure as for the binary measurements. This procedure was repeated until sufficient tie lines were obtained between the binary pair mutual solubility and the plait point
6. Composition uncertainty was minimized by ensuring that phase composition samples were within 1% of the repeatability error. At least 3 three samples were taken, and at most five samples were required. The uncertainty calculations as well as composition deviations are detailed in Appendix B.

# 6

## CHAPTER SIX

### EXPERIMENTAL RESULTS

This chapter serves to summarize and present the primary results obtained from this investigation. This includes primarily the ternary liquid-liquid equilibrium (LLE) experimental measurements undertaken. LLE measurements were undertaken for a test system to establish that the equipment utilized provided reliable and accurate results. New experimental measurements were generated for the following systems:

- *n*-Nonane + toluene + NFM at 1 atm and 303.15 K.
- *n*-Nonane + toluene + NFM at 1 atm and 323.15 K.
- *n*-Nonane + toluene + NFM at 1 atm and 343.15 K.
- *n*-Decane + toluene + NFM at 1 atm and 303.15 K.
- *n*-Decane + toluene + NFM at 1 atm and 323.15 K.
- *n*-Decane + toluene + NFM at 1 atm and 343.15 K.

## 6.1 Chemical Purity

**Table 6-1: Chemical purities and refractive indices for all reagents used in this study.**

Reagent	Refractive Index		GC Analysis (Peak Area %)	Min. Purity (mass %) <sup>d</sup>
	Experimental	Literature <sup>a</sup>		
<i>n</i> -Decane	1.4095	1.4102 <sup>b</sup>	99.7	> 99
<i>n</i> -Heptane	1.3867	1.3878 <sup>b</sup>	99.7	> 99
Methanol	1.3196	1.3288 <sup>b</sup>	99.9	> 99
N-Formylmorpholine (NFM)	1.4842	1.4848 <sup>c</sup>	99.8	99
<i>n</i> -Nonane	1.4044	1.4050 <sup>b</sup>	99.7	> 99
Propanol	1.3832	1.3840 <sup>b</sup>	99.8	> 99
Toluene	1.4882	1.4961 <sup>b</sup>	99.8	99.9

<sup>a</sup> at 293.15 K, <sup>b</sup> Weast *et al.* (1984), <sup>c</sup> Lange (1999), <sup>d</sup> Stated by supplier

The purity of the chemicals used in this investigation were confirmed using gas chromatography. This analysis necessitated use of a thermal conductivity detector due to its capability in detecting non-hydrocarbon impurities. No significant impurities were detected for the reagents used, therefore no further purification of the chemicals was required. Additionally, the purities were confirmed by comparison of experimental refractive index measurements with values from the literature. These measurements together with the gas chromatography analysis is reported in Table 6-1.

## 6.2 Phase Equilibrium of Test Systems

The Shimadzu 2014 gas chromatograph (GC) was used for the composition analysis of the test system measurements undertaken in this study. The GC detector calibration results and optimized parameters for the GC operation are presented in Appendix B.

## 6.2.2 Liquid-Liquid Equilibrium Result

### 6.2.2.1 Methanol (1) + *n*-Heptane (2)

The liquid-liquid equilibrium (LLE) system of methanol (1) + *n*-heptane (2) was measured and compared to literature to ascertain the capability of the apparatus to measure LLE data. The experimental data measured at 101.3 kPa in this study are reported in Table 6-2 and graphically presented as a  $T$ - $x^I$ - $x^{II}$  plot in Figure 6-1. The experimental data of the test systems demonstrated that the apparatus can produce reliable LLE measurements. Uncertainties are reported in Appendix B, Table B-3.

**Table 6-2: Experimental LLE data for the methanol (1) + *n*-heptane (2) system at 101.3 kPa.**

T / K	Phase I		Phase II	
	x1	x2	x1	x2
298.15	0.911	0.089	0.190	0.810
303.15	0.904	0.096	0.196	0.804
308.15	0.900	0.100	0.230	0.770
313.15	0.890	0.110	0.249	0.751
318.15	0.847	0.152	0.342	0.658
323.15	0.766	0.234	0.491	0.509

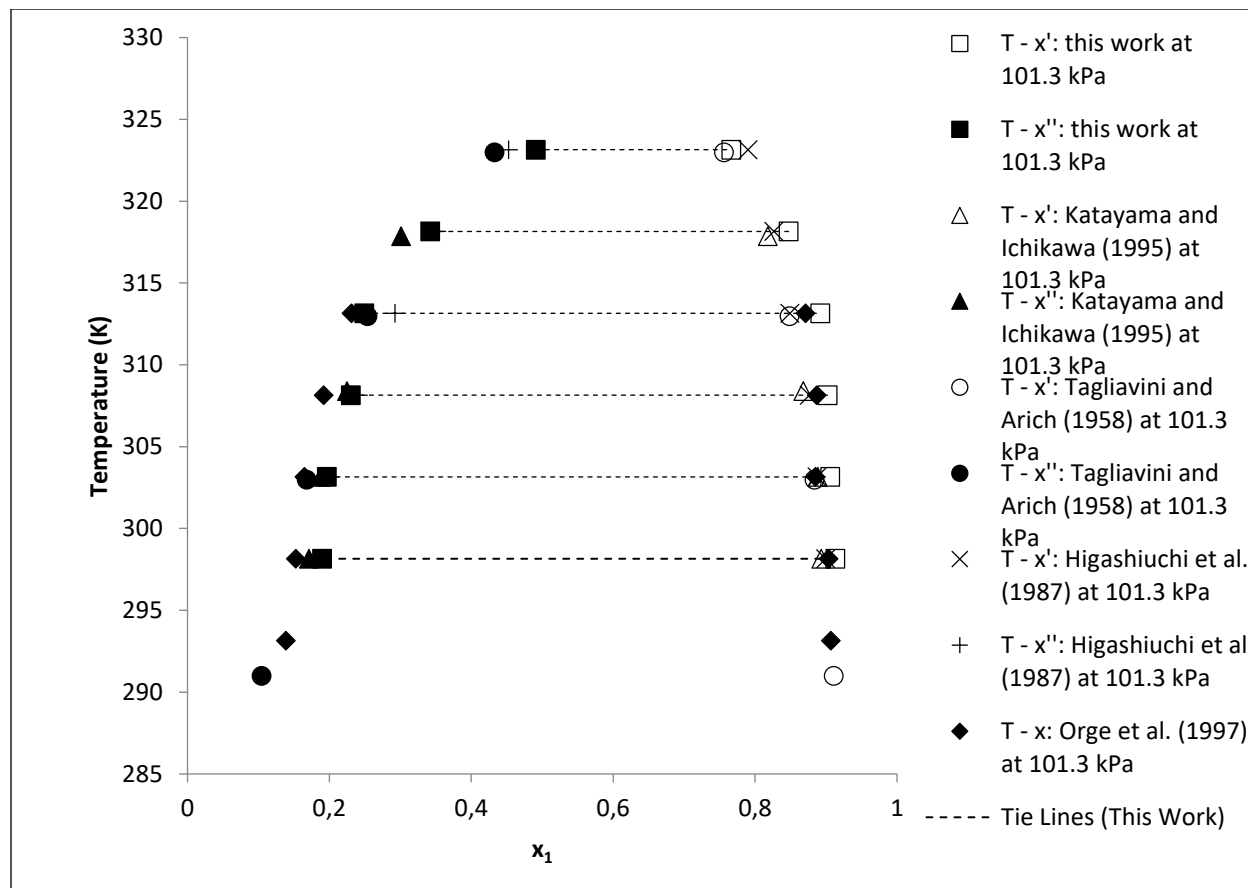


Figure 6-1: The T-x<sup>I</sup>-x<sup>II</sup> plot for the methanol (1) + n-heptane (2) system at 101.3 kPa.

## 6.4 Phase Equilibrium of New Systems

For all the systems, the GC detector calibration results and optimized parameters for the GC operation are presented in Appendix B. The mole fraction values for each phase sampled were within 1 % repeatability error (Appendix B, Equation B-1) for at least 3 samples taken and at most 5 samples. All the new systems experimentally measured in this work have not been previously reported in the open literature.

### 6.4.1 Ternary Liquid-Liquid Equilibrium (LLE)

#### 6.4.1.1 *n*-Nonane (1) + Toluene (2) + NFM (3)

This system has not been previously measured at 303.15 K, 323.15 K, 343 K, and 1 atm and is thus presented as new LLE data. The experimental data and the triangle diagram are presented below, and the gas chromatography detector calibration graphs as well as uncertainties in Appendix B.

**Table 6-3: Liquid-liquid equilibrium data for the *n*-nonane (1) + toluene (2) + NFM (3) system at 303.15 K and 101.3 kPa.**

Phase I			Phase II		
X1	X2	X3	X1	X2	X3
0.0105	0.0000	0.9895	0.9071	0.0000	0.0929
0.0110	0.0579	0.9311	0.7711	0.1155	0.1134
0.0137	0.1331	0.8532	0.6688	0.2327	0.0984
0.0163	0.1909	0.7928	0.5753	0.3115	0.1132
0.0182	0.2248	0.7571	0.5298	0.3511	0.1192
0.0205	0.3169	0.6626	0.4164	0.4854	0.0982
0.0269	0.3545	0.6185	0.3748	0.5211	0.1041

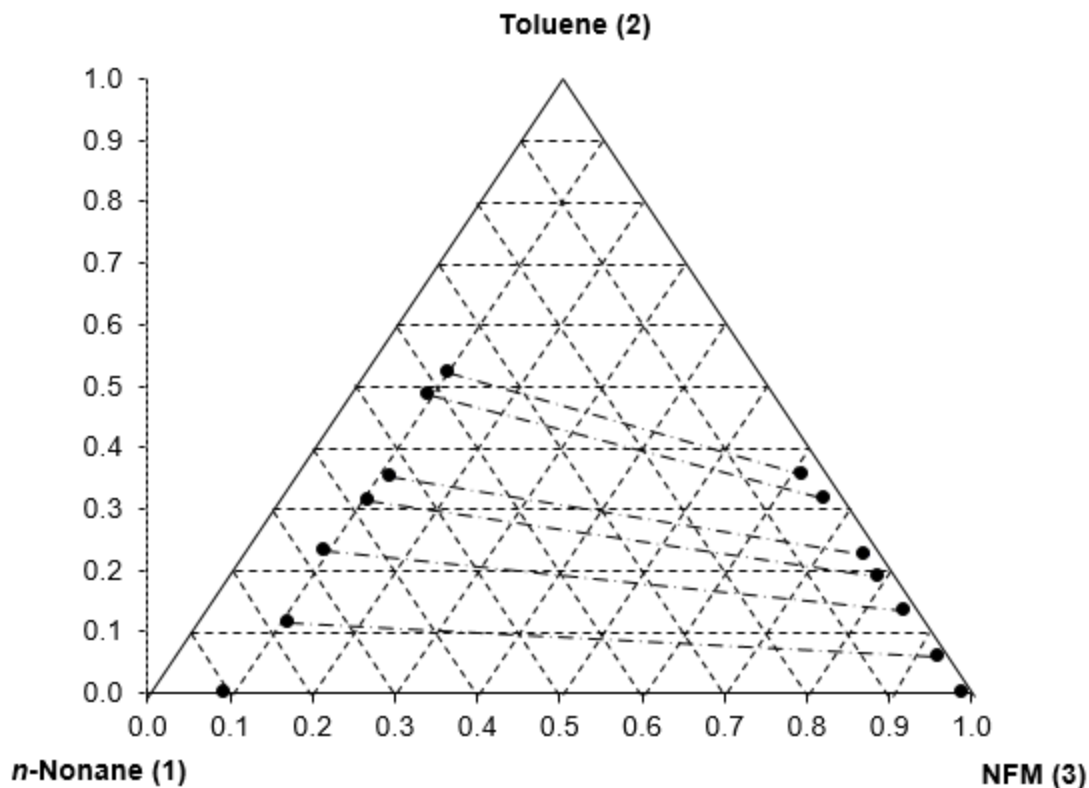


**Figure 6-2: Ternary diagram for the *n*-nonane (1) + toluene (2) + NFM (3) system at 303.15 K and 1 atm.**

**Table 6-4: Liquid-liquid equilibrium data for the *n*-nonane (1) + toluene (2) + NFM (3) system at 323.15 K and 101.3kPa.**

Phase I			Phase II		
$x_1$	$x_2$	$x_3$	$x_1$	$x_2$	$x_3$
0.0152	0.0000	0.9848	0.8968	0.0000	0.1032
0.0165	0.0673	0.9162	0.7744	0.1144	0.1111
0.0205	0.1365	0.8430	0.6471	0.2322	0.1207
0.0226	0.1756	0.8019	0.5960	0.2723	0.1317
0.0270	0.2369	0.7361	0.5035	0.3610	0.1355
0.0352	0.3269	0.6378	0.3899	0.4576	0.1525
0.0385	0.3573	0.6043	0.3698	0.4673	0.1629

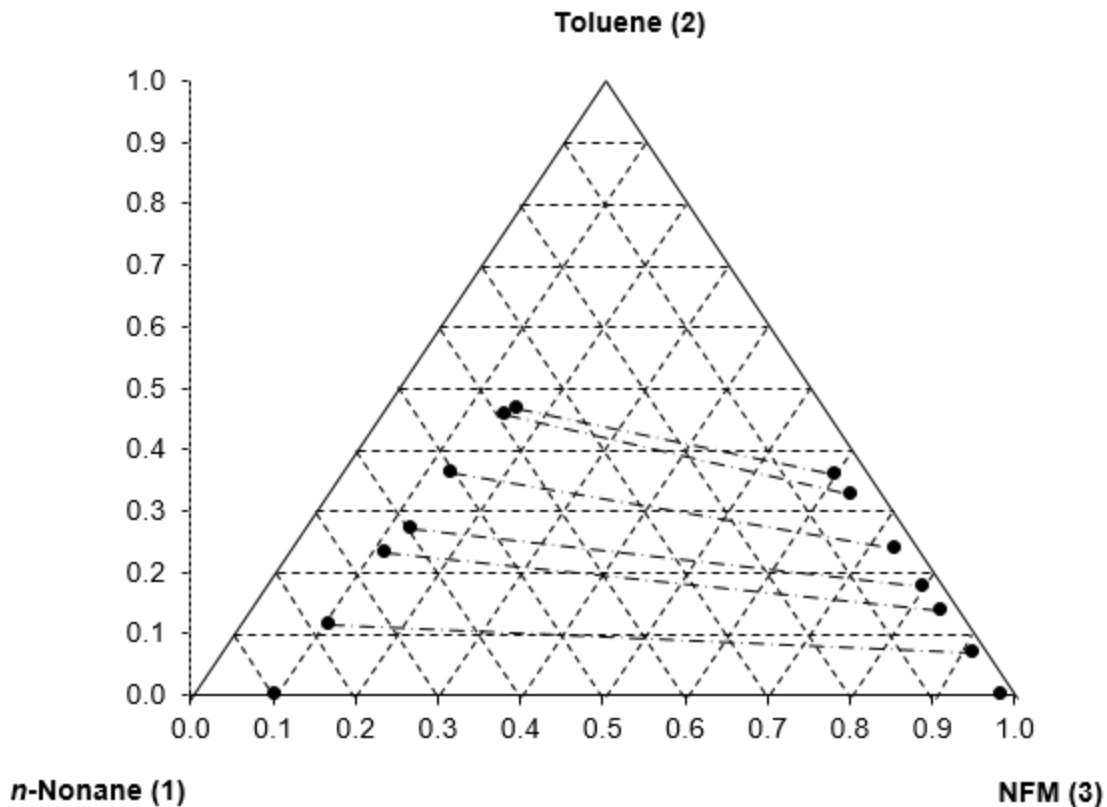
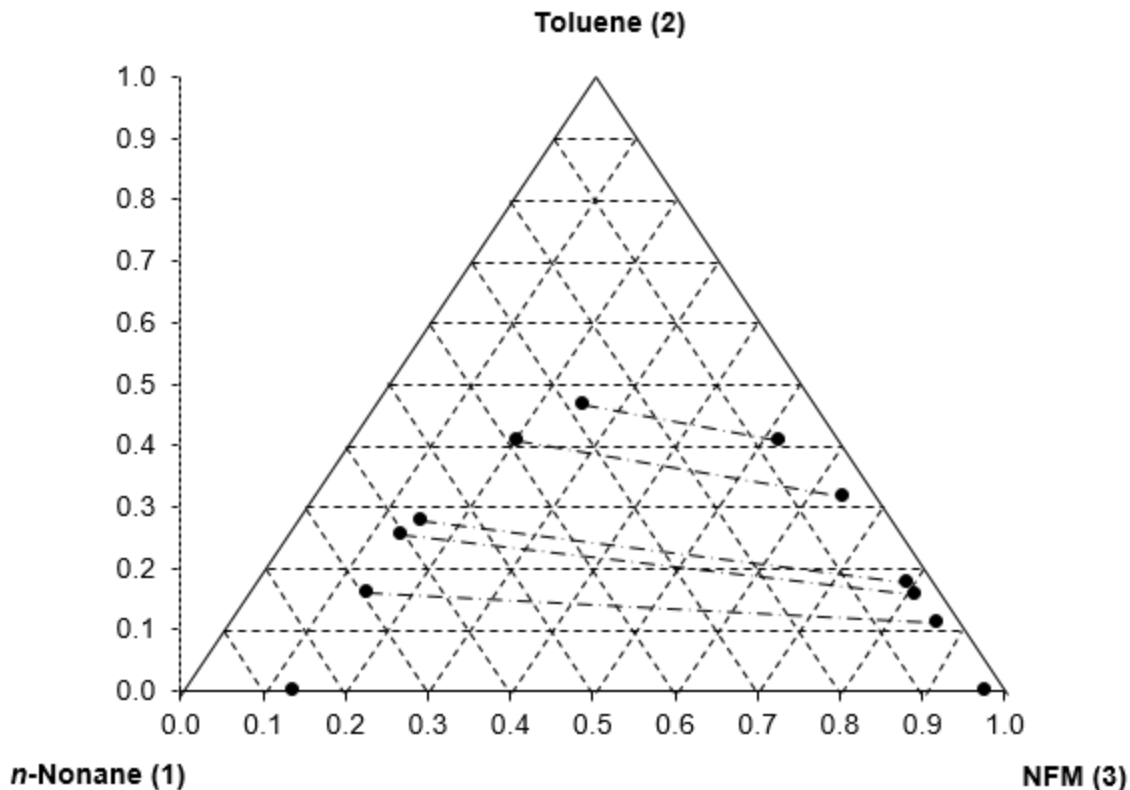


Figure 6-3: Ternary diagram for the *n*-nonane (1) + toluene (2) + NFM (3) system at 323.15 K and 1 atm.

Table 6-5: Liquid-liquid equilibrium data for the *n*-nonane (1) + toluene (2) + NFM (3) system at 343.15 K and 101.3kPa.

Phase I			Phase II		
$x_1$	$x_2$	$x_3$	$x_1$	$x_2$	$x_3$
0.0220	0.0000	0.9780	0.8622	0.0000	0.1378
0.0251	0.1105	0.8644	0.6922	0.1606	0.1472
0.0294	0.1567	0.8139	0.6043	0.2554	0.1403
0.0314	0.1747	0.7938	0.5699	0.2756	0.1545
0.0387	0.3152	0.6461	0.3875	0.4089	0.2035
0.0690	0.4061	0.5249	0.2768	0.4675	0.2557



**Figure 6-4: Ternary diagram for the *n*-nonane (1) + toluene (2) + NFM (3) system at 343.15 K and 1 atm.**

#### 6.4.1.2 *n*-Decane (1) + Toluene (2) + NFM (3)

This system has not been previously measured at 303.15 K, 323.15 K, 343 K, and 1 atm and is thus presented as new LLE data. The experimental data and the triangle diagrams are presented in Tables 6-6 to 6-8 and Figures 6-5 to 6-7, and the gas chromatography detector calibration graphs as well as uncertainties in Appendix B.

**Table 6-6: Liquid-liquid equilibrium data for the *n*-decane (1) + toluene (2) + NFM (3) system at 303.15 K and 101.3 kPa.**

Phase I			Phase II		
x <sub>1</sub>	x <sub>2</sub>	x <sub>3</sub>	x <sub>1</sub>	x <sub>2</sub>	x <sub>3</sub>
0.0072	0.0000	0.9928	0.9264	0.0000	0.0736
0.0079	0.0301	0.9620	0.8504	0.0632	0.0864
0.0116	0.0958	0.8926	0.7784	0.1207	0.1009
0.0146	0.1286	0.8568	0.6614	0.2406	0.0980
0.0317	0.1620	0.8062	0.6113	0.2886	0.1001
0.0204	0.2406	0.7390	0.4991	0.4121	0.0888
0.0406	0.3485	0.6109	0.2957	0.5787	0.1257

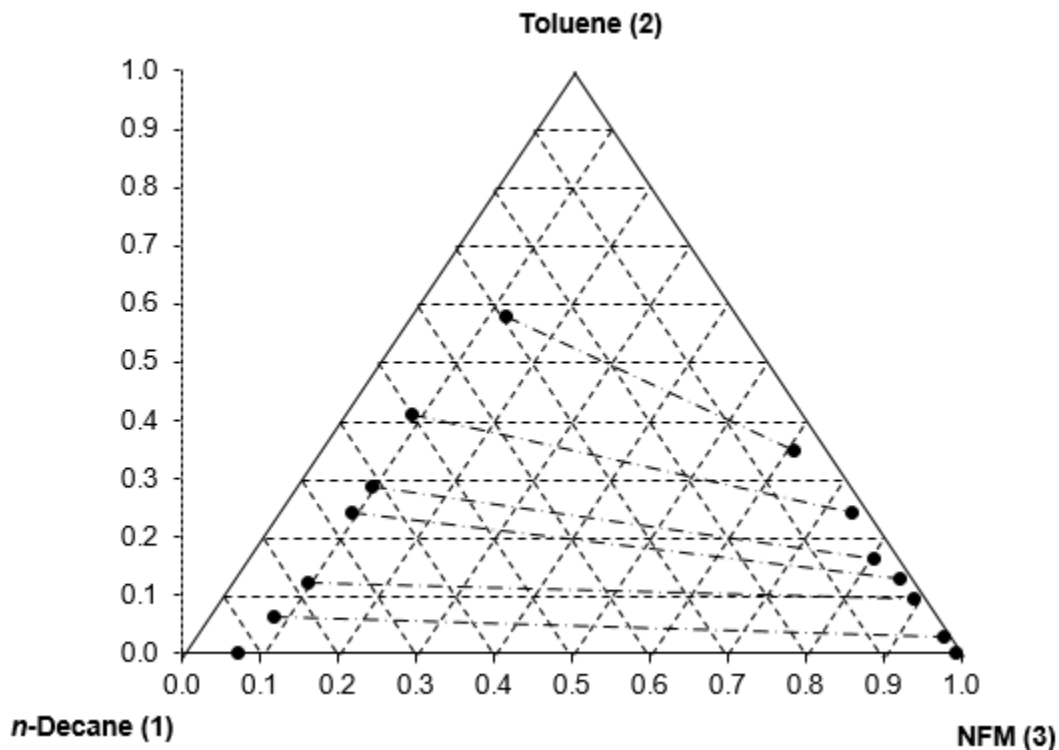


**Figure 6-5: Ternary diagram for the *n*-decane (1) + toluene (2) + NFM (3) system at 303.15 K and 1 atm.**

**Table 6-7: Liquid-liquid equilibrium data for the *n*-decane (1) + toluene (2) + NFM (3) system at 323.15 K and 101.3 kPa.**

Phase I			Phase II		
x <sub>1</sub>	x <sub>2</sub>	x <sub>3</sub>	x <sub>1</sub>	x <sub>2</sub>	x <sub>3</sub>
0.0126	0.0000	0.9874	0.9153	0.0000	0.0847
0.0109	0.0166	0.9726	0.8510	0.0491	0.0999
0.0142	0.0733	0.9124	0.7185	0.1626	0.1188
0.0201	0.1523	0.8277	0.5879	0.2806	0.1315
0.0237	0.1909	0.7854	0.5221	0.3451	0.1328
0.0453	0.3573	0.5975	0.3116	0.5049	0.1836

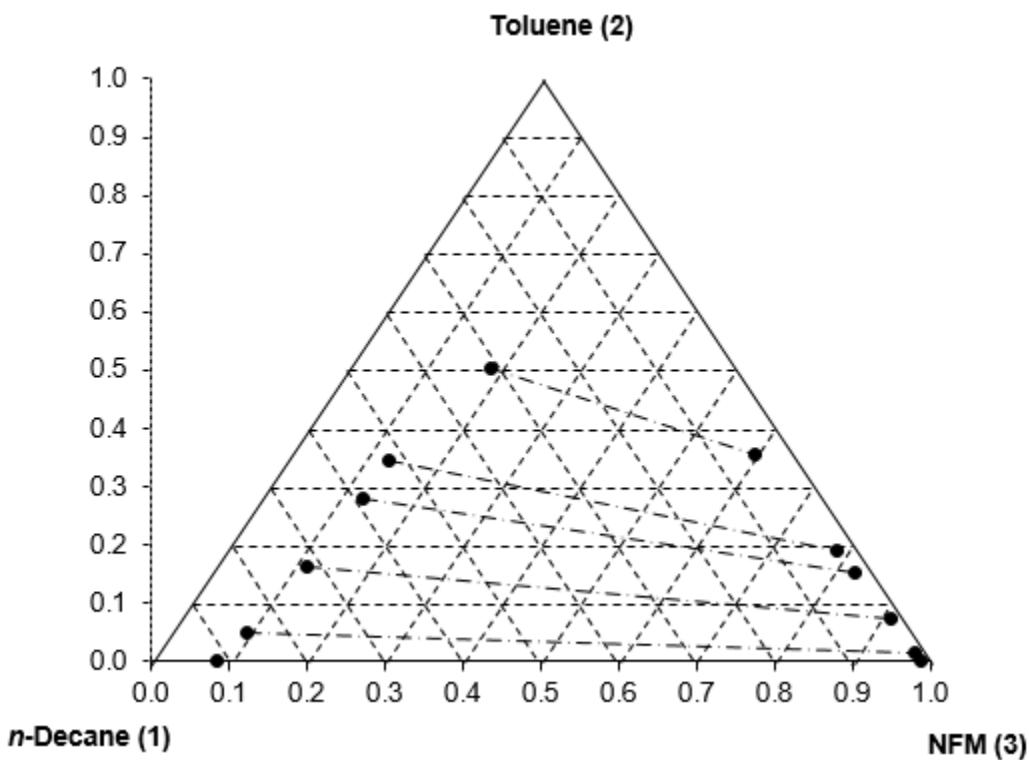


**Figure 6-6: Ternary diagram for the *n*-decane (1) + toluene (2) + NFM (3) system at 323.15 K and 1 atm.**

**Table 6-8: Liquid-liquid equilibrium data for the *n*-decane (1) + toluene (2) + NFM (3) system at 343.15 K and 101.3 kPa.**

Phase I			Phase II		
x <sub>1</sub>	x <sub>2</sub>	x <sub>3</sub>	x <sub>1</sub>	x <sub>2</sub>	x <sub>3</sub>
0.0176	0.0000	0.9824	0.9009	0.0000	0.0991
0.0174	0.0323	0.9503	0.8411	0.0468	0.1121
0.0155	0.0519	0.9325	0.7630	0.1170	0.1200
0.0260	0.1196	0.8545	0.6835	0.2232	0.0933
0.0299	0.1623	0.8077	0.6113	0.2886	0.1001
0.0388	0.2092	0.7520	0.4808	0.3750	0.1442
0.0605	0.3212	0.6183	0.3159	0.4630	0.2211

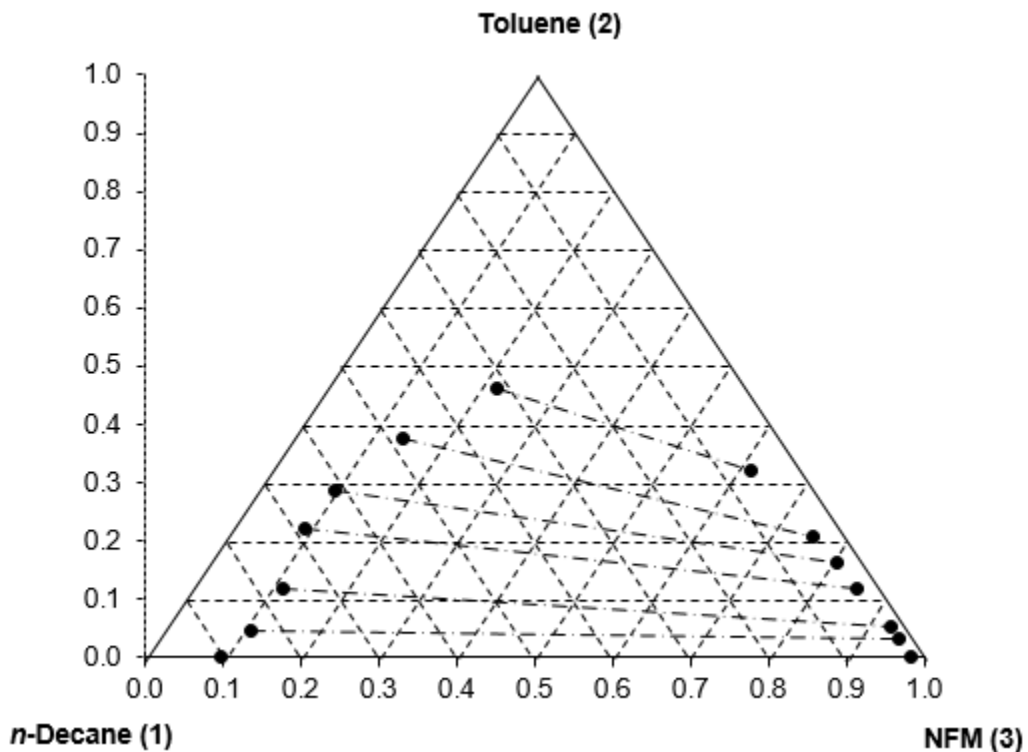


**Figure 6-7: Ternary diagram for the *n*-decane (1) + toluene (2) + NFM (3) system at 343.15 K and 1 atm.**

**Table 6-9: Experimental data of the distribution coefficient ( $\kappa$ ), separation factor ( $\beta$ ) and selectivity (S) of the *n*-nonane (1) + toluene (2) + NFM (3) system**

T / K	K	$\beta$	S
303.15	0.501	35.1	6.45
	0.572	28.0	3.51
	0.613	21.7	2.62
	0.640	18.7	2.32
	0.653	13.3	1.74
	0.680	9.5	1.59
323.15	0.589	27.6	6.23
	0.588	18.6	3.29
	0.645	17.0	2.82
	0.656	12.2	2.15
	0.714	7.90	1.67
	0.765	7.35	1.62
343.15	0.688	19.0	4.33
	0.614	12.6	2.83
	0.634	11.5	2.59
	0.771	7.71	1.73
	0.869	3.48	1.36

**Table 6-10: Experimental data of the distribution coefficient ( $\kappa$ ), separation factor ( $\beta$ ) and selectivity (S) of the *n*-decane (1) + toluene (2) + NFM (3) system**

T / K	K	$\beta$	S
303.15	0.477	51.35	11.46
	0.793	53.27	6.64
	0.535	24.20	3.37
	0.561	10.81	2.61
	0.584	14.28	2.04
	0.602	4.39	1.35
323.15	0.338	26.43	11.08
	0.451	22.74	4.54
	0.543	15.89	2.74
	0.553	12.18	2.24
	0.708	4.87	1.44
343.15	0.689	33.30	12.32
	0.444	21.82	5.79
	0.536	14.10	3.34
	0.563	11.49	2.63
	0.558	6.91	1.93
	0.694	3.62	1.42

# 7

## CHAPTER SEVEN

### DATA ANALYSIS AND DISCUSSION

#### 7.1 Ternary Systems Correlation

The data of the ternary systems measured in this work were analyzed and represented with the NRTL and UNIQUAC liquid phase activity coefficient models. The non-randomness parameter ( $\alpha_{ij}$ ) in the NRTL model was made equal for all applicable binary pairs and fixed at 0.20 to 0.40 in intervals of 0.05.

The tie lines were correlated using the in-built regression functionality in Aspen Plus v8.4. The experimental data was input into different data sets and the regression was generated per ternary system. The regression was implemented with the use of the Britt-Luecke algorithm (Britt and Luecke, 1973), with the binary interaction parameters being calculated by minimizing the deviation between the experimental data and calculated values from the model. This process determines the mole fractions of individual components for an initialized set of parameters using the Deming initialization method (Britt and Luecke, 1973), and thereafter a new set of parameters is determined iteratively until the value of the objective function is smaller than the prescribed tolerance. The best model was determined by the lowest value of the root mean square deviation (RMSD).

The GC detector was calibrated for the dilute regions of two pairs of components, with the calibration curves displayed in Appendix B. The response factor ratios displayed a quadratic relationship with the mole fraction ratios, except for the toluene-NFM pair which displayed a linear relationship. It was ensured that the correct calibration graph was used, corresponding to the dilute region samples drawn.

### 7.1.1 *n*-Nonane (1) + Toluene (2) + NFM (3)

The experimental data for this system was measured at 303.15 K, 323.15 K, and 343.15 K. The measurements exhibit a binodal curve typical of a type I system (Treybal, 1963). The tie-line regression showed that the NRTL model provided the best fit to the experimental data for *n*-nonane + toluene + NFM at the different temperatures. The parameters for the NRTL model for the  $\alpha$  value that produced the lowest RMSD and the UNIQUAC model are presented in Tables 7-1 to 7-3. The best tie-line model is illustrated together with the experimental values in Figures 7-1 to 7-3. The modelled data is presented in Table 7-4.

**Table 7-1: Model parameters for the tie-lines of the *n*-nonane (1) + toluene (2) + NFM (3) system at 303.15 K and 1 atm.**

Models			
<b>NRTL with <math>\alpha = 0.35</math></b>		<b>UNIQUAC</b>	
$g_{12} - g_{22}$ / (J/mol)	2363	$u_{12} - u_{22}$ / (J/mol)	4.330
$g_{21} - g_{11}$ / (J/mol)	785.0	$u_{21} - u_{11}$ / (J/mol)	374.1
$g_{13} - g_{33}$ / (J/mol)	563.6	$u_{13} - u_{33}$ / (J/mol)	110.4
$g_{31} - g_{11}$ / (J/mol)	1184	$u_{31} - u_{11}$ / (J/mol)	157.1
$g_{23} - g_{33}$ / (J/mol)	526.5	$u_{23} - u_{33}$ / (J/mol)	269.6
$g_{32} - g_{22}$ / (J/mol)	512.2	$u_{32} - u_{22}$ / (J/mol)	111.4
<b>RMSD</b>	0.0045	<b>RMSD</b>	0.0057

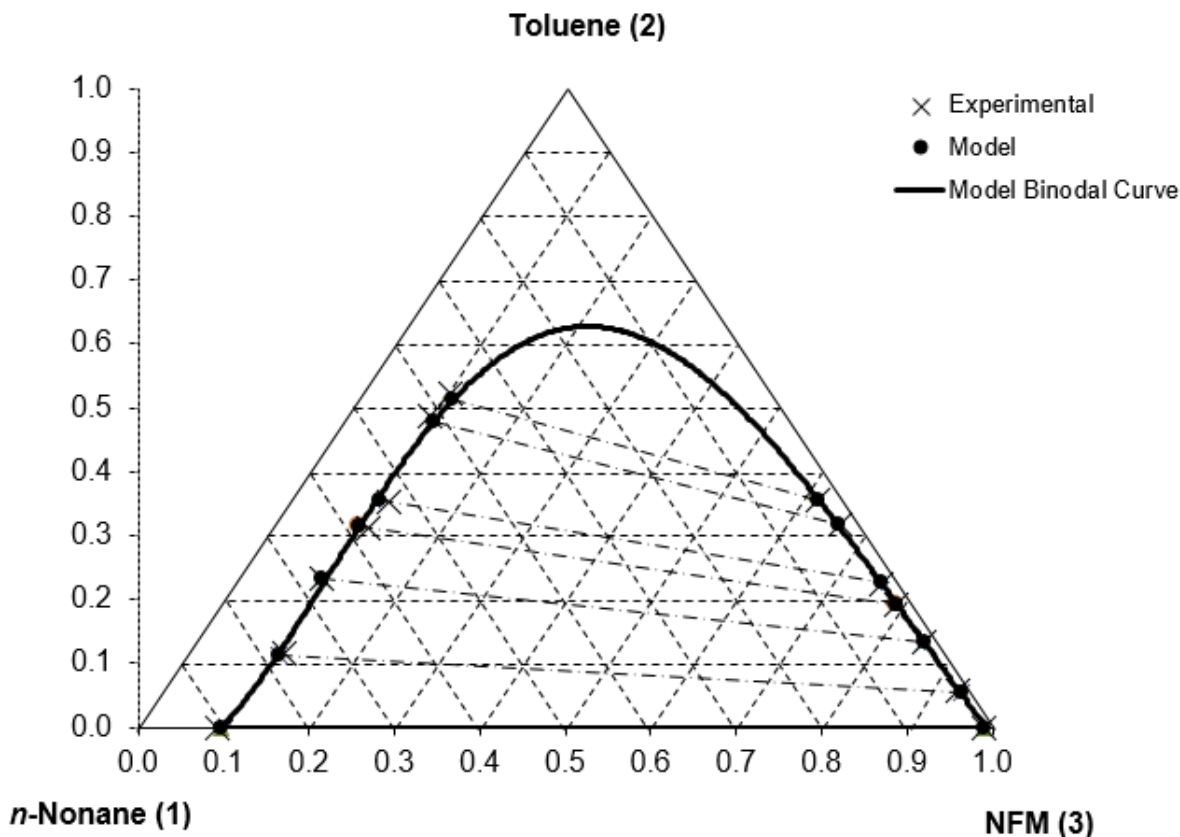
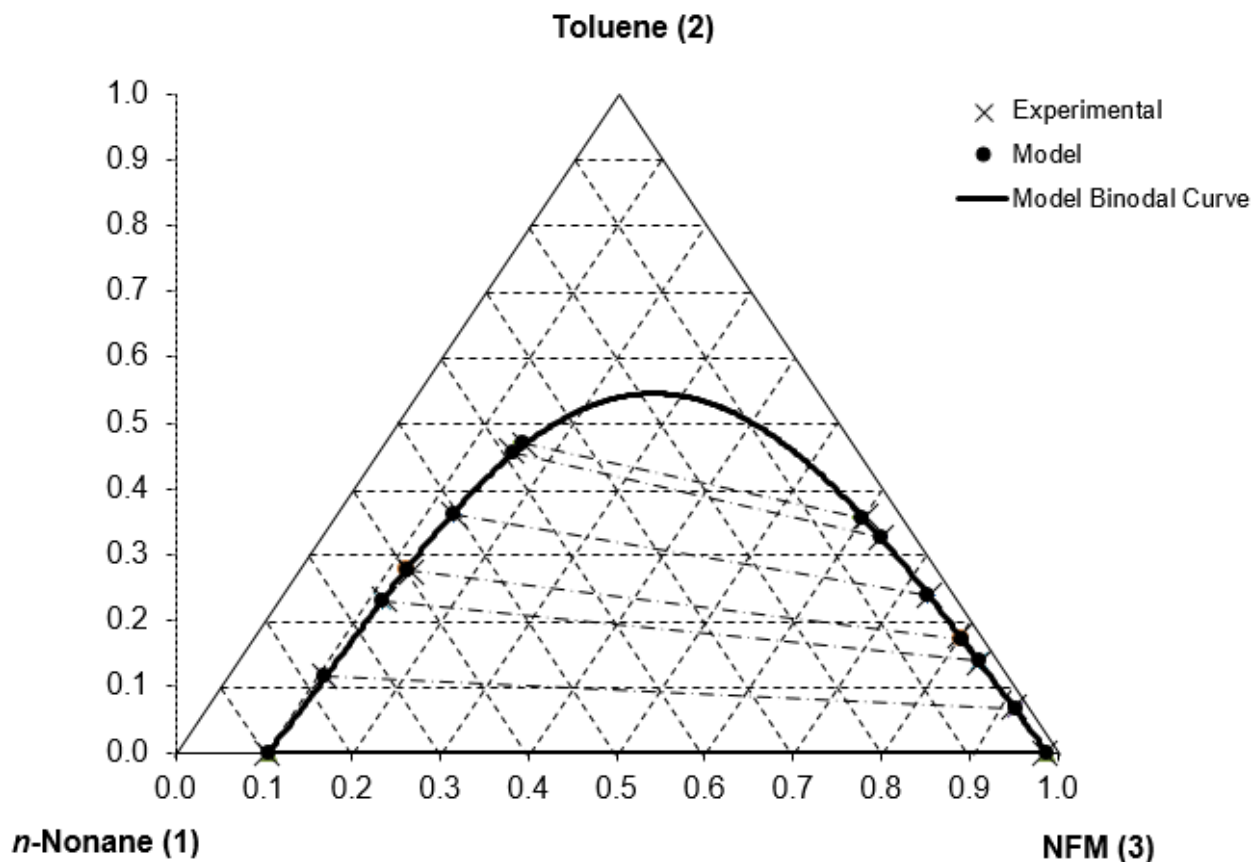


Figure 7-1: Fit of the NRTL model with  $\alpha = 0.35$  for the predicted tie-lines and binodal curve for the ternary plot of the *n*-nonane (1) + toluene (2) + NFM (3) system at 303.15 K and 1 atm.

Table 7-2: Model parameters for the tie-lines of the *n*-nonane (1) + toluene (2) + NFM (3) system at 323.15 K and 1 atm.

Models			
NRTL with $\alpha = 0.35$		UNIQUAC	
$g_{12} - g_{22}$ / (J/mol)	1933	$u_{12} - u_{22}$ / (J/mol)	37.08
$g_{21} - g_{11}$ / (J/mol)	680.0	$u_{21} - u_{11}$ / (J/mol)	172.1
$g_{13} - g_{33}$ / (J/mol)	631.6	$u_{13} - u_{33}$ / (J/mol)	120.9
$g_{31} - g_{11}$ / (J/mol)	1185	$u_{31} - u_{11}$ / (J/mol)	162.5
$g_{23} - g_{33}$ / (J/mol)	449.2	$u_{23} - u_{33}$ / (J/mol)	130.5
$g_{32} - g_{22}$ / (J/mol)	482.8	$u_{32} - u_{22}$ / (J/mol)	127.9
<b>RMSD</b>	0.0025	<b>RMSD</b>	0.0027



**Figure 7-2: Fit of the NRTL model with  $\alpha = 0.35$  for the predicted tie-lines and binodal curve for the ternary plot of the *n*-nonane (1) + toluene (2) + NFM (3) system at 323.15 K and 1 atm.**

**Table 7-3: Model parameters for the tie-lines of the *n*-nonane (1) + toluene (2) + NFM (3) system at 343.15 K and 1 atm.**

Models			
<b>NRTL with <math>\alpha = 0.2</math></b>		<b>UNIQUAC</b>	
$g_{12} - g_{22}$ / (J/mol)	3932	$u_{12} - u_{22}$ / (J/mol)	40.05
$g_{21} - g_{11}$ / (J/mol)	899.9	$u_{21} - u_{11}$ / (J/mol)	119.7
$g_{13} - g_{33}$ / (J/mol)	222.1	$u_{13} - u_{33}$ / (J/mol)	109.1
$g_{31} - g_{11}$ / (J/mol)	1257	$u_{31} - u_{11}$ / (J/mol)	175.7
$g_{23} - g_{33}$ / (J/mol)	340.6	$u_{23} - u_{33}$ / (J/mol)	89.08
$g_{32} - g_{22}$ / (J/mol)	888.7	$u_{32} - u_{22}$ / (J/mol)	124.6
<b>RMSD</b>	0.0055	<b>RMSD</b>	0.0058

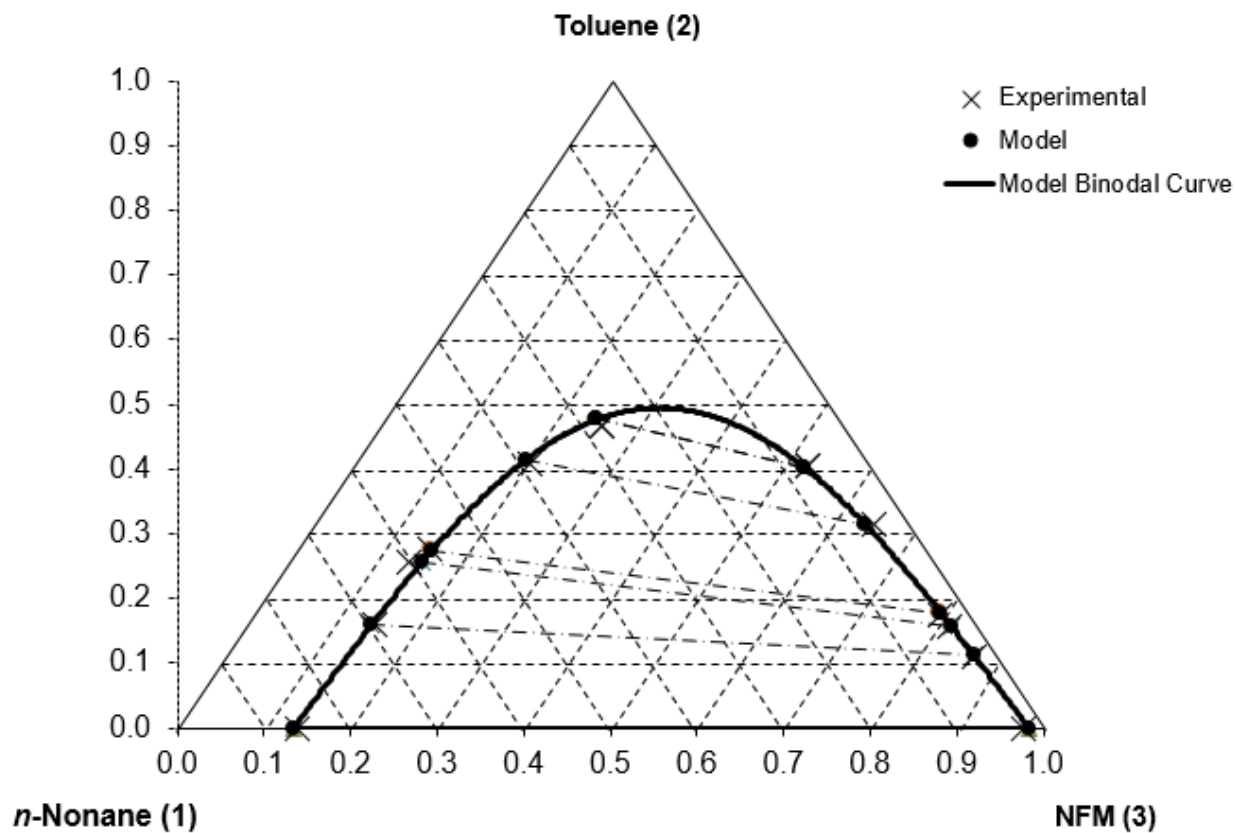


**Figure 7-3: Fit of the NRTL model with  $\alpha = 0.2$  for the predicted tie-lines and binodal curve for the ternary plot of the *n*-nonane (1) + toluene (2) + NFM (3) system at 343.15 K and 1 atm.**

**Table 7-4: Modelled liquid-liquid equilibrium data for the n-nonane (1) + toluene (2) + NFM (3) system at 303.15, 323.15, 343.15 K and 101.3 atm.**

NRTL Model						
T (K)	Phase I			Phase II		
	X1	X2	X3	X1	X2	X3
303.15	0.0091	0.0000	0.9909	0.9026	0.0000	0.0974
303.15	0.0088	0.0550	0.9362	0.7789	0.1119	0.1092
303.15	0.0147	0.1317	0.8536	0.6676	0.2330	0.0994
303.15	0.0158	0.1923	0.7919	0.5827	0.3152	0.1021
303.15	0.0168	0.2253	0.7579	0.5394	0.3539	0.1067
303.15	0.0215	0.3175	0.6610	0.4147	0.4786	0.1067
303.15	0.0262	0.3538	0.6200	0.3740	0.5145	0.1116
323.15	0.0122	0.0000	0.9878	0.8940	0.0000	0.1060
323.15	0.0152	0.0656	0.9192	0.7733	0.1155	0.1112
323.15	0.0195	0.1390	0.8415	0.6501	0.2307	0.1192
323.15	0.0218	0.1724	0.8058	0.5985	0.2777	0.1238
323.15	0.0273	0.2382	0.7345	0.5043	0.3608	0.1349
323.15	0.0376	0.3265	0.6359	0.3882	0.4554	0.1565
323.15	0.0422	0.3567	0.6010	0.3706	0.4685	0.1609
343.15	0.0169	0.0000	0.9831	0.8656	0.0000	0.1344
343.15	0.0236	0.1112	0.8652	0.6958	0.1604	0.1437
343.15	0.0274	0.1562	0.8164	0.5904	0.2546	0.1550
343.15	0.0295	0.1776	0.7930	0.5695	0.2726	0.1579
343.15	0.0494	0.3139	0.6367	0.3902	0.4126	0.1971
343.15	0.0746	0.4013	0.5241	0.2786	0.4767	0.2447

### 7.1.2 n-Decane (1) + Toluene (2) + NFM (3)

The experimental data for this system was measured at 303.15 K, 323.15 K, and 343.15 K. The measurements exhibit a binodal curve typical of a type I system (Treybal, 1963). The tie-line regression showed that the NRTL model provided the best fit to the experimental data for *n*-decane (1) + toluene (2) + NFM (3) at all of the temperatures considered in the study. The parameters for the NRTL model for the  $\alpha$  value that produced the lowest RMSD, and the UNIQUAC model, are

presented in Tables 7-5 to 7-7. The best tie-line model is illustrated together with the experimental values in Figures 7-4 to 7-6. The modelled data is presented in Table 7-8.

**Table 7-5: Model parameters for the tie-lines of the *n*-decane (1) + toluene (2) + NFM (3) system at 303.15 K and 1 atm.**

Models			
<b>NRTL with <math>\alpha = 0.25</math></b>		<b>UNIQUAC</b>	
$g_{12} - g_{22}$ / (J/mol)	-123.1	$u_{12} - u_{22}$ / (J/mol)	64.51
$g_{21} - g_{11}$ / (J/mol)	248.2	$u_{21} - u_{11}$ / (J/mol)	1.670
$g_{13} - g_{33}$ / (J/mol)	422.4	$u_{13} - u_{33}$ / (J/mol)	180.6
$g_{31} - g_{11}$ / (J/mol)	1182	$u_{31} - u_{11}$ / (J/mol)	86.73
$g_{23} - g_{33}$ / (J/mol)	1001	$u_{23} - u_{33}$ / (J/mol)	492.4
$g_{32} - g_{22}$ / (J/mol)	-113.8	$u_{32} - u_{22}$ / (J/mol)	-137.4
<b>RMSD</b>	0.0076	<b>RMSD</b>	0.0083

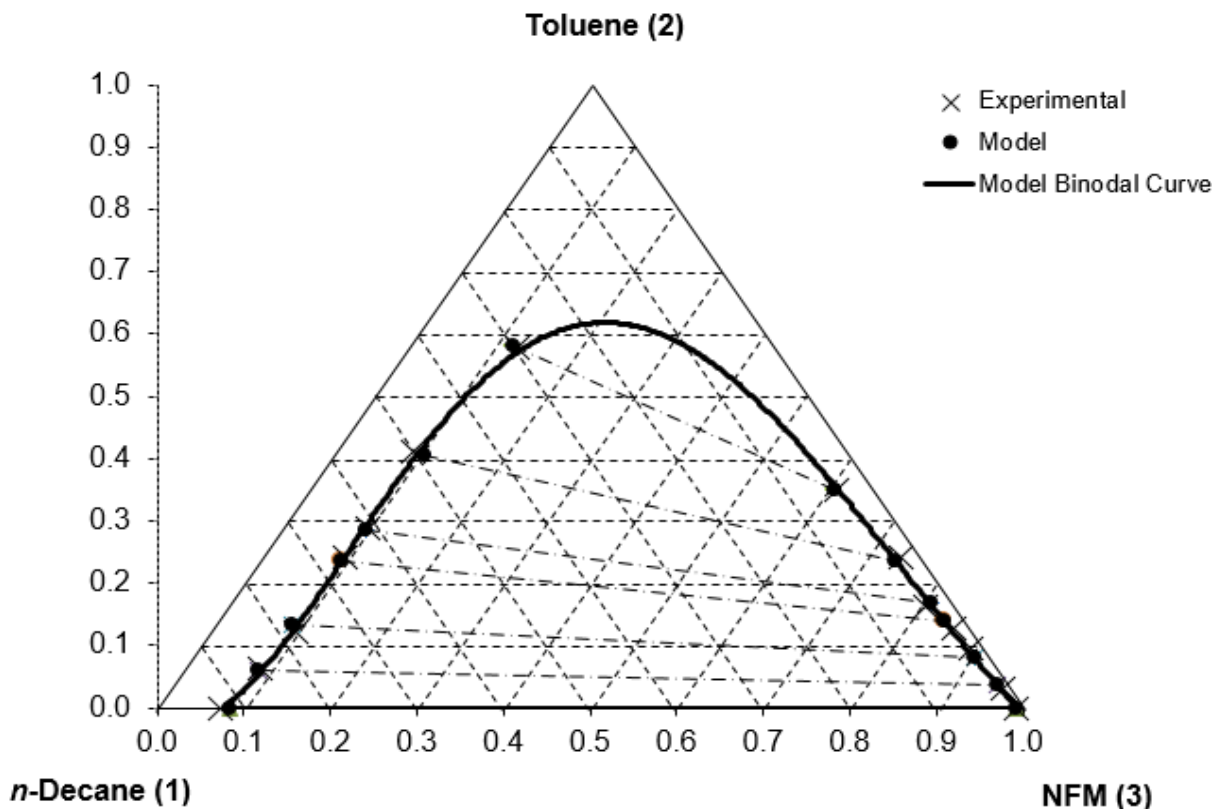


**Figure 7-4: Fit of the NRTL model with  $\alpha = 0.25$  for the predicted tie-lines and binodal curve for the ternary plot of the *n*-decane (1) + toluene (2) + NFM (3) system at 303.15 K and 1 atm.**

**Table 7-6: Model parameters for the tie-lines of the *n*-decane (1) + toluene (2) + NFM (3) system at 323.15 K and 1 atm.**

Models			
<b>NRTL with <math>\alpha = 0.4</math></b>		<b>UNIQUAC</b>	
$g_{12} - g_{22}$ / (J/mol)	-664.2	$u_{12} - u_{22}$ / (J/mol)	-61.76
$g_{21} - g_{11}$ / (J/mol)	659.5	$u_{21} - u_{11}$ / (J/mol)	-43.59
$g_{13} - g_{33}$ / (J/mol)	882.9	$u_{13} - u_{33}$ / (J/mol)	155.4
$g_{31} - g_{11}$ / (J/mol)	1305	$u_{31} - u_{11}$ / (J/mol)	128.0
$g_{23} - g_{33}$ / (J/mol)	494.6	$u_{23} - u_{33}$ / (J/mol)	8599
$g_{32} - g_{22}$ / (J/mol)	248.3	$u_{32} - u_{22}$ / (J/mol)	-345.0
<b>RMSD</b>	0.0026	<b>RMSD</b>	0.0035

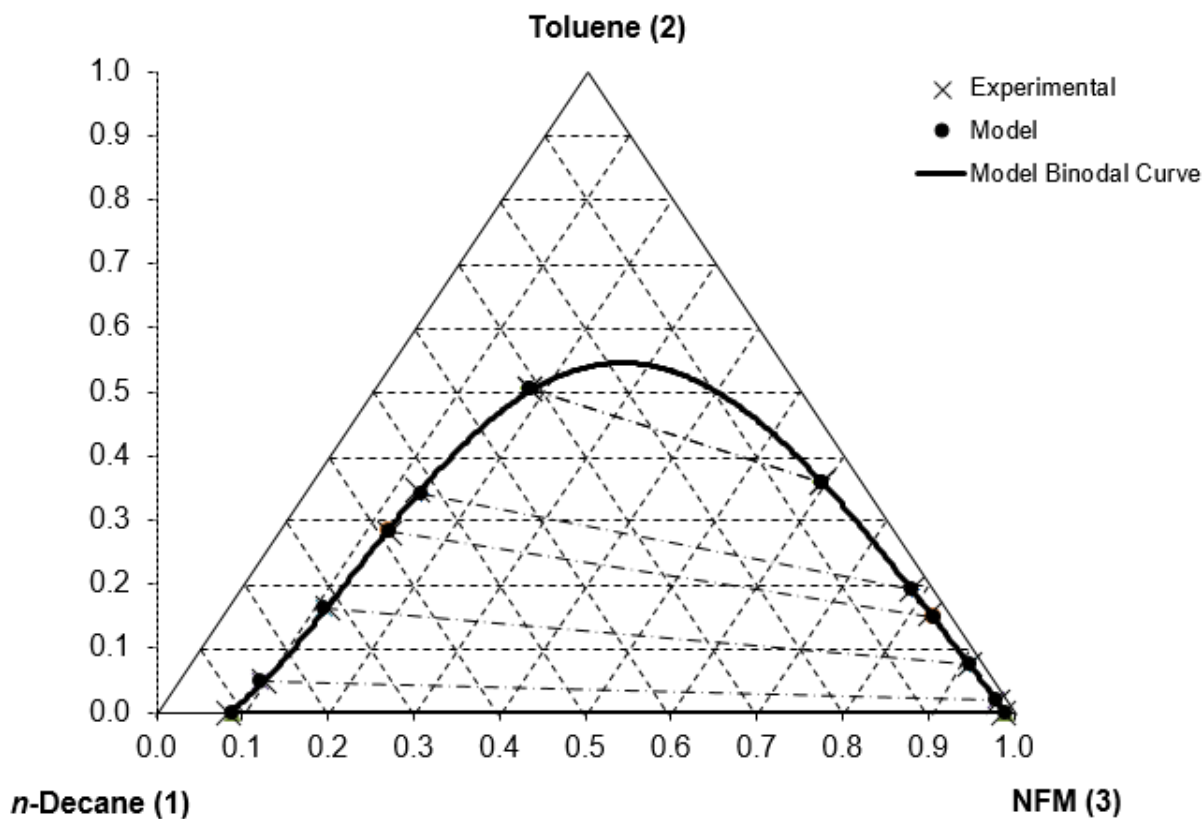


**Figure 7-5: Fit of the NRTL model with  $\alpha = 0.4$  for the predicted tie-lines and binodal curve for the ternary plot of the *n*-decane (1) + toluene (2) + NFM (3) system at 323.15 K and 1 atm.**

**Table 7-7: Model parameters for the tie-lines of the *n*-decane (1) + toluene (2) + NFM (3) system at 343.15 K and 1 atm.**

Models			
<b>NRTL with <math>\alpha = 0.2</math></b>		<b>UNIQUAC</b>	
$g_{12} - g_{22} / (\text{J/mol})$	1492	$u_{12} - u_{22} / (\text{J/mol})$	140.1
$g_{21} - g_{11} / (\text{J/mol})$	1142	$u_{21} - u_{11} / (\text{J/mol})$	186.7
$g_{13} - g_{33} / (\text{J/mol})$	336.5	$u_{13} - u_{33} / (\text{J/mol})$	195.4
$g_{31} - g_{11} / (\text{J/mol})$	1099	$u_{31} - u_{11} / (\text{J/mol})$	92.68
$g_{23} - g_{33} / (\text{J/mol})$	297.9	$u_{23} - u_{33} / (\text{J/mol})$	96.39
$g_{32} - g_{22} / (\text{J/mol})$	810.9	$u_{32} - u_{22} / (\text{J/mol})$	260.8
<b>RMSD</b>	0.0084	<b>RMSD</b>	0.0214

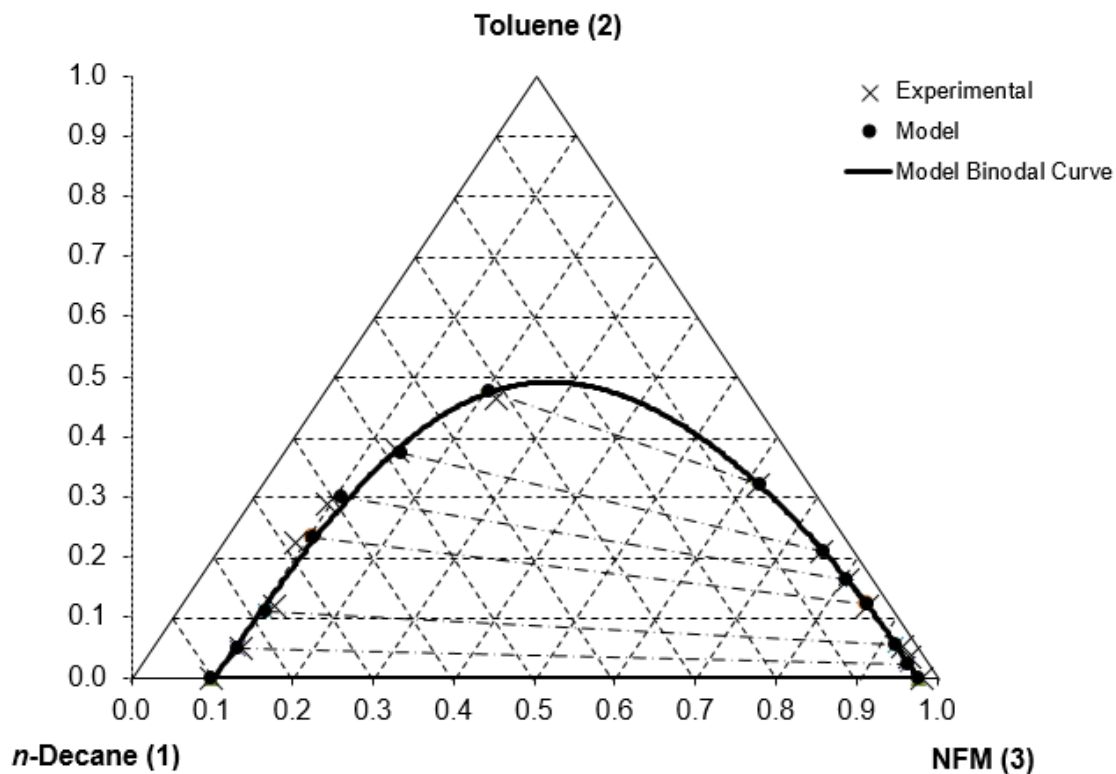


**Figure 7-6: Fit of the NRTL model with  $\alpha = 0.2$  for the predicted tie-lines and binodal curve for the ternary plot of the *n*-decane (1) + toluene (2) + NFM (3) system at 343.15 K and 1 atm.**

**Table 7-8: Modelled liquid-liquid equilibrium data for the *n*-decane (1) + toluene (2) + NFM (3) system at 303.15, 323.15, 343.15 K and 101.3 atm.**

NRTL Model						
T (K)	Phase I			Phase II		
	x1	x2	x3	x1	x2	x3
303.15	0.0085	0.0000	0.9915	0.9155	0.0000	0.0845
303.15	0.0109	0.0377	0.9514	0.8532	0.0600	0.0868
303.15	0.0143	0.0815	0.9042	0.7769	0.1331	0.0900
303.15	0.0198	0.1398	0.8405	0.6696	0.2351	0.0953
303.15	0.0228	0.1683	0.8089	0.6154	0.2862	0.0984
303.15	0.0304	0.2350	0.7346	0.4891	0.4044	0.1065
303.15	0.0424	0.3488	0.6088	0.2982	0.5811	0.1206
323.15	0.0099	0.0000	0.9901	0.9109	0.0000	0.0891
323.15	0.0109	0.0198	0.9693	0.8540	0.0484	0.0976
323.15	0.0141	0.0748	0.9111	0.7231	0.1625	0.1144
323.15	0.0195	0.1484	0.8321	0.5872	0.2826	0.1302
323.15	0.0234	0.1921	0.7845	0.5197	0.3414	0.1389
323.15	0.0454	0.3581	0.5965	0.3119	0.5043	0.1837
343.15	0.0228	0.0000	0.9772	0.9006	0.0000	0.0994
343.15	0.0254	0.0231	0.9515	0.8433	0.0488	0.1079
343.15	0.0256	0.0534	0.9210	0.7768	0.1103	0.1129
343.15	0.0245	0.1225	0.8531	0.6568	0.2339	0.1093
343.15	0.0320	0.1627	0.8053	0.5900	0.2993	0.1108
343.15	0.0356	0.2096	0.7548	0.4782	0.3720	0.1498
343.15	0.0596	0.3207	0.6198	0.3187	0.4746	0.2067

## 7.2 Systems Comparison

The phase behaviour does not change drastically in form between the ternary system containing either *n*-nonane or *n*-decane. It can be seen in Figures 7-1 to 7-6 that the solubility of NFM is higher in the alkane rich phase at higher temperatures, with the solubility of alkanes in the NFM rich phase not significantly impacted. Increasing the concentration of toluene and the system temperature results in an increase in solubility of the alkane + NFM binary pair. Table 7-8 lists the plait point of all systems measured using the Coolidge method (Treybal, 1963), indicating that increasing temperature decreases the two-liquid phase region.

**Table 7-9: Plait point of ternary systems measured at different temperatures.**

<b>System</b>	<b>Temperature</b>	<b>Plait Point mole fraction (alkane, toluene, NFM)</b>
<i>n</i> -Nonane (1) + Toluene (2) + NFM (3)	303.15 K	(0.108, 0.611, 0.281)
<i>n</i> -Nonane (1) + Toluene (2) + NFM (3)	323.15 K	(0.146, 0.521, 0.333)
<i>n</i> -Nonane (1) + Toluene (2) + NFM (3)	343.15 K	(0.161, 0.481, 0.358)
<i>n</i> -Decane (1) + Toluene (2) + NFM (3)	303.15 K	(0.103, 0.608, 0.284)
<i>n</i> -Decane (1) + Toluene (2) + NFM (3)	323.15 K	(0.133, 0.536, 0.331)
<i>n</i> -Decane (1) + Toluene (2) + NFM (3)	343.15 K	(0.174, 0.461, 0.365)

### 7.3 Solvent Parameters

The experimental separation factors, distribution coefficients, and selectivity for the systems measured are presented in Chapter 6, Tables 6-9 and 6-10. These parameters were also determined with the NRTL model predicted mole fractions as shown in Table 7-4 and Table 7-8. The comparison against the experimental data is illustrated in Figures 7-7 to 7-12.

It was observed that higher temperatures or increased toluene concentrations in either phase resulted in increased distribution coefficient values. Figures 7-7 and 7-8 indicate good agreement between experimental and predicted distribution coefficients for the ternary systems measured.

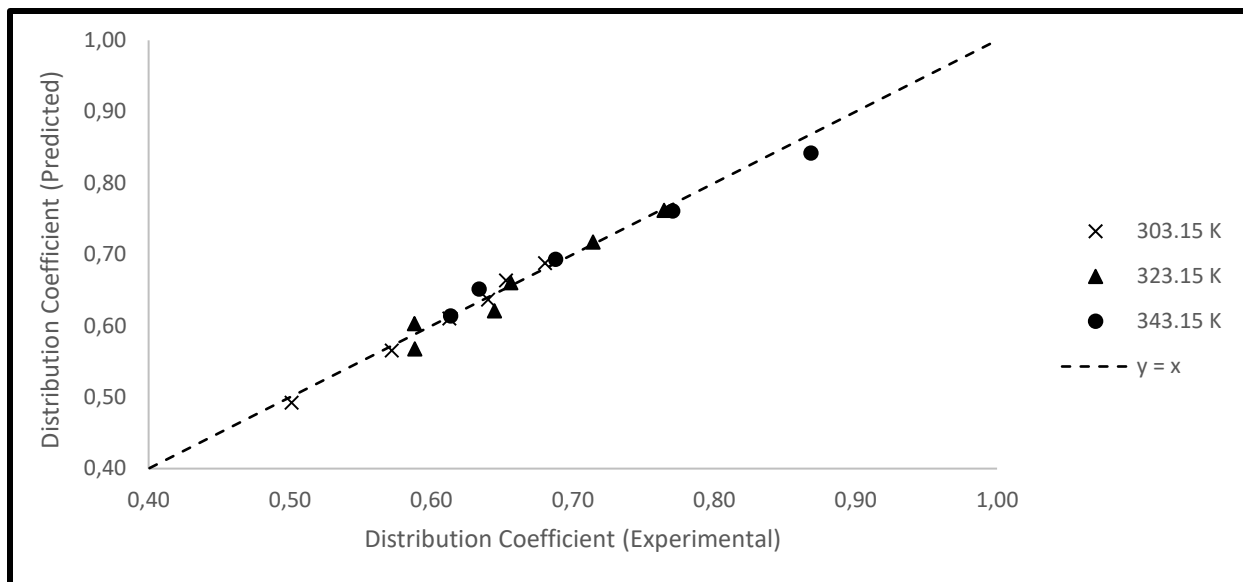


**Figure 7-7: Measured and predicted distribution coefficients with NRTL model for the *n*-nonane (1) + toluene (2) + NFM (3) system.**

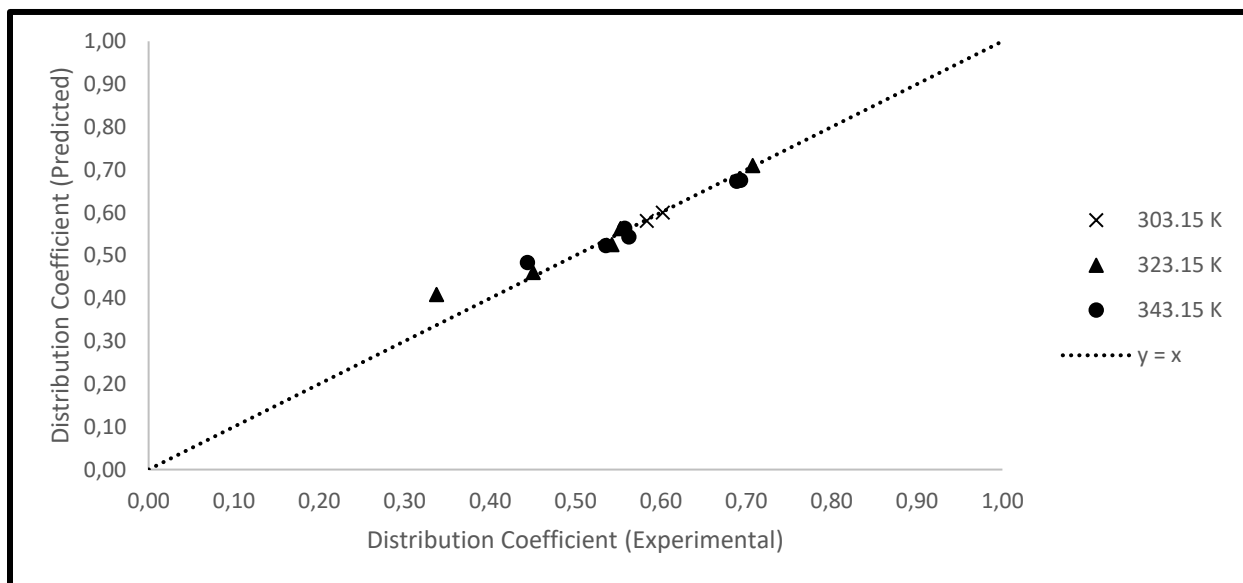


**Figure 7-8: Measured and predicted distribution coefficients with NRTL model for the *n*-decane (1) + toluene (2) + NFM (3) system.**

The experimental values of the separation factor are compared to the results predicted using the NRTL model in Figures 7-9 and 7-10. It is indicative of varying separation factors across the whole two-phase region. Figures 7-10 and 7-10 indicate that the separation factor is lower at higher

temperatures. The separation factor appeared to be dependent on the toluene content in a phase, indicating that optimal toluene feed conditions exist to maximize the separation factor. In all instances, the separation factors are more than one, indicating that the extraction is feasible.

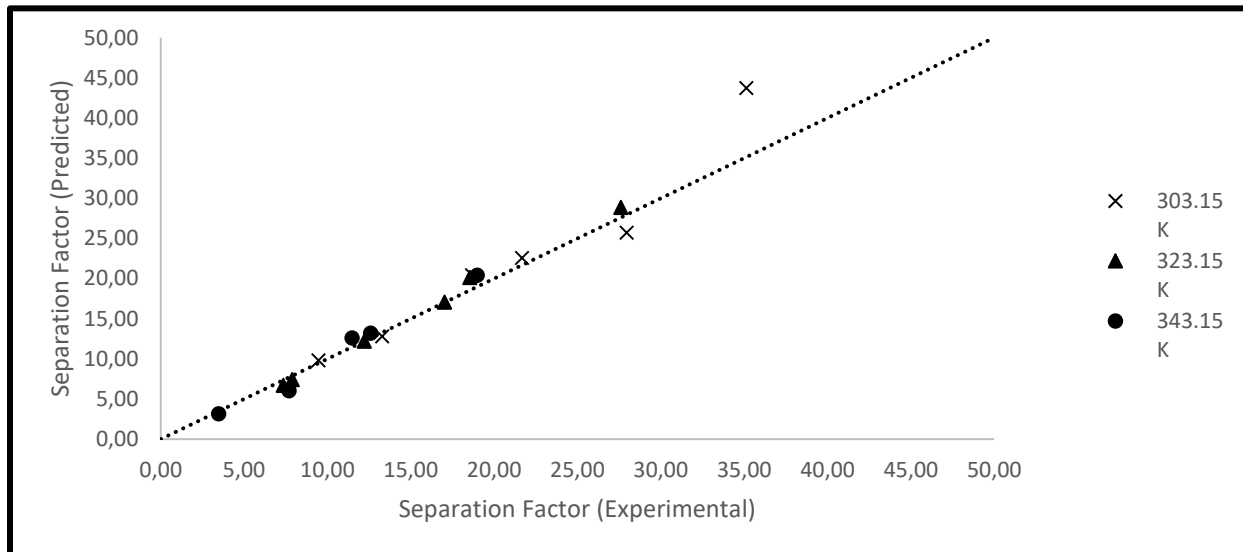


**Figure 7-9: Measured and predicted separation factor by NRTL model for the *n*-nonane (1) + toluene (2) + NFM (3) system.**

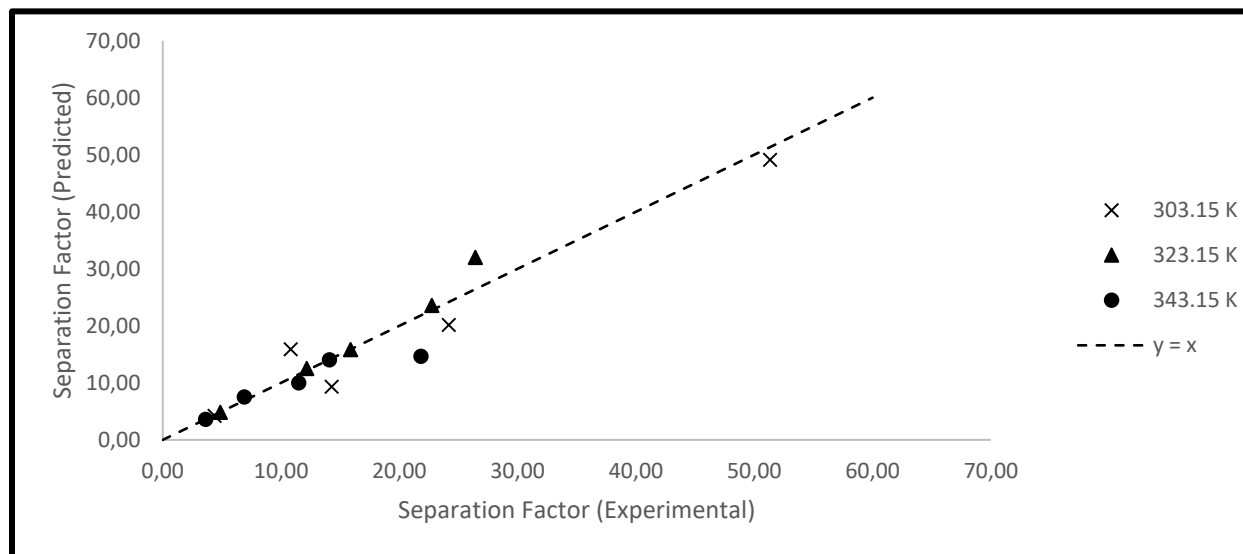


**Figure 7-10: Measured and predicted separation factor by NRTL model for the *n*-decane (1) + toluene (2) + NFM (3) system.**

The experimental selectivity values are compared to the results predicted using the NRTL model in Figures 7-11 and 7-12. Selectivity serves as an indication of the extent to which the solvent will be suitable for the extraction of toluene. As shown in Figures 7-11 and 7-12, selectivity in all instances is more than 1, decreasing with decreasing concentrations of toluene in tie-line end compositions. This suggests that a greater composition of toluene in the feed results in a lower selectivity of NFM to toluene.

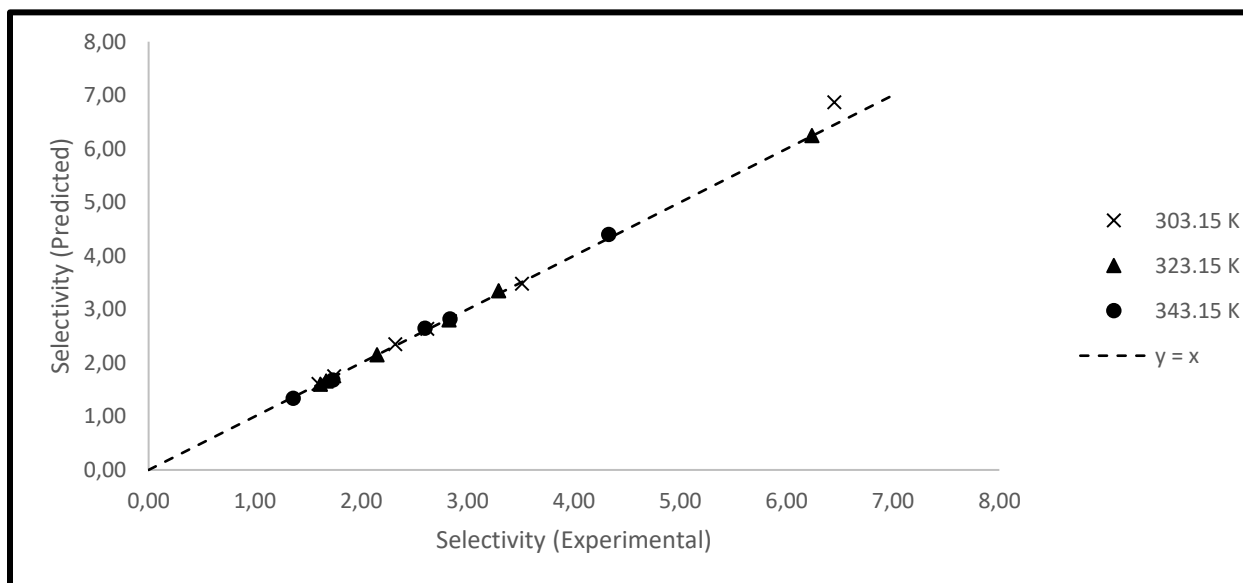


**Figure 7-11: Measured and predicted selectivity by NRTL model for the *n*-nonane (1) + toluene (2) + NFM (3) system.**

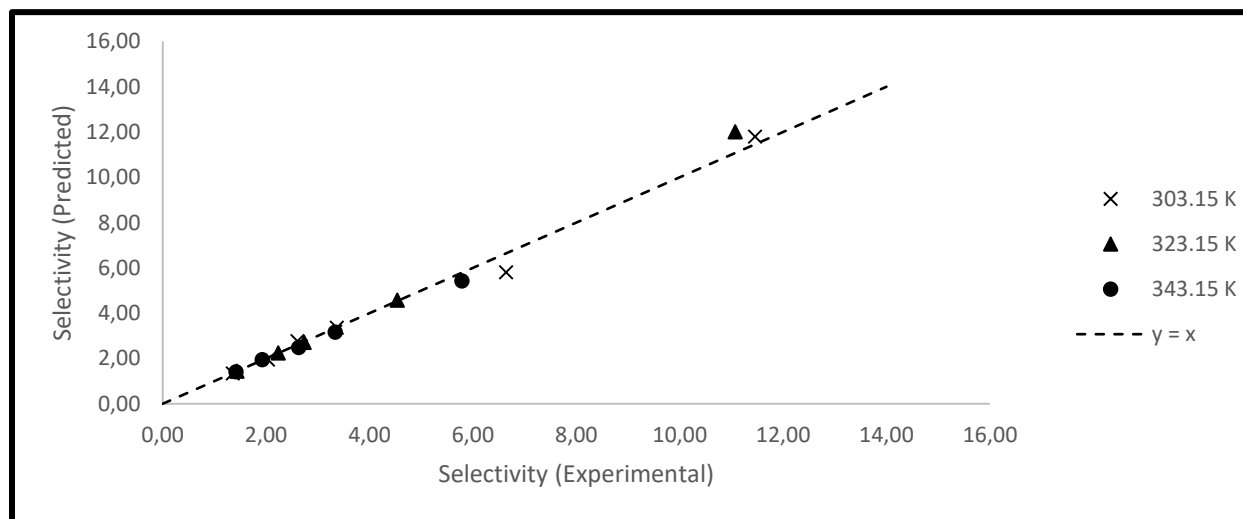


**Figure 7-12: Measured and predicted selectivity by NRTL model for the *n*-nonane (1) + toluene (2) + NFM (3) system.**

# 8

## CHAPTER EIGHT

### PROCESS DESIGN SIMULATION

This chapter serves to present a process design simulation for the separation of benzene, toluene, ethylbenzene and xylene isomers from a process stream consisting of a mixture of olefins and aromatics, using NFM as the solvent. The target recovery of aromatics was set to be at least 99%, and the process was developed and simulated using Aspen Plus V8.4 to achieve the target recovery. This process involves a combination of solvent extraction and extractive distillation using NFM as the solvent to effect the separation. The resulting process is then compared to the existing sulfolane process.

#### 8.1 Process Requirements

It is desired to extract aromatic compounds benzene, toluene, ethylbenzene, and xylene isomers from the feed naphtha in the naphtha cracking process, as opposed to extraction of aromatics from the products of the cracking process. The advantages offered by extraction from the feed stream include higher thermal efficiencies and less fouling thus leading to lower operational costs. The cracking process is illustrated in Chapter 2, Figure 2-5. A typical composition of feed naphtha containing 10 wt.% aromatics is presented in Table 8-1. This feed was used since it contains all variations of aromatics (BTEX) with a relatively low feed composition, and numerous other

components. The intention is to generate a simulation using a real process stream with many inherent complications to achieve recovery of aromatics at worst-case conditions.

**Table 8-1: Typical composition of feed naphtha (Meindersma and de Haan, 2008).**

<b>Component</b>	<b>wt. %</b>
<i>n</i> -Butane	1.5
<i>i</i> -Pentane	4.2
<i>n</i> -Pentane	10.3
Cyclopentane	1.5
2,3-Dimethyl-butane	0.8
2-Methyl-pentane	6.0
3-Methyl-pentane	4.0
<i>n</i> -Hexane	8.6
Me-cyclopentane	4.1
Benzene	1.8
Cyclohexane	2.8
2-Methyl-hexane	2.8
3-Methyl-hexane	3.8
<i>n</i> -Heptane	4.4
Methyl-cyclohexane	4.8
Toluene	3.0
2-Methyl-heptane	2.4
1,3-Dimecyclohexane	7.0
<i>n</i> -Octane	5.4
Ethyl-cyclohexane	2.0
2,6-Dimethyl-heptane	1.9
Ethyl benzene	2.0
<i>p</i> -Xylene	1.9
3-Methyl-octane	2.7
<i>o</i> -Xylene	1.0
<i>n</i> -Nonane	2.6
<i>n</i> -Decane	3.0
<i>i</i> -Decane	4.0

The primary requirement is separation and purification of the aromatic components in the above stream to achieve a minimum recovery of 99 wt.%. The capital cost is comparative to that of the existing processes using conventional solvents, as it is ensured that the process design simulation design results are within the scope of existing processes.

## 8.2 Thermodynamic Modelling

The choice of using the NRTL equation is founded on the model's capability in representing variations in ideality at low pressure, and the fact that its use was successfully demonstrated in similar investigations by Ko et al. (2002), DongChu et al. (2007), and Zhu et al. (2007). Additionally, the NRTL model was shown to represent the ternary systems better than the UNIQUAC model for the systems measured in this work, as discussed in Chapter 7. The binary interaction parameters resulting from regression of the ternary measurements of the *n*-nonane/*n*-decane-toluene-NFM system were provided as a user input. Due to the number of components in the feed mixture, 812 binary interaction parameters are required for a representative simulation. These are drawn automatically from the APV84 VLE-LIT and APV84 LLE-ASPEN databanks, while the UNIFAC model was used to estimate parameters for systems without existing experimental data. Ko et al. (2008) determined that the NRTL equation capably aided the simulation of extractive distillation using NFM, after using existing vapour-liquid equilibrium data and the binary interaction parameters of NFM with a variety of hydrocarbons to simulate the process using Aspen Plus. On the other hand, Zhu et al. (2002) predicted VLE data of NFM and numerous hydrocarbons using the UNIFAC group contribution method, finding the model data to agree with actual industrial operating data.

## 8.3 Process Modelling and Simulation

A sequence of columns was used to effect the aromatics recovery. This consists of a counter-current liquid-liquid extraction column, followed by four distillation columns in series. The final configuration of processing units is depicted in Figure 8-1. The following section details the process followed in determining the optimal configuration.

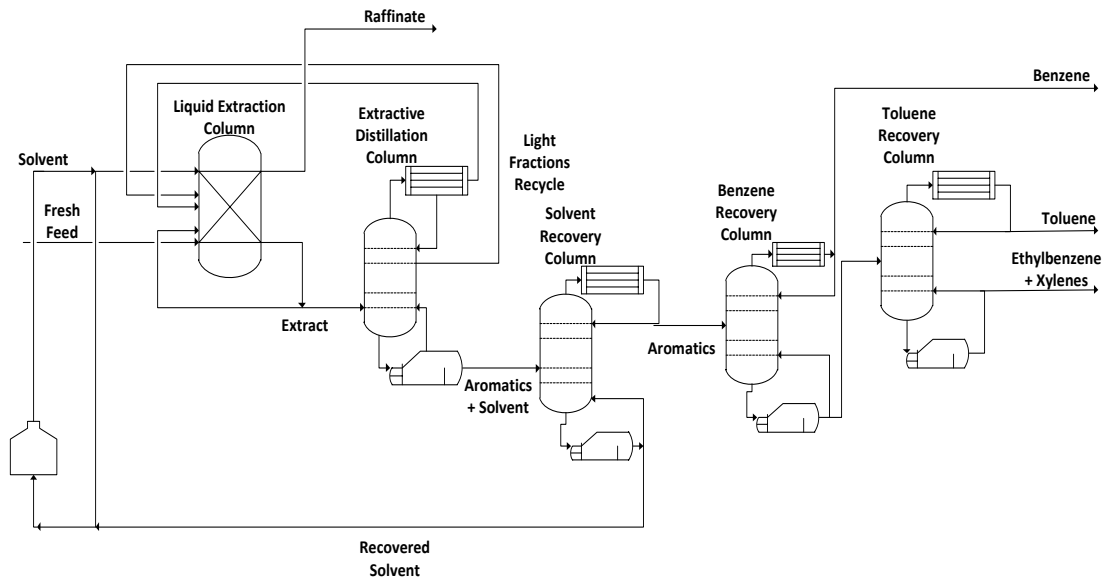


**Figure 8-1: Process flow diagram illustrating aromatics recovery process using NFM as the solvent.**

**Table 8-2: Operating conditions of main streams in separation process.**

	Mass Flow	Volume Flow	Temperature	Pressure	Molar Enthalpy	Enthalpy Flow
	Tons/h	L/min	°C	bar	cal/mol	kcal/sec
<b>Fresh Feed</b>	272	6439	20	1	-44377	-35773
<b>Aromatics + Solvent</b>	1000	13926	208	1	-74067	-179600
<b>Toluene</b>	9	184	110	1	4282	109
<b>Ethylbenzene + Xylenes</b>	14	321	138	1	-3001	-112
<b>Aromatics</b>	28	601	111	1	2514	201
<b>Recovered Solvent</b>	972	13771	240	1	-74691	-175130
<b>Solvent</b>	304	3510	20	1	-87873	-64431
<b>Benzene</b>	5	100	80	1	13590	235
<b>Extract</b>	1092	13300	20	1	-81267	-218510
<b>Raffinate</b>	257	6021	20	1	-50527	-38187

In developing the above process, a single liquid-liquid extractive unit was initially used with the fresh feed entering at the bottom and NFM at the top. The minimum solvent rate was then established by varying the solvent feed with the recovery of aromatics in the extract exiting at the bottom. The number of stages was fixed at 50 stages with the intent of optimization at the final stage of the design. The temperature profile and pressure at the feed stages was specified to be that of the inlet feed, such that the column operation is isothermal and isobaric.

Reviewing of the extract composition indicated that substantial portions of non-aromatics were being recovered in the extract by the solvent. The remaining aspects of the design focused on minimizing the recovery of non-aromatics while maintaining the achieved aromatic recovery. This was realized with the use of optimizing process conditions such as the solvent feed rate and temperature, as well as an extractive distillation column operating synchronously with the liquid-liquid extraction column.

As with the solvent extraction column, the extractive distillation column was specified with an overstated number of stages of 35 and reflux ratio of 5 with Murphree efficiencies of 0.8 incorporated per stage. The distillate of this column consists primarily of light fractions of paraffins, olefins, benzene, toluene and NFM. This is recycled to the solvent extraction column, allowing for the light fraction non-aromatics to be maximized in the raffinate. The same principle is applied to the raw extract, with which a portion is recycled to the solvent extraction column for recovery in the raffinate of heavy fractions such as *n*-octane, *n*-nonane and *n*-decane. A side stream is also recycled to maximize recovery of components such as methyl-cyclohexane, 2-methyl-heptane, 1,3-dimethylcyclohexane and 2,6-dimethyl-heptane.

The bottoms of the extractive distillation column consist of aromatics and NFM, and is transported to the next distillation column in the process, the solvent recovery column. The bottoms rate of this column was specified to be the solvent rate of NFM in the column feed, with the aim of achieving complete recirculation of the solvent between the liquid extraction and distillation units. Due to the high difference in boiling point between NFM and aromatic components, this separation is easily achieved. A buffer tank for the solvent is provided to the recirculating solvent to prevent accumulation of NFM within the system and to aid with control of the solvent to feed ratio.

The two columns successive to the solvent recovery column are for the individual recovery of benzene and toluene respectively. The separation of benzene from the aromatics stream is also easily achieved because of the high difference in volatilities. The same is true of the separation of toluene from the remaining aromatic components. The bottoms of the last column is a mixture of ethylbenzene and xylenes. This separation is not easily achieved because of the similarity in

boiling point between ethylbenzene, *p*-xylene and *o*-xylene. This separation process utilizes alternate techniques such as azeotropic distillation and does not form part of the scope of this investigation. Table 8-3 summarizes the primary outcomes of the simulation in terms of recovery.

**Table 8-3: Aromatics recovery achieved in separation process.**

<b>Component</b>	<b>Recovery</b>	<b>Target Recovery Met</b>
Benzene	99.9%	Yes
Toluene	99.8%	Yes
Ethylbenzene	99.5%	Yes
<i>p</i> -Xylene	99.8%	Yes
<i>o</i> -Xylene	99.8%	Yes
NFM	100%	Yes

## 8.4 System Specifications

After realizing the desired recovery of the aromatic components, the simulation operating parameters were then optimized to find the optimum process conditions and equipment specifications. These parameters include the solvent feed rate, column stages, feed stages, reflux ratio and boilup ratio. This was accomplished primarily with use of sensitivity analyses of each simulation block.

### 8.4.1 Liquid-Liquid Extraction Column

Table 8-4 lists the main column specifications and operating conditions. Due to the complex interaction effects between the liquid-liquid extraction column and extractive distillation column, a sensitivity analysis altering column specifications is not feasible because of the number of dependent variables involved, subsequently causing numerous simulation errors. Therefore, the column stages and feed stages were determined by manually determining different feasible solutions and selecting the most efficient.

**Table 8-4: Specifications for the liquid-liquid extraction column.**

Configuration	Number of Stages	22
	Valid Phases	Liquid-Liquid
	Solvent/Feed Ratio	4
	Solvent Rate from Storage (Tons/h)	304
	Fresh Feed Rate (Tons/h)	272
Stream Stage	Solvent Feed	1
	Fresh Feed	22
	Recycle Stream Feed	20
	Recycle Stream Feed	21
Pressure	Top Stage Pressure (bar)	1
	Bottom Stage Pressure (bar)	1
Temperature	Top Stage Temperature (°C)	20
	Bottom Stage Temperature (°C)	20

#### 8.4.2 Extractive Distillation Column

The distillate rate and reflux ratio were initially specified to be 25 Tons/h and 0.1 on a mass basis respectively. Isolated sensitivity analyses are not feasible due to the interactions between the two columns. If the reflux ratio is varied, the distillate and bottoms rate is affected which in turn affects the recycle streams. This influences the raffinate composition and extraction composition profiles and thereafter impacts the liquid-liquid extraction column extract rate. Different solvent rates and column specifications are required because of the change in recycle stream composition.

An optimization block was created in Aspen which varied the above parameters for both columns while setting the aromatic recoveries as an objective function, with the constraints being minimization of non-aromatic component recoveries in the bottoms of the extractive distillation column. The computing requirement proved excessive due to the number of variables and iterations involved (approximately 10 000), with the simulation subsequently not converging either. The distillate rate and reflux ratio were then fixed and the number of stages, feed stage, and side stream stage were varied incrementally while monitoring the aromatic and non-aromatics recovery in the bottoms. This resulted in several feasible scenarios generated with the optimal

selected and applied for the liquid-liquid extraction column and extractive distillation column simultaneously. Table 8-5 summarizes the column specifications and process conditions.

**Table 8-5: Specifications for the extractive distillation column simulated using Radfrac.**

Configuration	Number of Stages	15
	Condenser	Total
	Reboiler	Kettle
	Valid Phases	Vapour-Liquid-Liquid
	Distillate Rate (kmol/h)	500
	Reflux Ratio (mass basis)	0.1
	Murphree Efficiency	0.8
Streams	Feed	Above-Stage 2
	Side Stream	14
Pressure	Top Stage Pressure (bar)	1
	Bottom Stage Pressure (bar)	1
Condenser	Temperature (°C)	53
	Duty (MW)	5
Reboiler	Temperature	208
	Duty (MW)	120

### 8.4.3 Solvent Feed

The quantity of required solvent was optimized by varying the solvent rate and examining the resulting toluene recovery in the form of the distillate rate from the toluene recovery column. Figure 8-2 indicates the effect of solvent rate on toluene recovery, showing that increasing the solvent rate beyond a certain point has no appreciable impact on aromatics recovery. Toluene was used as the determining component because it is the aromatic component present in largest quantity, and is subsequently most limiting in terms of solvent requirement. The minimum solvent rate from buffer storage was determined to be 304 kmol/h. After mixing with the recycle solvent, the total solvent rate to the column is 984 kmol/h. The solvent to feed ratio was then determined to be 4.

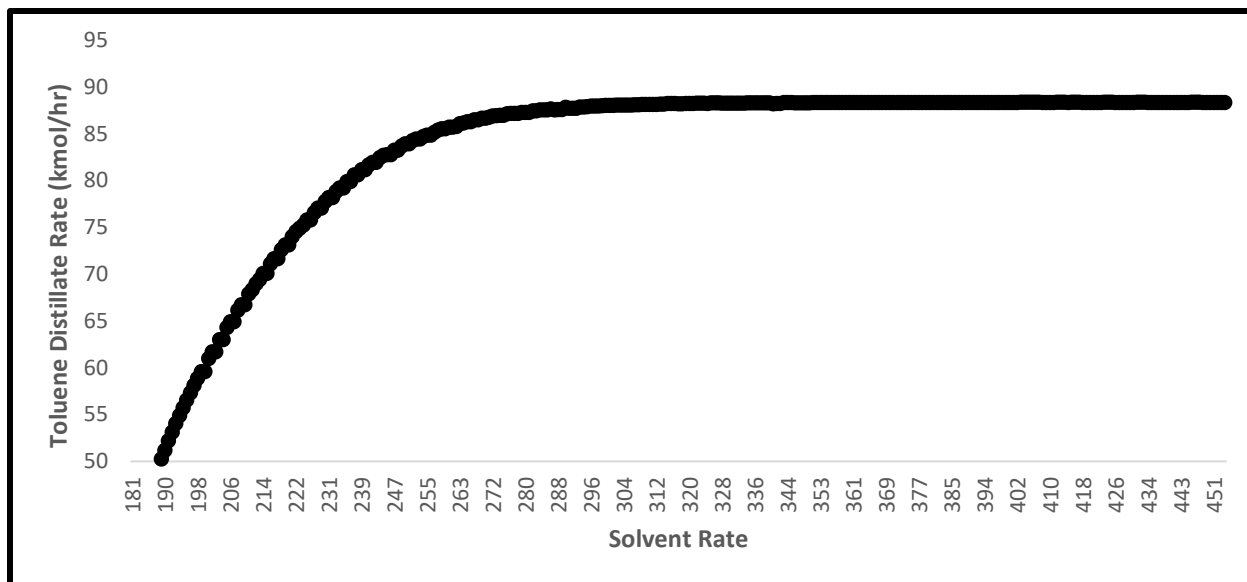


**Figure 8-2: Sensitivity analysis of solvent feed rate to extractor against toluene distillate rate.**

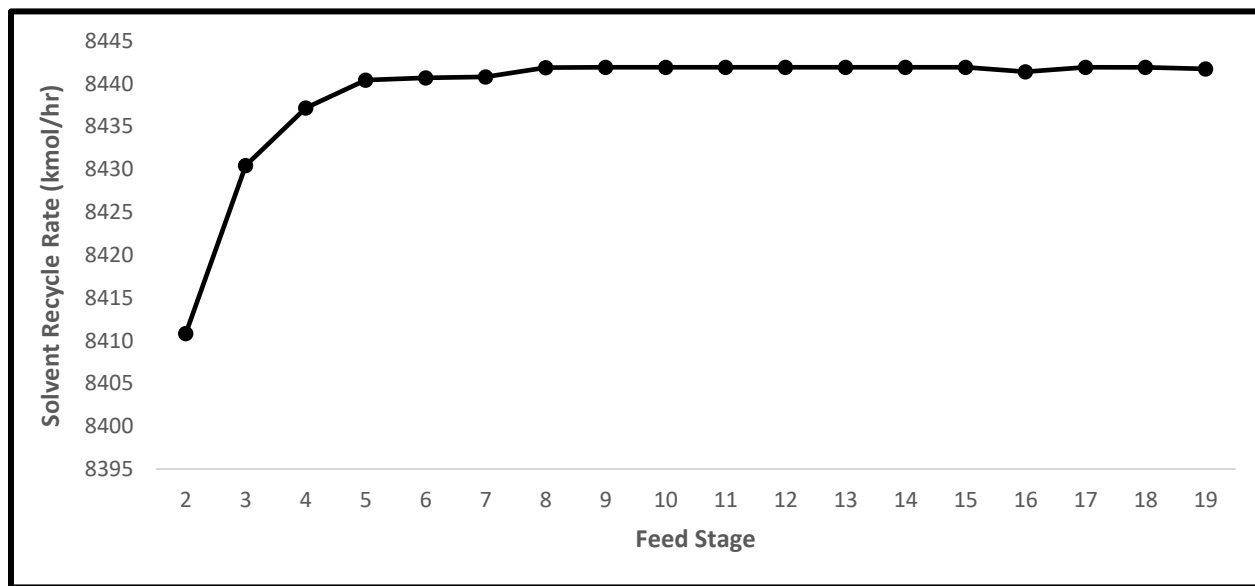
#### 8.4.4 Solvent Recovery Column

This column was initially specified at 30 stages with the bottoms rate at the NFM rate in the feed, and a boilup ratio of 1.2. The aim was to have complete recovery of the solvent i.e. all NFM in feed is returned to liquid-liquid extraction column. There were interacting effects on the entire system due to the NFM recycle. The quantity of NFM recycled varies with the solvent feed rate, implying that bottoms rate changes correspondingly, which will result in accumulation of solvent in either the extraction or distillation column. This in turn influences all previous column parameters. These issues were overcome with the inclusion of buffer storage, resulting in a portion of the recirculation recycled to the column and fresh solvent from buffer storage mixing with the recycle. This will also aid in improved control of the aromatic recovery under varying feed rates by allowing control of the solvent to feed ratio. There will also be improved energy efficiency in instances where the plant is operating under reduced feed and when reduced solvent rates are required, thereby reducing pumping costs. A Murphree efficiency of 0.8 was applied to all stages prior to optimization. This was to enable the process to be realistically compared to existing processes. Table 8-6 summarizes the final column conditions and specifications.

**Table 8-6: Specifications for the solvent recovery column simulated using Radfrac.**

Configuration	Number of Stages	21
	Condenser	Total
	Reboiler	Kettle
	Valid Phases	Vapour-Liquid
	Distillate Rate (kmol/hr)	288.37
	Boilup Ratio	1.2
Streams	Feed	Above-Stage 16
Pressure	Top Stage Pressure (bar)	1
	Bottom Stage Pressure (bar)	1
Condenser	Temperature (°C)	111
	Duty (MW)	117
Reboiler	Temperature	240
	Duty (MW)	136

This separation is effected more easily due to the high difference in boiling point between NFM and aromatics. The aromatic component with the largest boiling point is *o*-xylene at 144°C compared to NFM with a normal boiling point of 237°C. As there were no side streams, and the feed and number of stages did not affect solvent bottoms rate drastically, it was possible to run sensitivity analyses on the number of stages and feed stage, which are depicted in Figures 8-3 and 8-4. The feed stage and number of stages beyond which the recycle rate remained constant was taken as the optimal and is specified as such in Table 8-6.

**Figure 8-3: Sensitivity analysis of solvent recycle rate against feed stage.**

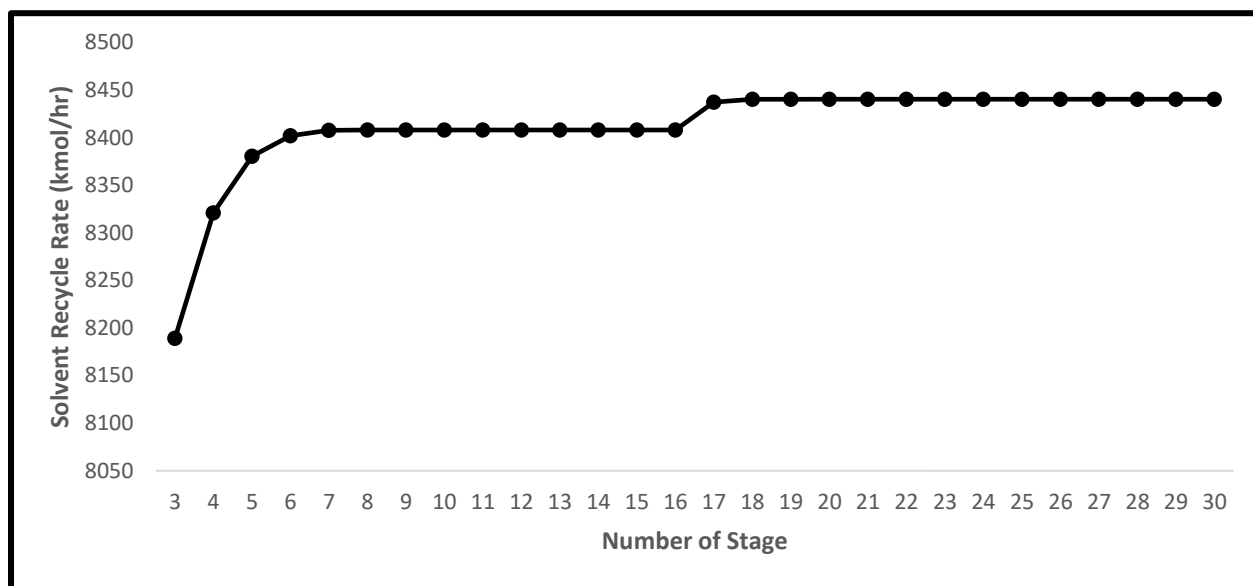


Figure 8-4: Sensitivity analysis of solvent recycle rate against number of stages.

#### 8.4.5 Benzene Recovery Column

The column was initially specified with the distillate rate at the benzene rate in the feed. The column stages were specified at 30 with the feed entering above stage 7, and the boilup ratio at 5. Benzene has the lowest boiling point of 80.1°C with toluene as the next lowest at 110.6°C at 1 atm. Therefore, this separation is achieved with simple distillation. The initial specified conditions were then subjected to sensitivity analyses to obtain optimal column specifications. The column feed stage, number of stages, and boilup ratio were varied against the benzene distillate, illustrated in Figures 8-5, 8-6, and 8-7, to achieve the best column specifications summarized in Table 8-7. The anomalous behaviour observed in Figure 8-6 is as a result of convergence issues in the simulation at that specific stage. Murphree efficiencies were specified for each stage.

**Table 8-7: Specifications for the benzene recovery column simulated using Radfrac.**

Configuration	Number of Stages	26
	Condenser	Total
	Reboiler	Kettle
	Valid Phases	Vapour-Liquid
	Distillate Rate (kmol/hr)	62.37
	Boilup Ratio	5.22
	Murphree Efficiency	0.8
Streams	Feed	Above Stage 15
Pressure	Top Stage Pressure (bar)	1
	Bottom Stage Pressure (bar)	1
Condenser	Temperature (°C)	80
	Duty (MW)	12
Reboiler	Temperature (°C)	125
	Duty (MW)	12

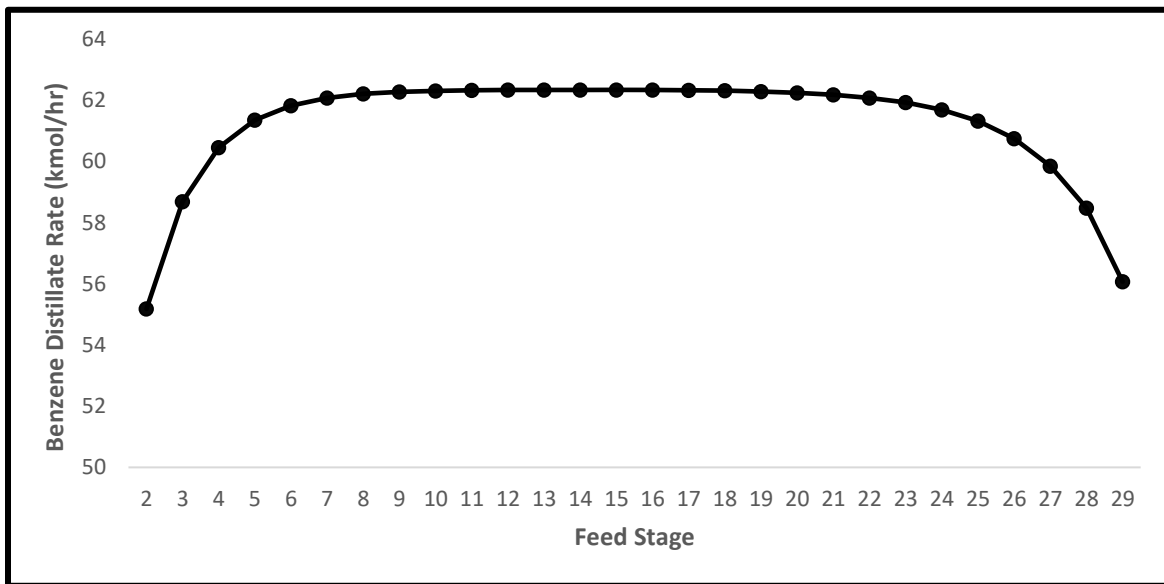


**Figure 8-5: Sensitivity analysis of benzene distillate rate against feed stage.**

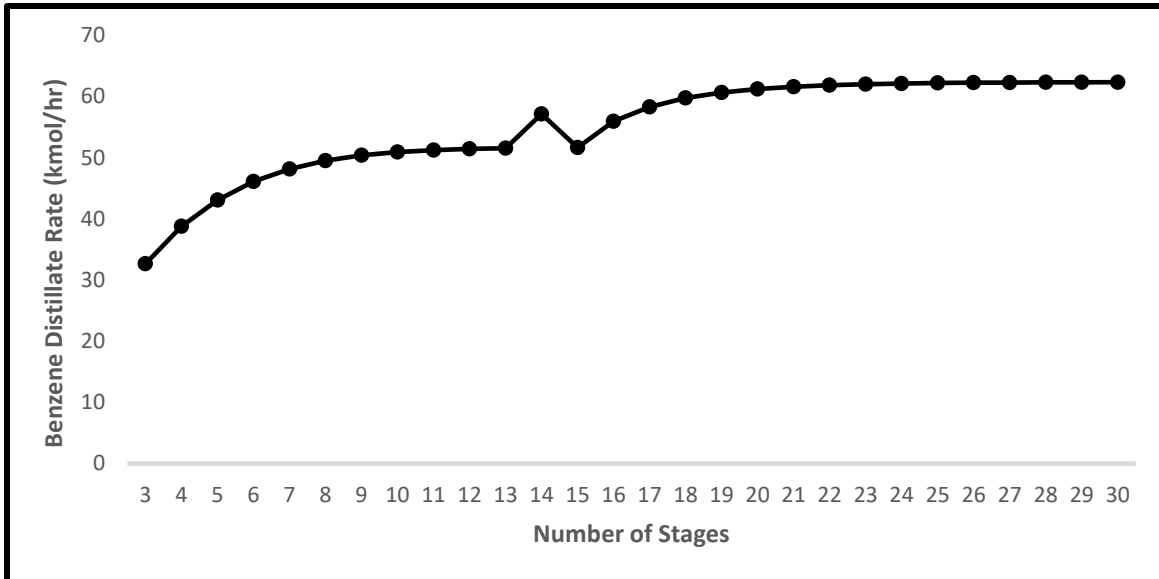


Figure 8-6: Sensitivity analysis of benzene distillate rate against number of stages.

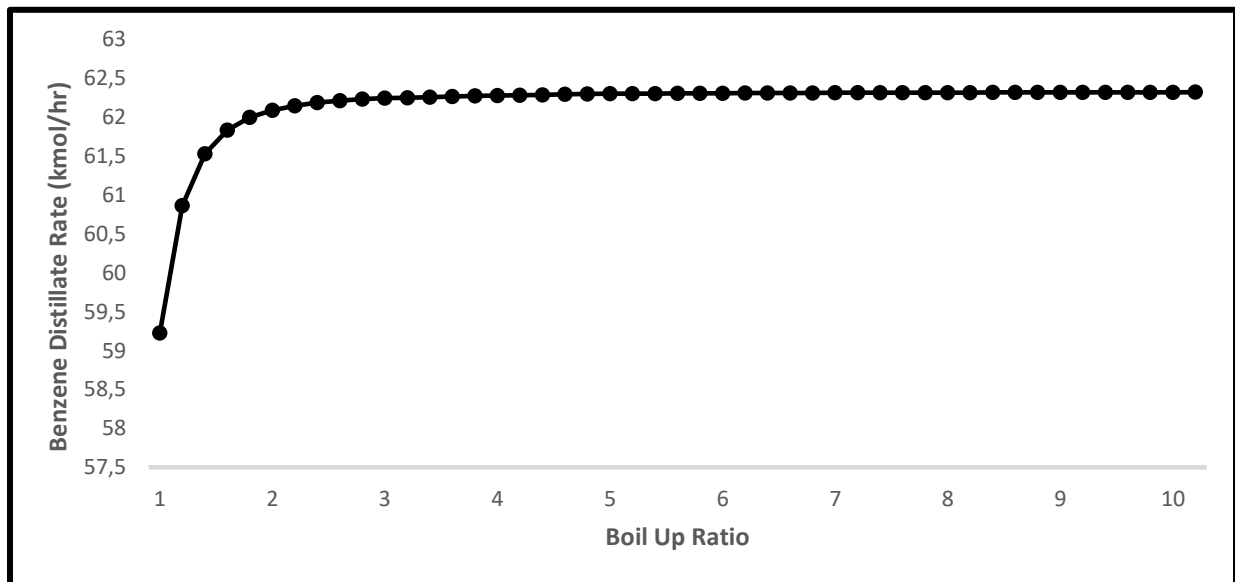


Figure 8-7: Sensitivity analysis of benzene distillate rate against benzene column boil up ratio.

#### 8.4.6 Toluene Recovery Column

The column was initially specified with the distillate rate equal to the toluene rate in the feed. The column stages were specified at 25 with the feed entering above stage 8, and the boilup ratio at 10.

Toluene has the lowest normal boiling point of the species considered in this system at 110.6°C with ethylbenzene as the next lowest at 136°C. Therefore, this separation is achieved with simple distillation. The initial specified conditions were then subjected to sensitivity analyses to obtain optimal column specifications. The column feed stage, number of stages, and boilup ratio were varied against the benzene distillate, illustrated in Figures 8-8, 8-9, and 8-10, to achieve the best column specifications summarized in Table 8-8. The anomalous behaviour observed in Figure 8-9 is as a result of convergence issues in the simulation at that specific stage. Murphree efficiencies were specified for each stage.

**Table 8-8: Specifications for the toluene recovery column simulated using Radfrac.**

Configuration	Number of Stages	25
	Condenser	Total
	Reboiler	Kettle
	Valid Phases	Vapour-Liquid
	Distillate Rate (kmol/hr)	92
	Boilup Ratio	5.95
	Murphree Efficiency	0.8
Streams	Feed	Above-Stage 12
Pressure	Top Stage Pressure (bar)	1
	Bottom Stage Pressure (bar)	1
Condenser	Temperature (°C)	110
	Duty (MW)	8
Reboiler	Temperature (°C)	138
	Duty (MW)	8

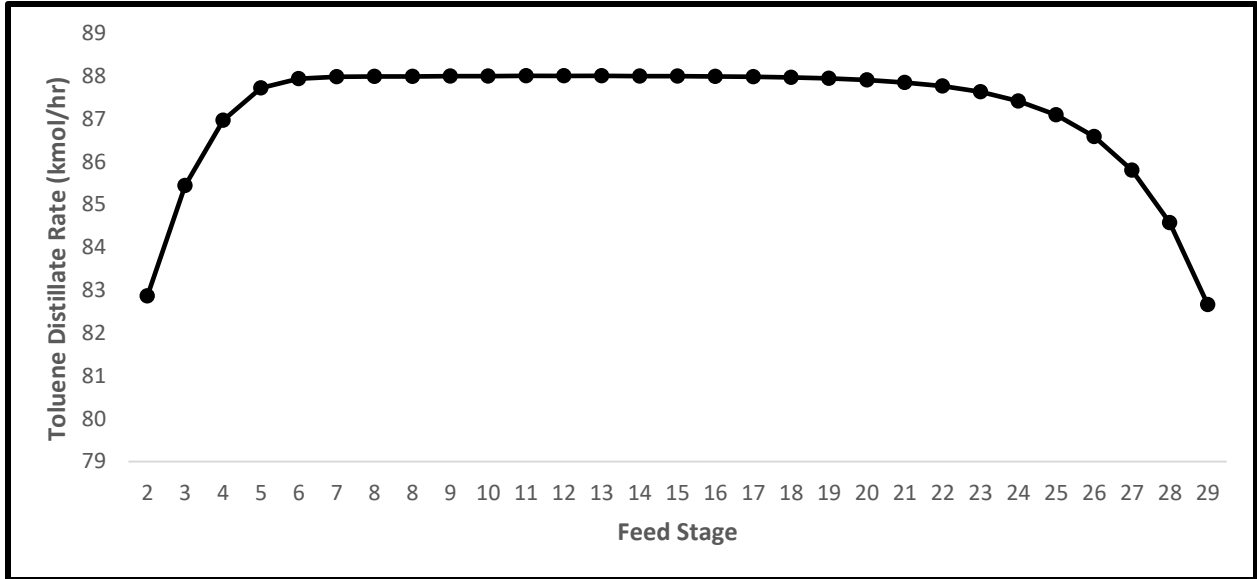


Figure 8-8: Sensitivity analysis of toluene distillate rate against feed stage.

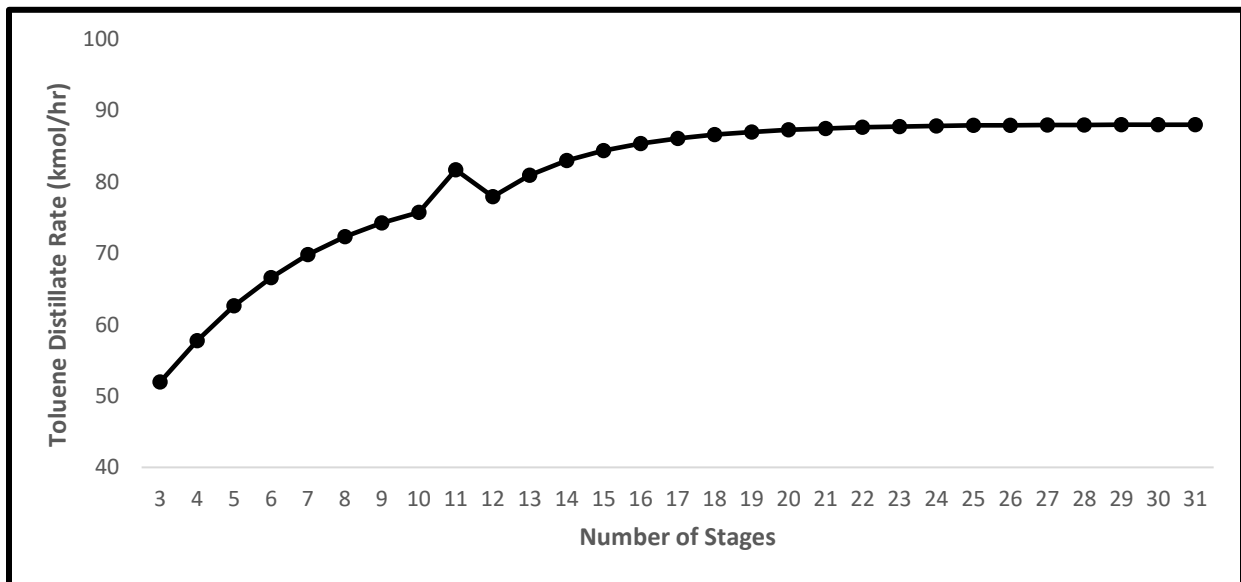
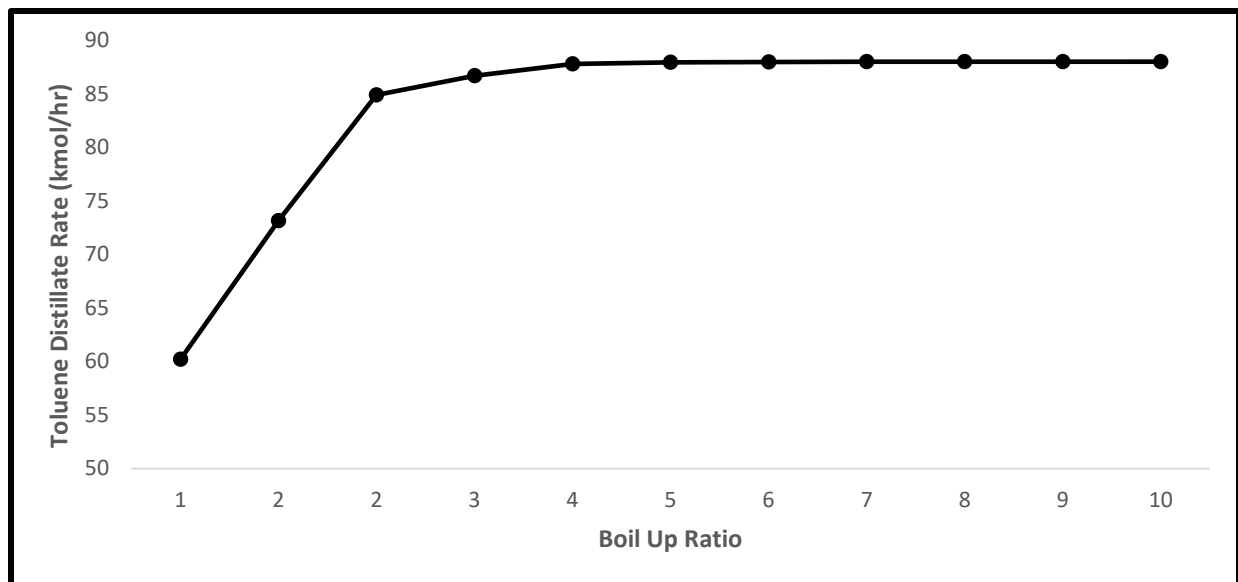


Figure 8-9: Sensitivity analysis of toluene distillate rate against number of stages.



**Figure 8-10: Sensitivity analysis of toluene distillate rate against column boil up ratio.**

The bottoms of this column contain a mixture of ethylbenzene, *p*-xylene and *o*-xylene. This separation is difficult due to the small differences in boiling point. Ethylbenzene has a normal boiling point of 136 °C, with *p*-xylene and *o*-xylene having normal boiling points of 138.4 °C and 144 °C respectively. Alternative separation processes such as azeotropic distillation should be considered.

## 8.5 Energy Comparison

As mentioned in Chapter 2, the sulfolane process consumes approximately 275-300 kcal of energy per kg of extract produced. The equivalent energy consumption was determined for this process using NFM as the solvent to gauge a comparison. This was achieved by a preliminary analysis on the heating and cooling requirements in the process. Table C-2 in Appendix C lists all the heat exchanges utilizing either HP or MP steam for heating and air for cooling. In general, the benzene and toluene recovery columns are not regarded as being part of the sulfolane process, which can be seen in Chapter 2, Figure 2-5. Therefore, the energy consumption of this specific process was calculated using only the condensers and reboilers of the extractive distillation column and solvent recovery column, utilizing HP steam. As this is a simulation of a conceptual design, the energy consumption of pumps and auxiliary equipment was not included. These are small energy

consumers comparatively, with their effect on the energy comparison being minor. The total duty of each energy transfer source is presented in Table 8-9.

**Table 8-9: Duty of major energy consumers and specific energy consumption.**

<b>Energy Source</b>	<b>Duty (kcal/h)</b>
High Pressure (HP) Steam	203 384 000
Air	85 096 800
<b>Total Duty (kcal/h)</b>	<b>288 480 800</b>
<b>Extract (kg/h)</b>	<b>1 091 500</b>
<b>Specific Energy Consumption (kcal/kg)</b>	<b>264</b>

Usage of HP steam is the major energy consumer in this process, accounting for approximately 71% of total energy consumption. The extract was taken to be the feed to the extractive distillation column and not the total extract from the column, as a portion of that is recycled. After converting this to kg/hr, the specific energy consumption was determined to be 264 kcal/kg. Comparing to the sulfolane process energy consumption in the literature of 275 – 300 kcal/kg (Meindersma and de Haan, 2008), the simulation indicates that the process developed consumes at least 11 kcal/kg less energy. At the process conditions simulated, this translates to an energy saving of 288 156 000 kcal/day, which converts to 334 901 kWh/day. If coal is the fuel source used to generate steam in a boiler, the energy saved manifests in coal saving. MacDonald et al. (2009) reported a coal calorific value of 35 MJ/Kg, which was converted to 9.7 kWh/kg, signifying a coal saving of 34.5 Tons/day. A price quotation of coal in the region of R1500/Ton was obtained from a local anthracite coal supplier on the 29/08/2017. Therefore, the saving in terms of coal is R51 789 a day and R19 million per year. This is approximately 5% of the total coal usage. Coal is used as an illustration here, however the nature of the monetary savings depends on the boiler type, conditions, and type of fuel used.

A detailed comparison of the two processes must be conducted to ascertain a complete picture of the differences in energy consumption. Energy use for a given period is governed by changing process conditions such as feed composition, feed rate, feed temperature, solvent rate, desired aromatics recovery, optimal process integration, level of equipment maintenance, and actual

optimal plant operation. To obtain the most accurate comparison of energy comparison, the sulfolane process feed rates and composition must align with the process feed conditions and the energy consumption determined in the developed process.

Developing this simulation offers existing processes the opportunity to become more energy efficient and substantially reduce costs by implementing process improvements and optimization techniques to operating conditions. It is possible to modify this simulation to match an existing aromatics recovery process that uses NFM or even other solvents, and find alignment between the simulation results and plant data by varying the column efficiencies. Once alignment is reached, operating parameters such as solvent rates, solvent to feed ratio, operating temperatures and pressures, as well as column parameters such as reflux ratios, can be varied to find the best operating point of the actual facility while achieving the desired recovery. Thereafter, implementation of these optimized parameters offers costs benefits with improved energy efficiency and a reduced carbon footprint. Future legislation in the form of carbon tax is likely to impose further penalties on carbon-emitting industrial facilities. Adopting such process modifications is forward-thinking in this regard, even if return on investments are lower in the short term.

# 9

## CHAPTER NINE

### CONCLUSION

The focus of this work consisted of two elements. One was concerned with phase equilibrium studies of two ternary systems which each comprised of a heavy hydrocarbon and toluene, with the suitability of NFM as an extraction solvent investigated. Liquid-liquid equilibrium measurements were conducted at three temperatures for each ternary system. The other aspect of this study was the development and simulation of a conceptual process design using Aspen Plus V8.4 to demonstrate the separation and recovery of aromatics, and make a comparison to an existing process which uses a different solvent.

The LLE measurements were conducted with the modified apparatus of Raal and Brouckaert (1992), with modifications introduced by Ndlovu (2005) that improved thermal insulation and sampling procedures, and later modifications incorporating an adjustable temperature sleeve and magnetic stirrer (Narasigadu et al., 2014). The binary *n*-heptane + methanol system at 1 atm was used as a test system to verify the credibility of the equipment used and the procedures employed. The test system equilibrium measurements agreed with the data of Katayama and Ichikawa (1995), as well as Higashiuchi et al. (1987). The new ternary LLE data revealed that NFM can be used as a solvent to extract toluene from a mixture of heavy hydrocarbons containing *n*-nonane and *n*-decane. This was supported by the calculated results of the distribution coefficient, separation factor, and selectivity. The selectivity varied between 1.35 – 6.64 for both systems at varying

concentrations of toluene at the measured temperatures. Extraction using NFM is feasible due to the selectivity values being greater than one.

The resulting data of the ternary system measurements were analyzed and regressed with the NRTL and UNIQUAC liquid phase activity coefficient models. It was observed that both ternary systems at each temperature exhibited a type I system (Treybal, 1963). The NRTL model was found to provide the best fit to the tie-lines of all the systems at all temperatures on the basis of the calculated Root Mean Square Deviation (RMSD) which was between 0.002 and 0.02 for all systems measured.

A process design simulation for the separation of benzene, toluene, ethylbenzene and xylenes from a process stream consisting of a mixture of olefins and aromatics, using NFM as the solvent was developed using Aspen Plus V8.4. The aim was to target a recovery of at least 99% aromatics, which was achieved. A sequence of columns was used to effect the aromatics recovery consisting of a counter-current liquid-liquid extraction column, followed by four distillation columns in series. Process conditions and column specifications were optimized by investigating numerous unit configurations and running sensitivity analyses on these parameters. The simulated process was determined to consume at least 11 kcal/kg extract less energy than the sulfolane process. This manifests as lower heating and steam requirements, resulting in reduced costs of at least R19 million per annum.

# 10

## CHAPTER TEN

### RECOMMENDATIONS

To improve the versatility of the LLE measurements and the conceptual design simulation results, the following recommendations can be considered:

- 1) An alternative GC column be used to reduce the retention time of NFM. A single run takes 55 minutes to complete for a single injection with the column used in this investigation. This impacts the number of samples that can be analyzed in a given time period.
- 2) Measurements can be conducted on other ternary systems with other alkanes and branched alkanes not currently available in the open literature to investigate the selectivity of NFM towards benzene, toluene, ethylbenzene and xylenes in these mixtures. This is due to the nature and complexity of actual process streams containing multiple components.
- 3) Other liquid phase activity coefficient models be considered such as the model of Tsuboka and Katayama (1975), to investigate if other models display superior representations to the NRTL model.
- 4) The simulated process design be modified with the usage of different solvents to ensure a consistent comparison of the energy consumption and operating costs of different processes.
- 5) The simulation be calibrated with an existing aromatics recovery process such that process operating parameters be optimized to realize maximum energy efficiency and cost reduction.

---

## REFERENCES

Alders, L, (1959), "Liquid-Liquid Extraction", 2nd edition, Elsevier, Amsterdam.

Aspen Plus, (2004), "Physical Properties and Methods", Cambridge, MA: Aspen Technology Incorporation.

Bhownath, N, (2008), "The Use of n-Dodecane as a Solvent in the Extraction of Light Alcohols from Water", Master of Science in Engineering (Chemical Engineering) Thesis, University of KwaZulu-Natal, South Africa.

Briggs, S W and Comings, E W, (1943), "Effect of Temperature on Liquid-Liquid Equilibrium: Benzene - Acetone - Water and Docosane - 1,6-Diphenylhexane - Furfural System", *Industrial and Engineering Chemistry*, Vol. 35, pp. 411- 417.

Cincotti, A, Murru, M, Cao, G, Marongiu, B, Masia, F and Sannia, M, (1999), "Liquid-Liquid Equilibria of Hydrocarbons with N-Formylmorpholine", *Journal of Chemical Engineering Data*, Vol. 44, pp. 480-483.

Chen, Q L, Wang, Q, Zhang, B J, He, C and He, C C, (2017), "Optimal design of a new aromatic extractive distillation process aided by a co-solvent mixture", *Energy Procedia*, Vol. 105, pp. 4927-4934

Cho, J, Ko, M S, Na, S, Kim, H, (2002), "Simulation of the Aromatic Recovery Process by Extractive Distillation", *Korean Journal of Chemical Engineering*, Vol. 19, pp. 996-1000

DongChu, C, HongQi, Y and Hao, W, (2007), "(Liquid + liquid) equilibria of three ternary systems: (heptane + benzene + N-formylmorpholine), (heptane + toluene + N-formylmorpholine), (heptane + xylene + N-formylmorpholine) from T = (298.15 to 353.15) K", *Journal of Chemical Thermodynamics*, Vol. 39, pp. 1182-1188.

Delancey, G, (2013), "Principles of Chemical Engineering Practice", John Wiley & Sons, New Jersey

DongChu, C, HongQi, Y and Hao, W, (2007), "Measurement and Correlation of Liquid-Liquid Equilibria of Methylcyclohexane + Toluene + N-Formylmorpholine at (293, 303, 313, and 323) K", *Journal of Chemical Engineering Data*, Vol. 52, pp. 1297-1301.

Gary, J H, Handwerk, G E, (1984), *Petroleum refining. Technology and economics*, Marcel Dekker, New York-Basel.

Higashiuchi, H, Sakuragi, Y, Iwai, Y, Arai, Y, Nagatani, M, (1987), "Measurement and correlation of liquid-liquid equilibria of binary and ternary systems containing methanol and hydrocarbons", *Fluid Phase Equilibria*, Vol. 36, pp. 35-47

Humphrey, J L, Rocha, J A and Fair, J R, (1984), "Essentials of Extraction", *Chemical Engineering (New York)*, Vol. 91, pp. 76-95.

Johnson, J A, (1986), *Handbook of petroleum refining processes*, McGraw-Hill, New York-London.

Jones, D S J and Pujado, P R, (2006), "Handbook of Petroleum Processing", Springer, Netherlands

Katayama, H, Ichikawa, M, (1995), "Liquid-liquid equilibria of three ternary systems: methanol-heptane including 1,3-dioxolane, 1,4-dioxane and tetrahydropyran in the range of 253.15 to 303.15K", *Journal of Chemical Engineering Japan.*, Vol. 28, pp. 412-418

Ko, M, Na, S, Cho, J, Kim, H, (2002), "Simulation of the recovery process by extractive distillation" *Korean Journal of Chemical Engineering*, Vol. 19(6), pp. 996-1000

Ko, M, Na, S, Cho, J, Kim, H, (2002), "Liquid-liquid equilibria for binary systems containing N-formylmorpholine", *Journal of Chemical Engineering Data*, Vol. 47, pp. 923-926

Ko, M, Na, S, Lee, S, Kim, H, (2003), "Liquid-liquid equilibria for the binary systems of N-formylmorpholine with cycloalkanes" *Journal of Chemical Engineering Data*, Vol. 48, pp. 249-252

Ko, M, Na, S, Kwon, S, Lee, S, Kim, H, (2003), "Liquid-liquid equilibria for the binary systems of N-formylmorpholine with branched cycloalkanes", *Journal of Chemical Engineering Data*, Vol. 48, pp. 699-702

Lasich, M, Moodley, T, Bhowanath, R, Naidoo, P, Ramjugernath, D, (2011), "Liquid-Liquid Equilibria of Methanol, Ethanol and Propan-2-ol with Water and Dodecane", *Journal of Chemical Engineering Data*, Vol. 56, pp. 4139-4146.

Lange, N A, (1999), "Handbook of Chemistry", 15<sup>th</sup> Edition, Handbook Publishers, Ohio

Letcher, T M, Siswana, P M, van der Watt, P and Radloff, S, (1989), "Phase Equilibria for (an Alcohol + p-Xylene + Water) at 298.2 K", *Journal of Chemical Thermodynamics*, Vol. 21, pp. 1053-1060.

MacDonald, M, Chadwick, Aslanian, G, (2009), "The Environmental Management of Low-Grade Fuels", Volume 5, Earthscan, UK.

Meindersma, G W, de Haan, A B, (2008), "Conceptual process design for aromatic/aliphatic separation with ionic liquids", *Chemical Engineering Research and Design*, Vol. 86, pp. 745-752.

Moriyoshi, T, Uosaki, Y, Sakamoto, T and Hayashi, Y, (1989), "(Liquid + Liquid) Equilibria of (Water + Ethanol + 2,6-Dimethyl-4-heptanone) from 0.1 to 200 MPa at 298.15 and 323.15 K", *Journal of Chemical Thermodynamics*, Vol. 21, pp. 219-224.

Naicker, P K, (1997), "Thermodynamics of liquid mixtures containing N-methyl-2-Pyrrolidone", Master of Science (Chemistry) Thesis, University of KwaZulu-Natal, South Africa.

Naidoo, R D, (2003), "The Thermodynamics of Liquids in Solution at 298 K and 1 atm", Master of Science (Chemistry) Thesis, University of KwaZulu-Natal, South Africa.

Narasigadu, C, (2006), "Phase Equilibrium Investigation of the Water and Acetonitrile Solvent with Heavy Hydrocarbons", Master of Science in Engineering (Chemical Engineering) Thesis, University of Natal, South Africa.

Narasigadu, C, Naidoo, M and Ramjugernath, D, (2014), "Ternary Liquid-Liquid Equilibrium Data for the Water + Acetonitrile + {Butan-1-ol or 2-Methylpropan-1-ol} Systems at (303.2, 323.2, 343.2) K and 1 atm", *Journal of Chemical Engineering Data*, Vol. 59, pp. 3820-3824.

Narasigadu, C, Raal, J D, Naidoo, P, Ramjugernath, D, (2011), "Ternary Liquid-Liquid Equilibria of Acetonitrile and Water with Heptanoic Acid and Nonanol at 323.15 K and 1 atm", *Journal of Chemical Engineering Data*, Vol. 54, pp. 735-738.

Ndlovu, M, (2005), "Development of a Dynamic Still for Measuring Low Pressure Vapour Liquid-Liquid Equilibria (Systems of Partial Liquid Miscibility)", Master of Science in Engineering (Chemical Engineering) Thesis, University of KwaZulu-Natal, South Africa.

Novak, J P, Matous, J and Pick, J, (1987), "Liquid-Liquid Equilibria", Elsevier, Amsterdam.

Null, H R, (1980), "Phase Equilibrium in Process Design", Robert E Krieger, New York.

Orge, B, Casas, L M, Ferreira, O, (2008), "Liquid-Liquid Equilibria of Mixtures Containing Methyl Acetate + Methanol + Hexane or Heptane", *Journal of Chemical Engineering Data*, Vol. 53, pp. 89-93.

Orge, B, Iglesias, M, Rodriguez, A, Canosa, J M, Tojo, J, (1997), "Mixing properties of (methanol, ethanol, or 1-propanol) with (n-pentane, n-hexane, n-heptane and n-octane) at 298.15 K", *Fluid Phase Equilibria*, Vol. 133, pp. 231-227

Raal, J D and Brouckaert, C J, (1992), "Vapour-Liquid and Liquid-Liquid Equilibria in the System Methyl Butenol-Water", *Fluid Phase Equilibria*, Vol. 74, pp. 253-270.

Redhi, G, (2003), "Thermodynamics of Liquid Mixtures Containing Carboxylic Acids", Doctor of Philosophy (Chemistry) Thesis, University of Natal, South Africa.

Reinhardt, H, Rydeberg, J, "Solvent Extraction Studies AKUFVE Method: A new Centrifuge for absolute phase separation", *Acta Chemical Scandinavia*, (1969), Vol. 23, pp. 2773.

Rifai, I and Durandet, J, (1962), *Rev. Inst. France di Petrol*, Vol. 17, pp. 1232, as given by Novak et al. (1987).

Saha, M, Rawat, B S, Khanna M K and Nautiyal, B R, (1998), "Liquid-Liquid Equilibrium Studies on Toluene + Heptane + Solvent", *Journal of Chemical Engineering Data*, Vol. 43, pp. 422-426.

Saha, M, Rawat, B S, Khanna M K and Nautiyal, B R, Raghuram, M V, (1999), "Extraction of aromatics from naphtha reformat using combination solvents", *Indian Journal of Chemical Technology*, Vol. 6, pp. 85-89.

Sherwood, T. K., (1937), "Absorption and Extraction," McGraw-Hill Book Company, Inc., New York

Skoog, D A, West, D M and Holler, F J, (1991), "Fundamentals of Analytical Chemistry", 6<sup>th</sup> edition, Saunders College Publishing, Florida.

Sørensen, J M, Magnussen, T, Rasmussen, P and Fredenslund, A, (1979), "Liquid-Liquid Equilibrium Data: Their Retrieval, Correlation and Prediction, Part I: Retrieval", *Fluid Phase Equilibria*, Vol. 2, pp. 297-309.

Sørensen, J M, Magnussen, T, Rasmussen, P and Fredenslund, A, (1979), "Liquid-Liquid Equilibrium Data: Their Retrieval, Correlation and Prediction, Part II: Correlation", *Fluid Phase Equilibria*, Vol. 3, pp. 47-82.

Sørensen, J M, Magnussen, T, Rasmussen, P and Fredenslund, A, (1980), "Liquid-Liquid Equilibrium Data: Their Retrieval, Correlation and Prediction, Part III: Prediction", *Fluid Phase Equilibria*, Vol. 4, pp. 151-163.

Tagliavini, G, Arich, G, (1958), "Liquid-liquid equilibrium in the system methanol + heptane + morpholine", *Ric. Sci.*, Vol. 28, pp. 1902-1910

Treybal, R. E., (1963), "Liquid Extraction", 2<sup>nd</sup> Edition, McGraw-Hill, New York

Weissermel, K, Arpe, H J, (2003), "Industrial Organic Chemistry", 4<sup>th</sup> Edition, Wiley Verlag GmbH & Co. KGaA, Weinheim

Xia, S, Huang, X, Ma, P, Song, S and Ma, B, (2008), "Vapor-Liquid Equilibrium of N-Formylmorpholine with Toluene and Xylene at 101.33 kPa", *Journal of Chemical Engineering Data*, Vol. 53, pp. 252-255.

Zahed, A. H., Yorulmaz, Y, Gashghari, M. A, (1992), "Extraction of BTX Hydrocarbons from Saudi Arabian Refinery Platformates", *JKAU: Eng. Sci.*, Vol. 4, pp. 101-114.

Zhigang, L, Biaohuca, C, Zhongwei, D, (2005), "Special Distillation Processes", 1<sup>st</sup> Edition, Elsevier, Amsterdam

Zhu, H, Shi, X, Zhou, W, (2008), "Process simulation and parameter optimization of separating aromatics and non-aromatics by extractive distillation with N-formylmorpholine", *Journal of East China University of Science and Technology (Natural Science Edition)*, Vol. 34, pp. 309-314

## APPENDIX A

### Criterion for Phase Equilibrium

Thermodynamic properties relate the temperature and pressure of a closed system using the definition of the Gibbs energy:

$$d(nG) = (nV)dP - (nS)dT \quad (\text{A-1})$$

If there are no chemical reactions in a single-phase system to which Equation (A-1) is applied then the implication is that the composition of the system is constant, leading to the following deductions:

$$\left[ \frac{\partial(nG)}{\partial P} \right]_{T,n} = nV \quad (\text{A-2})$$

$$\left[ \frac{\partial(nG)}{\partial T} \right]_{P,n} = -nS \quad (\text{A-3})$$

The subscripts mean that those properties are held constant while  $n$  denotes the number of moles the chemical species in the system.

For an open system, the Gibbs energy is still a function of temperature and pressure, however also becomes a function of the number of moles due to the fact that the system interacts with the surroundings. Hence:

$$nG = g(P, T, n) \quad (\text{A-4})$$

Taking the differential of Equation (A-4) results in:

$$d(nG) = (nV)dP - (nS)dT + \sum_i \mu_i dn_i \quad (\text{A-5})$$

and:

$$\mu_i = \left[ \frac{\partial(nG)}{\partial n_i} \right]_{P,T,n_j} \quad (\text{A-6})$$

where Equation (A-6) is defined as the chemical potential ( $\mu_i$ ) of species  $i$  in the mixture.

Consider two phases  $\alpha$  and  $\beta$  that are in equilibrium in an overall closed system. The system can be modeled with each phase being considered an open system that interact with mass transfer between phases. After applying a constraint of constant temperature and pressure across the system, Equation (A-5) can be expressed individually for each phase:

$$d(nG)^\alpha = (nV)^\alpha dP - (nS)^\alpha dT + \sum_i \mu_i^\alpha dn_i^\alpha \quad (\text{A-7})$$

$$d(nG)^\beta = (nV)^\beta dP - (nS)^\beta dT + \sum_i \mu_i^\beta dn_i^\beta \quad (\text{A-8})$$

The sum of Equations (A-7) and (A-8) gives the change in the total Gibbs energy for this system.

The total system property can be expressed by the following relation:

$$nM = (nM)^\alpha + (nM)^\beta \quad (\text{A-9})$$

where  $M$  represents any extensive thermodynamic property. Application of Equation (A-9) shows:

$$d(nG) = (nV)dP - (nS)dT + \sum_i \mu_i^\alpha dn_i^\alpha + \sum_i \mu_i^\beta dn_i^\beta \quad (\text{A-10})$$

Equation (A-1) can be applied due to the assumption of a closed system. A comparison of Equation (A1) and (A-10) at equilibrium indicates that:

$$\sum_i \mu_i^\alpha dn_i^\alpha + \sum_i \mu_i^\beta dn_i^\beta = 0 \quad (\text{A-11})$$

The terms  $dn_i^\alpha$  and  $dn_i^\beta$  represent changes in mole fraction due to mass transfer between phases. For a non-reactive system, the law of mass conservation requires that  $dn_i^\alpha = dn_i^\beta$ . Hence Equation (A-11) becomes:

$$\sum_i (\mu_i^\alpha - \mu_i^\beta) dn_i^\alpha = 0 \quad (\text{A-12})$$

Since the changes  $dn_i^\alpha$  are independent and arbitrary, Equation (A-12) is reduced to zero when the preceding term in brackets is zero, giving rise to the following conclusion:

$$\mu_i^\alpha = \mu_i^\beta \quad (\text{A-13})$$

A generalized form Equation (A-13) results when it is extended to multiple phases. Considering a closed system comprising  $N$  chemical species and  $\pi$  phases at the same temperature and pressure, results in:

$$\mu_i^\alpha = \mu_i^\beta = \dots = \mu_i^\pi \quad (\text{A-14})$$

where  $i = 1, 2, \dots, N$ .

The criterion for equilibrium is thus defined for a closed system consisting of multiple phases at the same temperature to pressure, to be that chemical potential of each species is the same in all phases (Smith et al., 2001).

## APPENDIX B

**Table B-1: Calibration results for temperature sensors in this investigation.**

Probe/Sensor Description	Calibration Equation	Temperature Range	Calibration Uncertainty $\Delta T$ / K
Equilibrium Cell 1	$T_{Actual} = 1.001851T_{Display} + 0.06471$	293.25 K to 373.25 K	0.02
Equilibrium Cell 2	$T_{Actual} = 1.001346T_{Display} + 0.1184$	293.25 K to 373.25 K	0.01

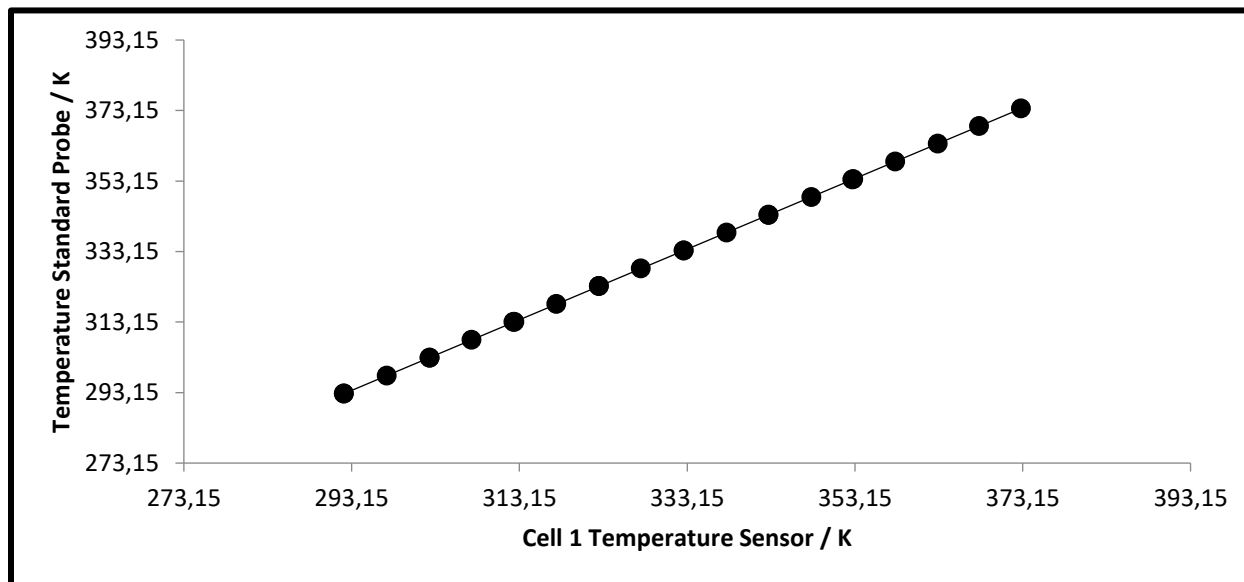


**Figure B-1: Temperature calibration plot of cell 1 temperature sensor.**

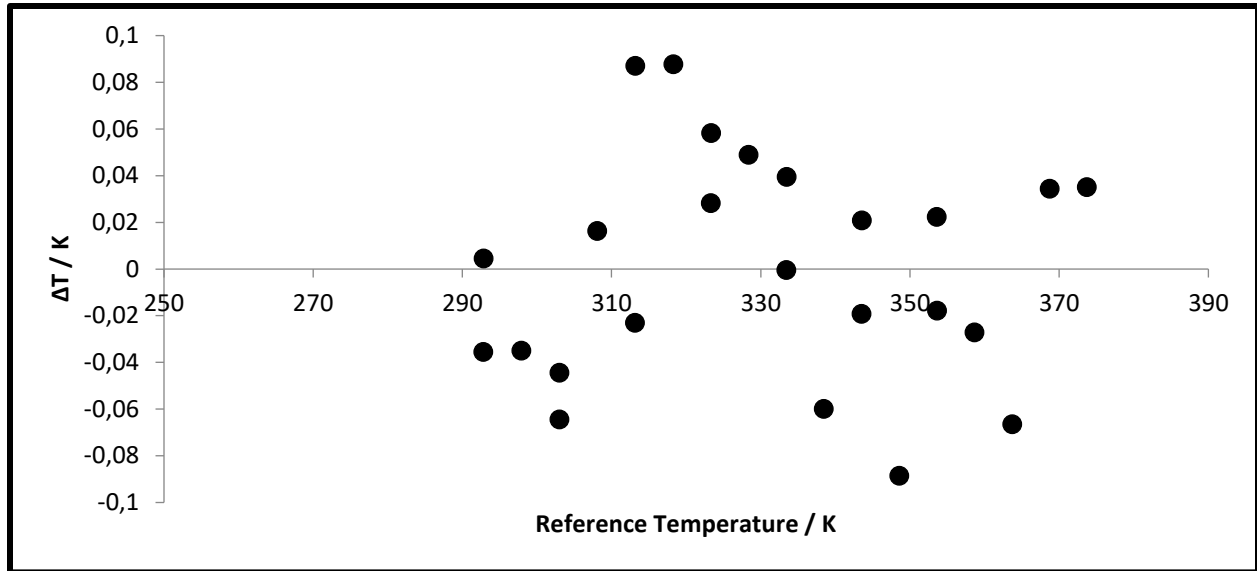


Figure B-2: Temperature deviation plot of cell 1 temperature sensor.

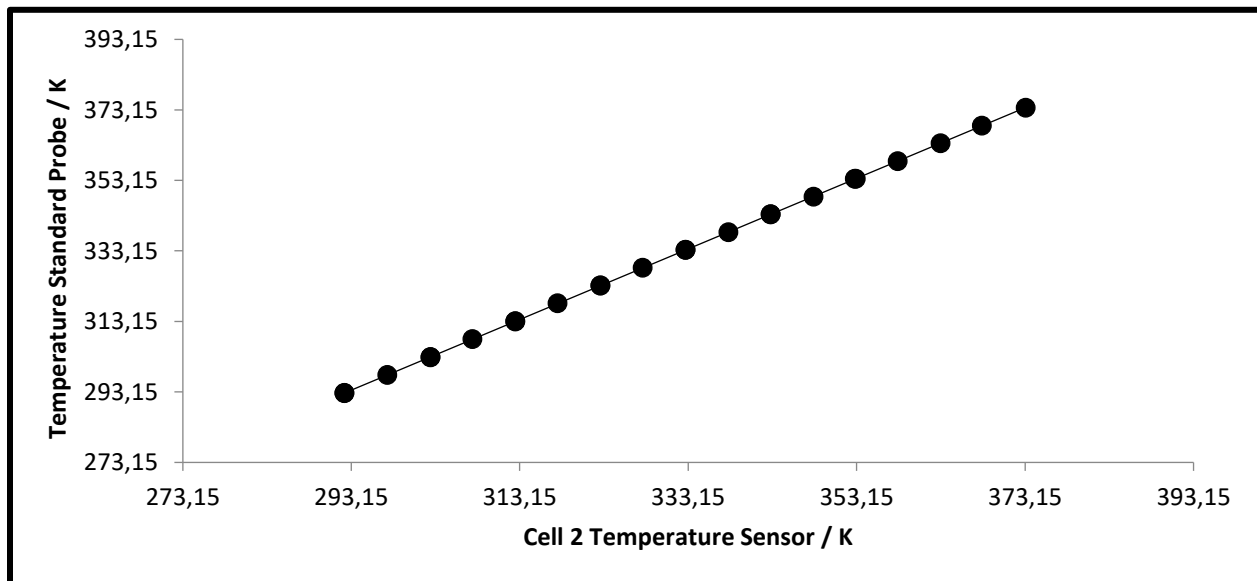
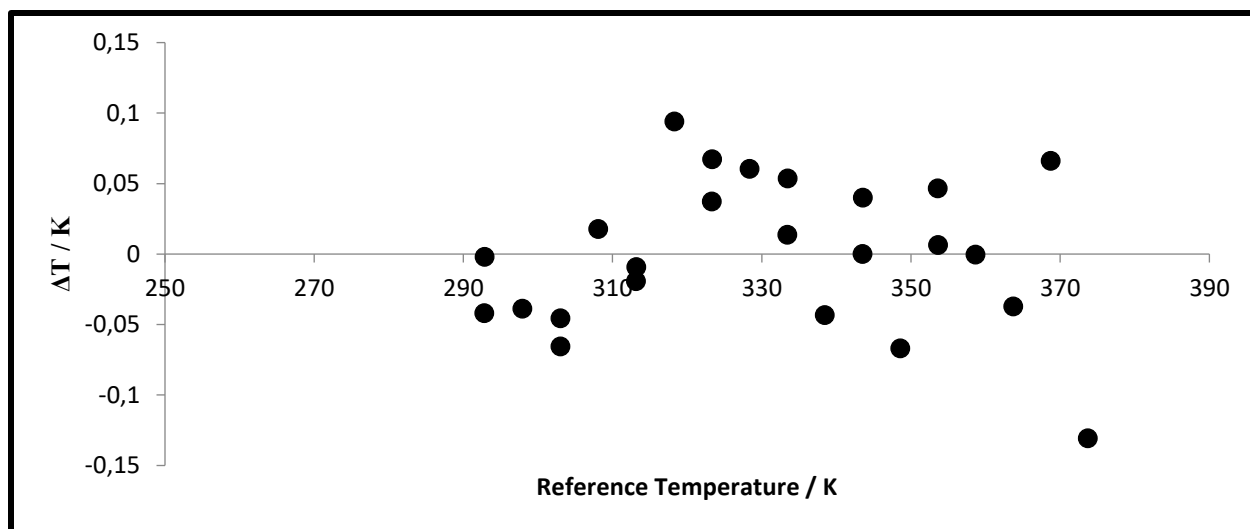


Figure B-3: Temperature calibration plot of cell 2 temperature sensor.



**Figure B-4: Temperature deviation plot of cell 2 temperature sensor.**

### Gas Chromatograph Operating Conditions

**Table B-2: Operating conditions for the Shimadzu 2014 gas chromatograph.**

Operating Condition	Test System	New Systems
Injector Temperature	240°C	250°C
L Pressure	316.5 kPa	345 kPa
R Pressure	0 kPa	0 kPa
L Carrier Gas	30 ml/min	30 ml/min
R Carrier Gas	3 ml/min	3 ml/min
Column Info	Poropak Q	Poropak Q
Hold Time	30 min	45 min
Column Temp	200°C	235°C
Equilibration Time	3 min	1 min
Detector Temperature	240°C	235°C
Sampling Rate	40 msec	40 msec
Stop Time	40 min	50 min
Subtract Detector	None	None
Current	80 mA	110 mA
Polarity	+(L-R)	+(L-R)
Preset Temp	240°C	250°C

### Gas Chromatograph Calibrations

At minimum, three sample injections were done for each calibration point to ensure that consistent area ratios were obtained as a measure of repeatability, quantified within a tolerance of 1% with the use of the following formula:

$$\text{Repeatability} = \frac{\text{Standard Deviation}}{\text{Average}} \times 100\% \quad (\text{B-1})$$

The absolute average deviation (AAD) was determined as follows:

$$\text{AAD} = \frac{\sum_{i=1}^k |\Delta x_i|}{k} \quad (\text{B-2})$$

Where:

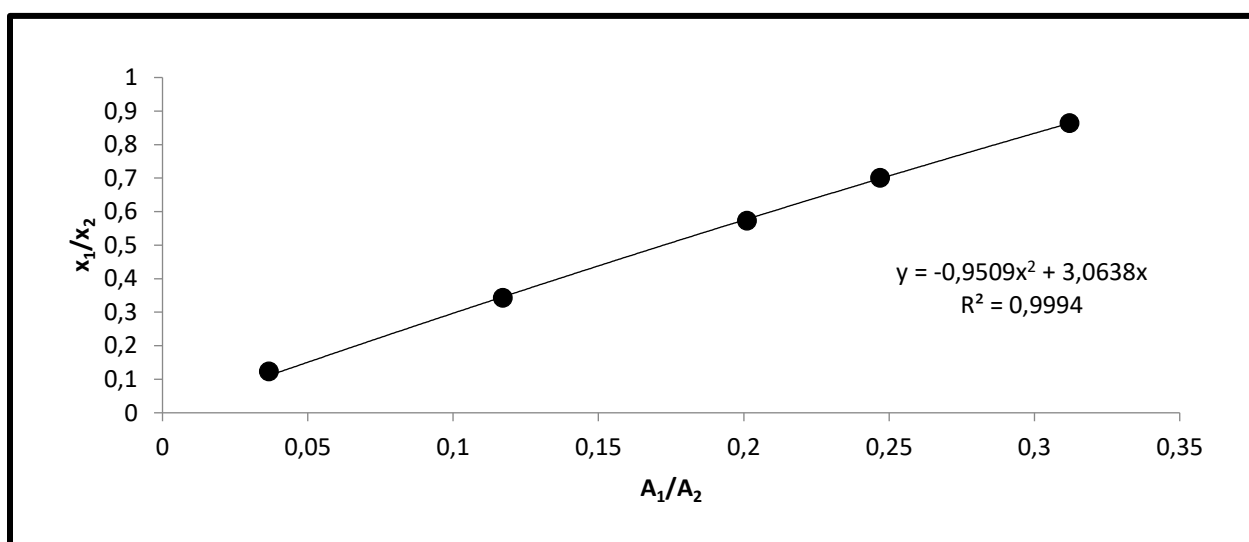
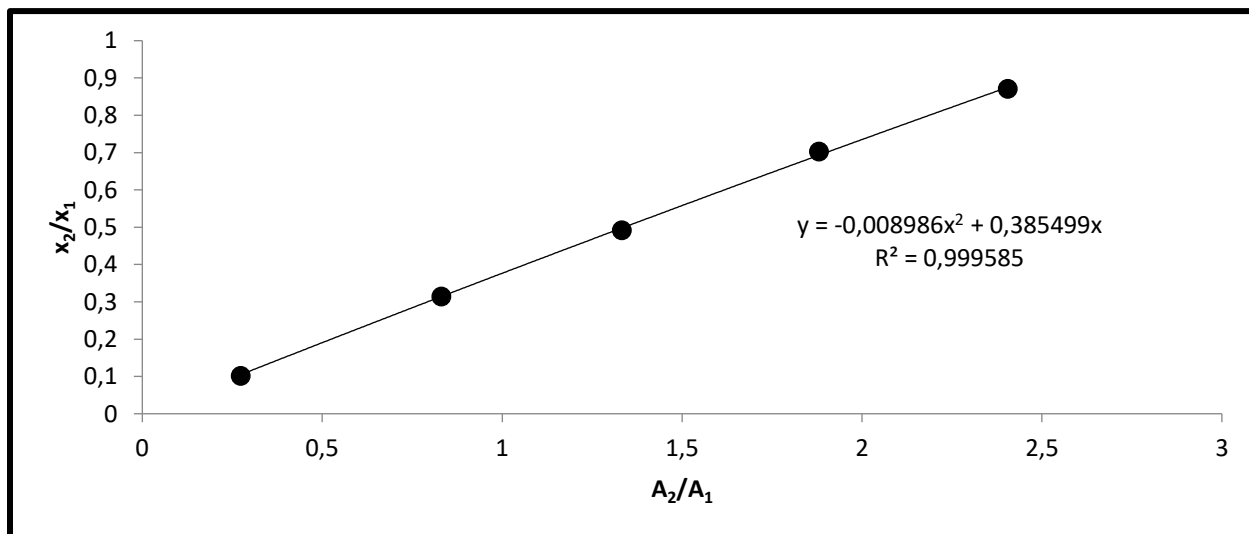
$$\Delta x_i = (x_i)_{\text{Calibration}} - (x_i)_{\text{Standard}} \quad (\text{B-3})$$

**Table B-3: Summary of calibrations with average absolute deviations**

System	Calibration	Dilute Region	AAD (Mole Fraction)
Methanol (1) +n-Heptane (2)	$\frac{A_1}{A_2} = -0.9509 \left( \frac{x_1}{x_2} \right)^2 + 3.0638 \left( \frac{x_1}{x_2} \right)$	Methanol	0.005
	$\frac{A_2}{A_1} = -0.008986 \left( \frac{x_2}{x_1} \right)^2 + 0.3855 \left( \frac{x_2}{x_1} \right)$	n-Heptane	0.005
n-Nonane (1) + NFM (2)	$\frac{A_1}{A_2} = 0.01585 \left( \frac{x_1}{x_2} \right)^2 + 0.5128 \left( \frac{x_1}{x_2} \right)$	n-Nonane	0.004
	$\frac{A_2}{A_1} = -0.5687 \left( \frac{x_2}{x_1} \right)^2 + 2.2384 \left( \frac{x_2}{x_1} \right)$	NFM	0.005
n-Decane (1) + NFM (2)	$\frac{A_1}{A_2} = -0.03375 \left( \frac{x_1}{x_2} \right)^2 + 0.5761 \left( \frac{x_1}{x_2} \right)$	n-Decane	0.004
	$\frac{A_2}{A_1} = -0.5897 \left( \frac{x_2}{x_1} \right)^2 + 2.1665 \left( \frac{x_2}{x_1} \right)$	NFM	0.005

**Table B-3: Summary of calibrations with average absolute deviations (continued)**

System	Calibration	Dilute Region	AAD (Mole Fraction)
Toluene (1) + NFM (2)	$\frac{A_1}{A_2} = -0.05568\left(\frac{x_1}{x_2}\right)^2 + 0.9456\left(\frac{x_1}{x_2}\right)$	Toluene	0.004
	$\frac{A_2}{A_1} = -0.1476\left(\frac{x_2}{x_1}\right)^2 + 1.2308\left(\frac{x_2}{x_1}\right)$	NFM	0.003

**Figure B-5: GC calibration graph of methanol (1) + n-heptane (2) (methanol dilute region)****Figure B-6: GC calibration graph of methanol (1) + n-heptane (2) (n-heptane dilute region)**

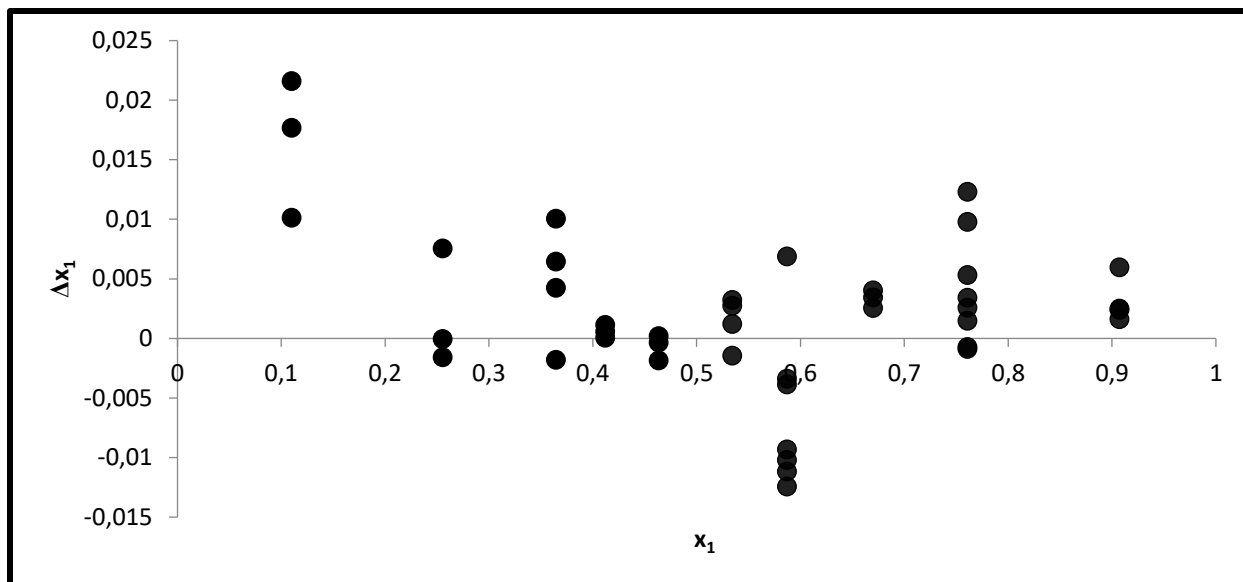


Figure B-7: Composition deviation plot for the methanol (1) + *n*-heptane (2) system

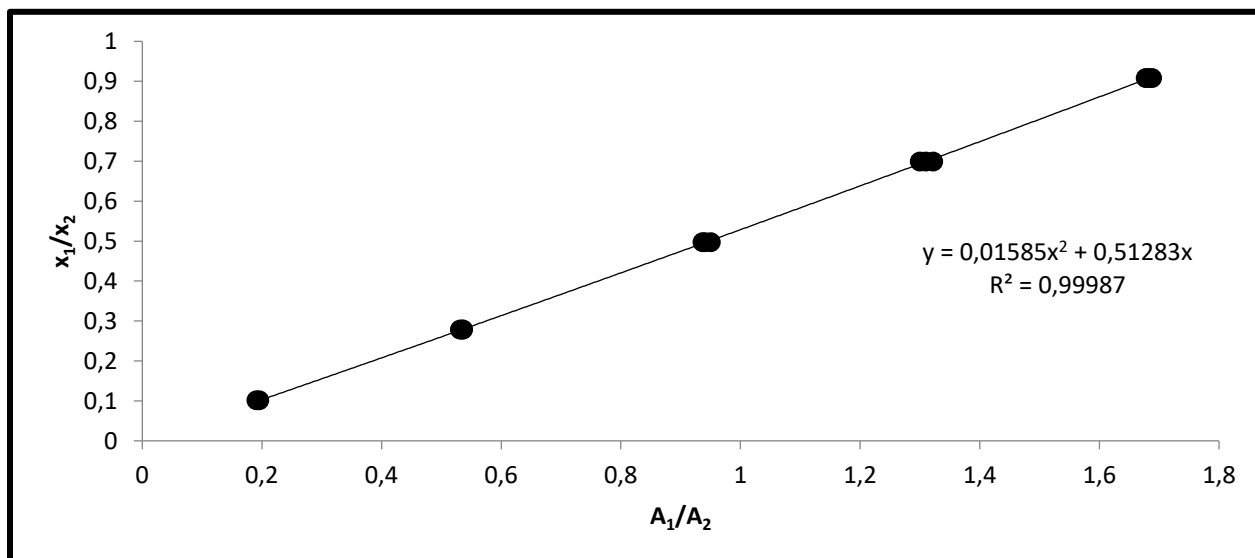


Figure B-8: GC calibration graph for the nonane (1) + NFM (2) pair (*n*-nonane dilute region)

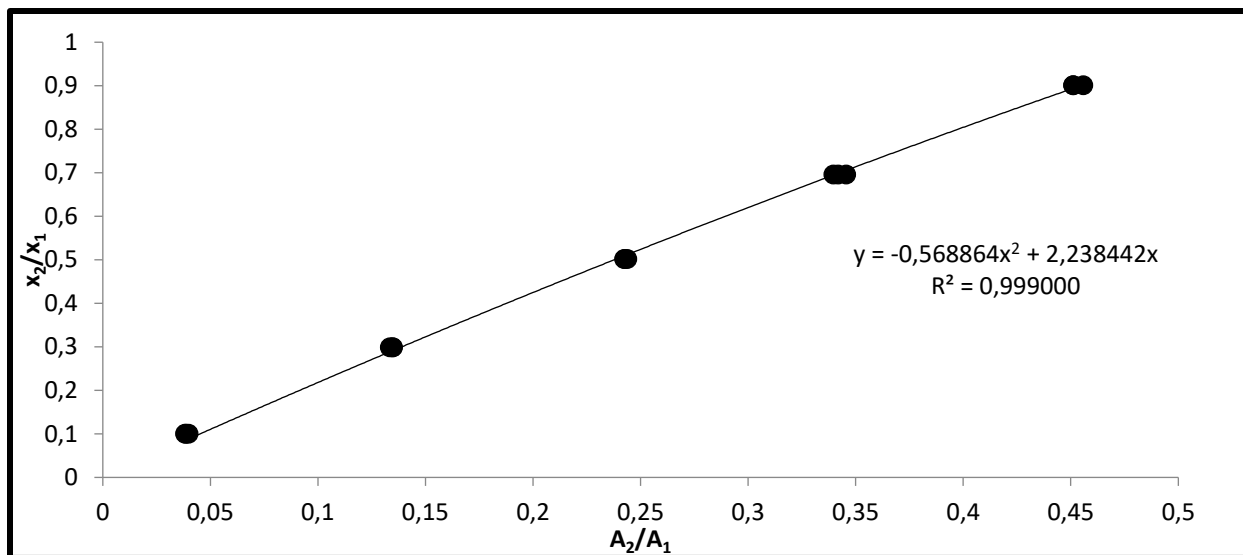


Figure B-9: GC calibration graph for the *n*-nonane (1) + NFM (2) pair (NFM dilute region)

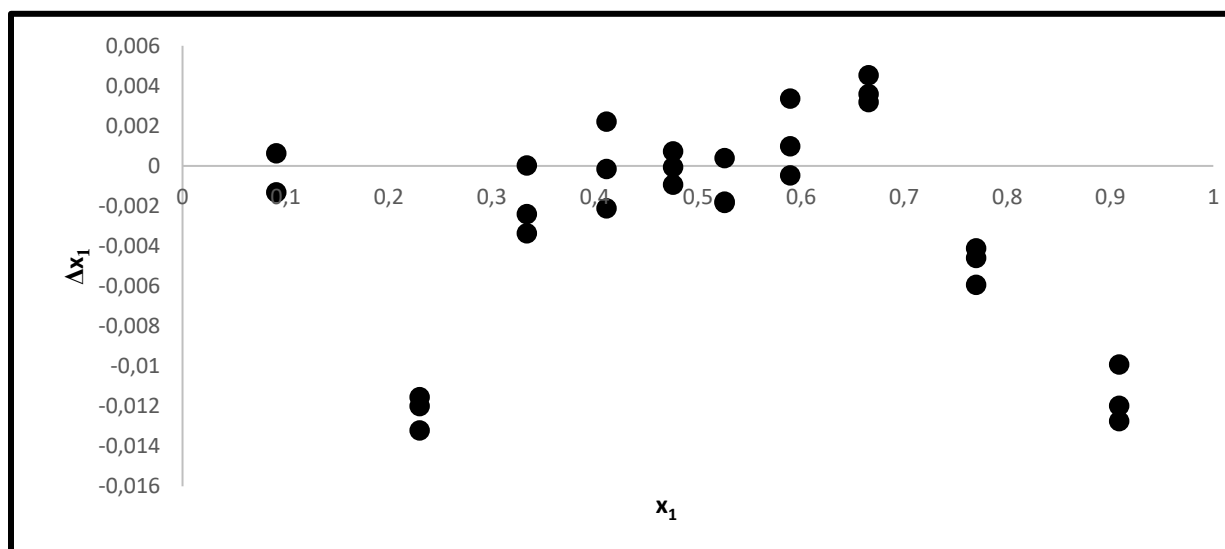
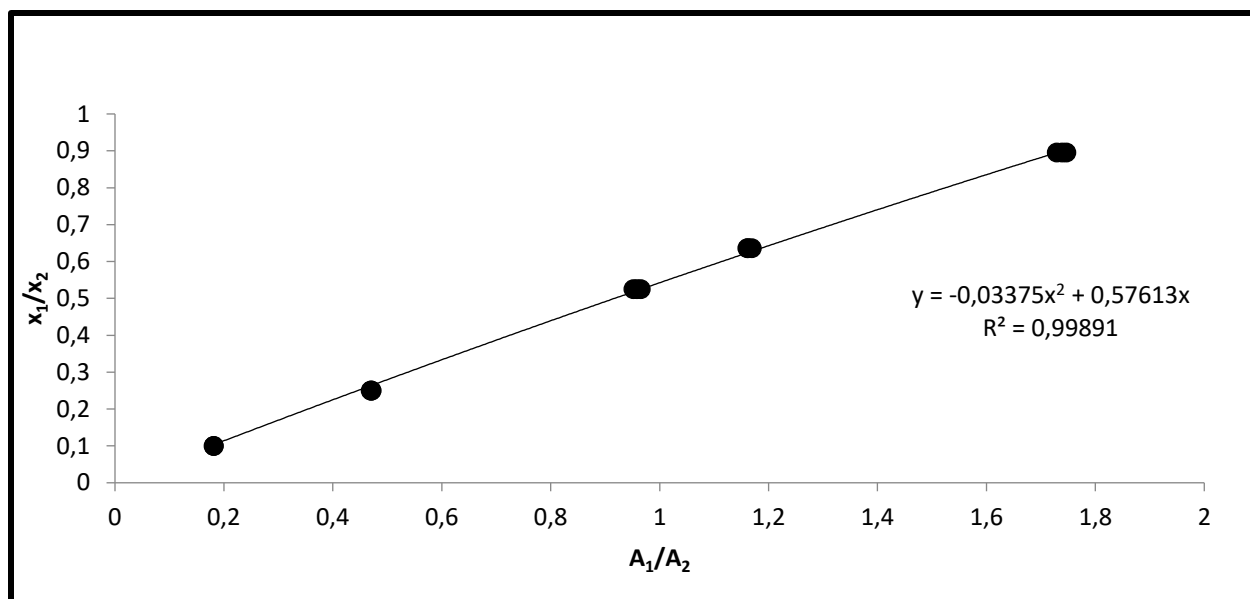
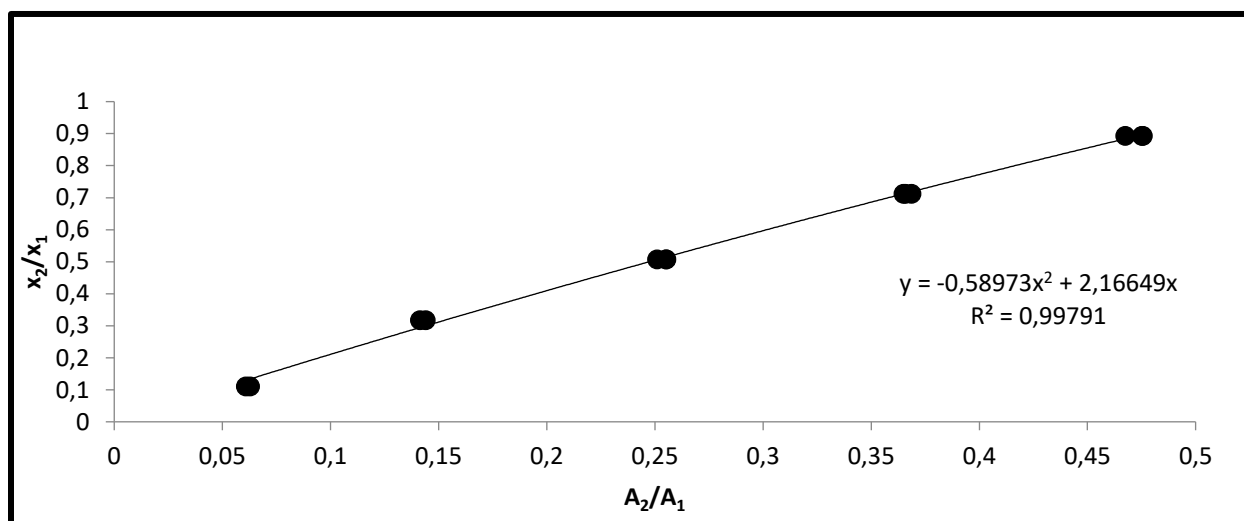


Figure B-10: Composition deviation plot for the *n*-nonane (1) + NFM (2) system



**Figure B-11: GC calibration graph for *n*-decane (1) + NFM (2) pair (*n*-decane dilute region)**



**Figure B-12: GC calibration graph for the *n*-decane (1) + NFM (2) pair (NFM dilute region)**

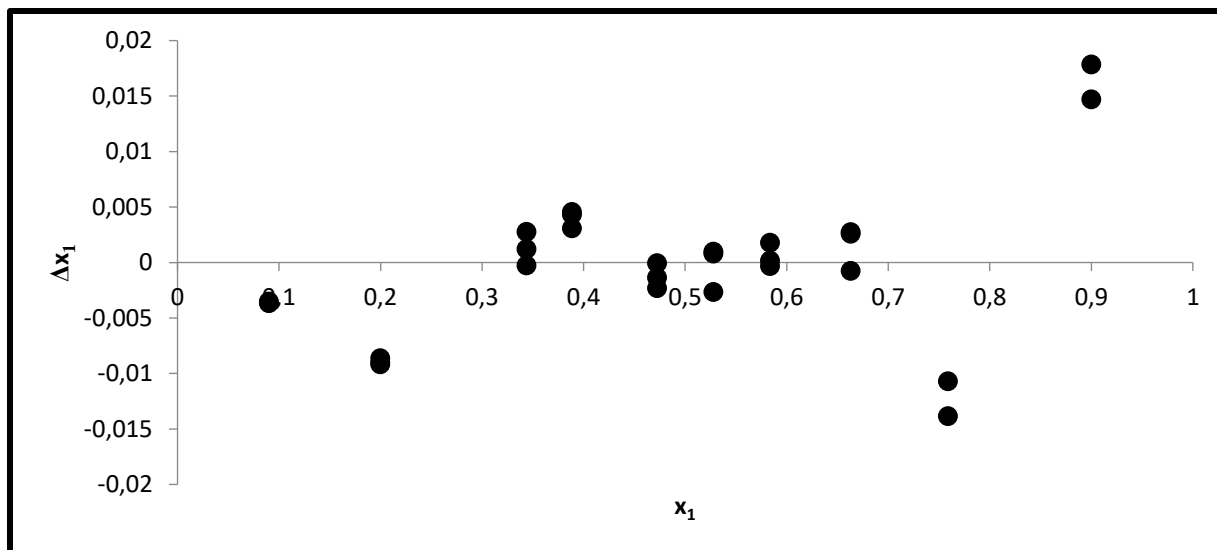


Figure B-13: Composition deviation plot for the *n*-decane (1) + NFM (2) system

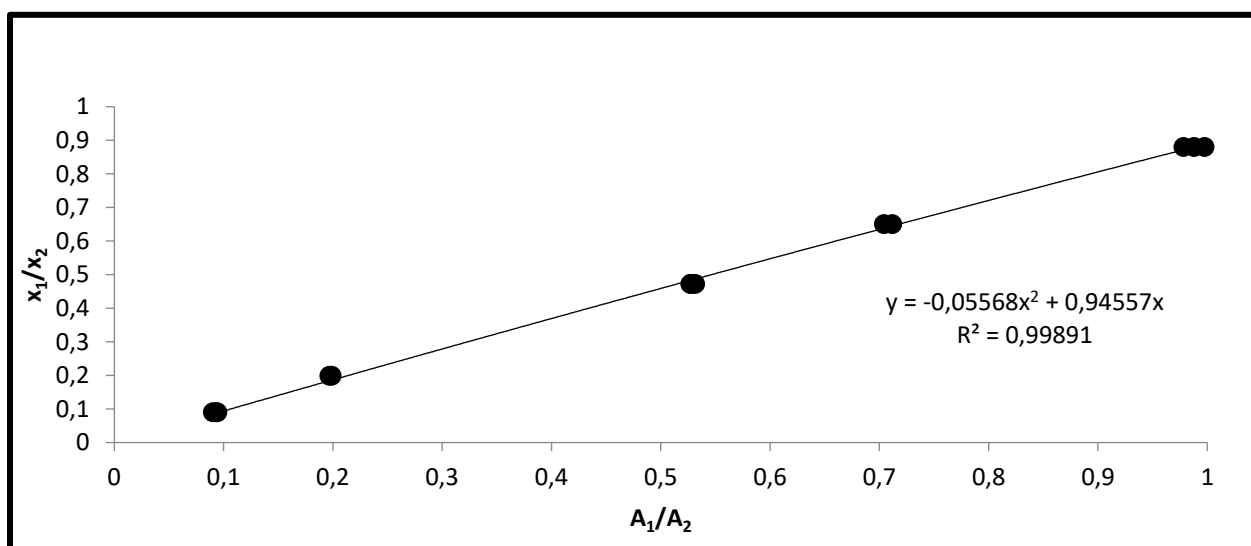


Figure B-14: GC calibration graph for the toluene (1) + NFM (2) pair (toluene dilute region)

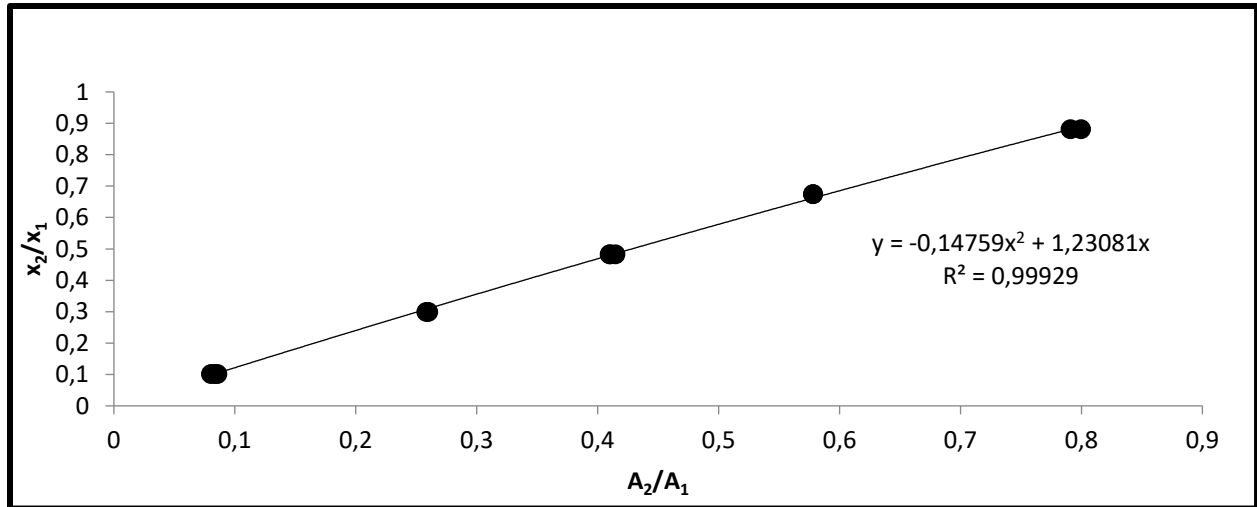


Figure B-15: GC calibration graph for the toluene (1) + NFM (2) pair (NFM dilute region)

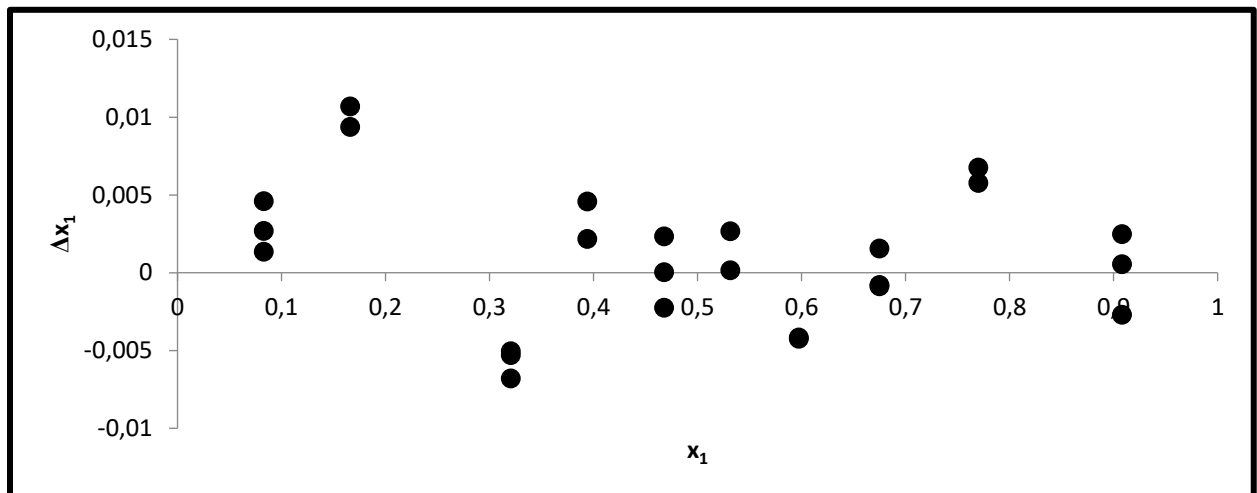


Figure B-16: Composition deviation plot for the toluene (1) + NFM (2) system

## APPENDIX C

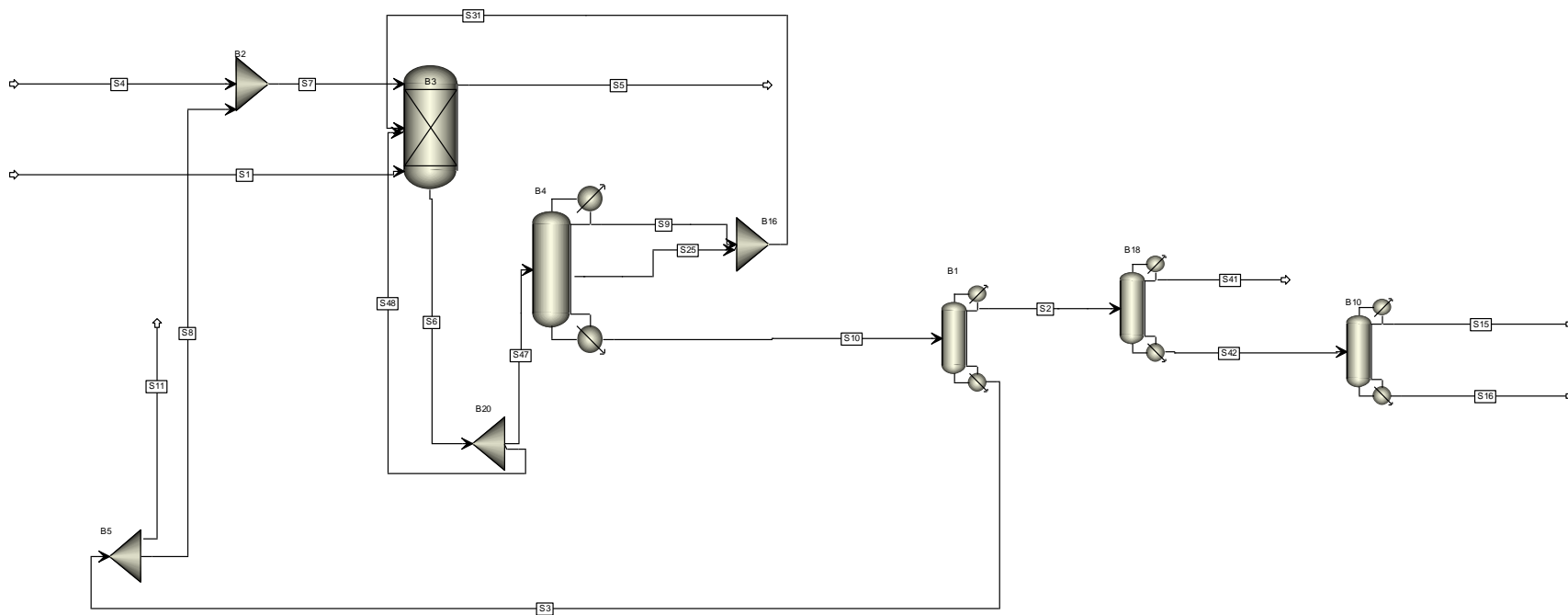


Figure C-1: Aspen Plus flowsheet for aromatics recovery unit using NFM as the solvent

Table C-1: Stream operating conditions and molar flows from Aspen Plus V8.4

	Units	S1	S10	S11	S15	S16	S2	S25	S3	S31	S4	S41	S42	S47	S48	S5	S6	S7	S8	S9
n-Butane	kmol/h	70.03	0.00	0.00	0.00	0.00	0.00	0.00	0.00	37.50	0.00	0.00	0.00	37.50	37.50	70.04	75.00	0.00	0.00	37.50
i-Pentane	kmol/h	157.95	0.00	0.00	0.00	0.00	0.00	0.00	0.00	59.51	0.00	0.00	0.00	59.51	59.51	157.98	119.03	0.00	0.00	59.51
n-Pentane	kmol/h	387.36	0.00	0.00	0.00	0.00	0.00	0.00	0.00	13.29	0.00	0.00	0.00	13.29	13.29	387.37	26.58	0.00	0.00	13.29
Cyclopentane	kmol/h	58.03	0.00	0.00	0.00	0.00	0.00	0.00	0.00	4.74	0.00	0.00	0.00	4.74	4.74	58.04	9.49	0.00	0.00	4.74
2,3-Dimethyl-butane	kmol/h	25.19	0.00	0.00	0.00	0.00	0.00	0.00	0.00	6.65	0.00	0.00	0.00	6.65	6.65	25.19	13.30	0.00	0.00	6.65
2-Methyl-pentane	kmol/h	188.92	0.00	0.00	0.00	0.00	0.00	0.00	0.00	46.97	0.00	0.00	0.00	46.97	46.97	188.94	93.94	0.00	0.00	46.97
3-Methyl-pentane	kmol/h	125.95	0.00	0.00	0.00	0.00	0.00	0.00	0.00	14.45	0.00	0.00	0.00	14.45	14.45	125.97	28.90	0.00	0.00	14.45
n-Hexane	kmol/h	270.78	0.00	0.00	0.00	0.00	0.00	0.00	0.00	16.89	0.00	0.00	0.00	16.89	16.89	270.79	33.78	0.00	0.00	16.89
Me-cyclopentane	kmol/h	132.19	0.00	0.00	0.00	0.00	0.00	0.00	0.00	11.02	0.00	0.00	0.00	11.02	11.02	132.20	22.05	0.00	0.00	11.02
Benzene	kmol/h	62.53	62.41	0.00	0.12	0.00	62.41	30.15	0.00	199.61	0.00	62.30	0.12	262.03	262.03	0.01	524.05	0.00	0.00	169.46
Cyclohexane	kmol/h	90.27	0.00	0.00	0.00	0.00	0.00	0.00	0.00	9.07	0.00	0.00	0.00	9.07	9.07	90.28	18.14	0.00	0.00	9.07
2-Methyl-hexane	kmol/h	75.82	0.00	0.00	0.00	0.00	0.00	0.00	0.00	13.96	0.00	0.00	0.00	13.96	13.96	75.83	27.93	0.00	0.00	13.96
3-Methyl-hexane	kmol/h	102.90	0.00	0.00	0.00	0.00	0.00	0.00	0.00	19.25	0.00	0.00	0.00	19.25	19.25	102.91	38.50	0.00	0.00	19.25
n-Heptane	kmol/h	119.15	0.00	0.00	0.00	0.00	0.00	0.00	0.00	8.95	0.00	0.00	0.00	8.95	8.95	119.15	17.90	0.00	0.00	8.95
Methyl-cyclohexane	kmol/h	132.65	0.01	0.00	0.00	0.00	0.01	0.01	0.00	13.86	0.00	0.00	0.00	13.86	13.86	132.65	27.73	0.00	0.00	13.85
Toluene	kmol/h	88.35	88.09	0.00	87.97	0.05	88.09	27.78	0.00	31.81	0.00	0.07	88.02	119.90	119.90	0.27	239.79	0.00	0.00	4.03
2-Methyl-heptane	kmol/h	57.01	0.02	0.00	0.02	0.00	0.02	0.03	0.00	7.56	0.00	0.00	0.02	7.58	7.58	57.00	15.16	0.00	0.00	7.54
1,3-Dimethylcyclohexane	kmol/h	169.26	0.92	0.00	0.91	0.01	0.92	0.98	0.00	30.64	0.00	0.00	0.92	31.55	31.55	168.37	63.10	0.00	0.00	29.66
n-Octane	kmol/h	128.27	2.36	0.00	1.34	1.01	2.36	1.50	0.00	7.16	0.00	0.00	2.36	9.51	9.51	125.92	19.03	0.00	0.00	5.65
Ethyl-cyclohexane	kmol/h	48.36	2.82	0.00	0.37	2.45	2.82	1.05	0.00	1.19	0.00	0.00	2.82	4.01	4.01	45.54	8.02	0.00	0.00	0.14
2,6-Dimethyl-heptane	kmol/h	40.20	0.42	0.00	0.05	0.37	0.42	0.57	0.00	3.41	0.00	0.00	0.42	3.83	3.83	39.78	7.66	0.00	0.00	2.84
Ethyl benzene	kmol/h	51.12	51.12	0.00	0.43	50.68	51.12	10.27	0.00	10.92	0.00	0.00	51.12	62.04	62.04	0.00	124.07	0.00	0.00	0.65
p-Xylene	kmol/h	48.56	48.56	0.00	0.17	48.39	48.56	9.00	0.00	9.50	0.00	0.00	48.56	58.06	58.06	0.00	116.12	0.00	0.00	0.50
3-Methyl-octane	kmol/h	57.12	1.99	0.00	0.01	1.98	1.99	2.25	0.00	3.41	0.00	0.00	1.99	5.40	5.40	55.14	10.79	0.00	0.00	1.16
o-Xylene	kmol/h	25.56	25.55	0.00	0.03	25.52	25.55	4.38	0.00	4.62	0.00	0.00	25.55	30.17	30.17	0.01	60.34	0.00	0.00	0.24
n-Nonane	kmol/h	55.01	0.70	0.00	0.42	0.28	0.70	3.35	0.00	3.88	0.00	0.00	0.69	4.57	4.57	54.31	9.15	0.00	0.00	0.53
n-Decane	kmol/h	57.21	0.59	0.00	0.15	0.43	0.59	2.51	0.00	2.55	0.00	0.00	0.59	3.14	3.14	56.63	6.28	0.00	0.00	0.04
i-Decane	kmol/h	76.28	2.81	0.00	0.00	2.81	2.81	2.51	0.00	2.63	0.00	0.00	2.81	5.44	5.44	73.48	10.88	0.00	0.00	0.13
NFM	kmol/h	0.00	8441.27	2532.37	0.00	0.02	0.02	353.67	8441.25	355.00	2639.64	0.00	0.02	8796.27	8796.27	107.02	17592.53	8548.51	5908.87	1.33
Mole Flow	kmol/h	2902.01	8729.62	2532.37	92.00	134.00	288.37	450.00	8441.25	950.00	2639.64	62.37	226.00	9679.62	9679.62	2720.80	19359.24	8548.51	5908.87	500.00
Mass Flow	Tons/h	272.2	999.7	291.6	8.6	14.4	27.9	50.1	971.9	91.8	303.9	4.9	23.0	1091.5	1091.5	256.6	2183.0	984.2	680.3	41.7
Volume Flow	L/min	6439.2	13926.3	4131.4	184.4	321.3	601.1	720.0	13771.5	78304.3	3510.3	99.7	504.6	13299.9	13299.9	6020.8	26602.9	13057.6	9640.0	993.7
Temperature	°C	20.0	207.8	240.0	110.0	137.6	110.8	133.0	240.0	69.8	20.0	80.2	124.8	19.8	19.8	20.0	20.0	179.2	240.0	53.0
Pressure	Bar	1.0	1.0	1.0	1.0	1.0	1.0	1.0	1.0	1.0	1.0	1.0	1.0	1.0	1.0	1.0	1.0	1.0	1.0	1.0
Molar Enthalpy	cal/mol	-44377.0	-74066.9	-74690.6	4281.7	-3000.9	2514.1	-64424.0	-74690.6	-43649.9	-87872.5	13590.2	-219.4	-81266.6	-81266.6	-50527.2	-81266.6	-78760.9	-74690.6	-24953.3
Enthalpy Flow	cal/sec	-35773000.0	-17960000.0	-52540000.0	109421.0	-111700.0	201385.0	-8053000.0	-17513000.0	-11519000.0	-64431000.0	235450.0	-13775.7	-21851000.0	-21851000.0	-38187000.0	-43702000.0	-18702000.0	-12259000.0	-3465700.0
Molar Entropy	cal/mol-K	-154.5	-137.3	-135.6	-75.3	-96.5	-79.5	-136.0	-135.6	-123.2	-168.5	-54.6	-87.0	-162.4	-162.4	-161.9	-162.4	-144.0	-135.6	-113.3
Average Molecular Weight		93.8	114.5	115.1	93.1	107.6	96.6	111.2	115.1	96.6	115.1	78.1	101.7	112.8	112.8	94.3	112.8	115.1	115.1	83.5

**Table C-2: Summary of process heat exchangers required - from Aspen Plus V8.4**

<b>Heat Exchanger</b>	<b>Type</b>	<b>Duty (kcal/s)</b>	<b>Hot Inlet (°C)</b>	<b>Hot Outlet (°C)</b>	<b>°Cold Inlet (°C)</b>	<b>°Cold Outlet (°C)</b>	<b>Area (m<sup>2</sup>)</b>	<b>Hot Side Fluid</b>	<b>Cold Side Fluid</b>
Extractive Distillation Condenser	Cooler	1128	79.1	53	30	35	1401.8	Column Distillate	Air
Solvent Recovery Condenser	Cooler	22510	122.1	110.8	30	35	10695.1	Column Distillate	Air
Benzene Recovery Condenser	Cooler	2270	80.2	80.2	30	35	1811.6	Column Distillate	Air
Toluene Recovery Condenser	Cooler	1551	110.5	110	30	35	768.2	Column Distillate	Air
Extractive Distillation Reboiler	Heater	28610	250	249	133	207.8	1245.1	HP Steam	Column Bottoms
Solvent Recovery Reboiler	Heater	32320	250	249	240	240.5	2589.4	HP Steam	Column Bottoms
Benzene Recovery Reboiler	Heater	1907	175	174	137.1	137.6	83.9	MP Steam	Column Bottoms
Toluene Recovery Reboiler	Heater	2780	175	174	120.4	124.8	130.3	MP Steam	Column Bottoms